

A Pictorial Assay of Ground Opacification of the Lungs

Ali Nawaz Khan^{1*}, Klaus Irion², Sara Al Ganem³, Hanaa Bamefleh⁴, Anthony Kodzo-Grey Venyo⁵, Prabhakar Rajiah⁶ and Carolyn Allen Carolyn⁷

¹Consultant Radiologist, North Manchester General Hospital, Manchester, United Kingdom

²Consultant Cardiothoracic Radiologist, Manchester Royal Infirmary, United Kingdom

³Consultant Chest Radiologist, Department of Radiology, King Saud Bin Abdul Aziz University for Health Sciences, Riyadh, Saudi Arabia

⁴Department of Pathology and Laboratory Medicine, King Saud Bin Abdul Aziz University for Health Sciences, Riyadh, Saudi Arabia

⁵Department of Urology, North Manchester General Hospital, Manchester, United Kingdom

⁶Associate Professor of Radiology, Associate Director of Cardiac CT and MR, Cardiothoracic Imaging, Department of Radiology, University of Texas Southwestern Medical Center, Dallas, Texas, United States

⁷Consultant Thoracic Radiologist and Clinical Director, North Manchester General Hospital, Manchester, United Kingdom

***Corresponding Author:** Ali Nawaz Khan, Consultant Radiologist, North Manchester General Hospital, Manchester, United Kingdom.

Received: August 18, 2017; **Published:** October 09, 2017

Abstract

Ground-glass opacification (GGO) of the lungs is caused by an accumulation of pathological products in the alveoli and alveolar septae. GGO is detectable on Chest-X-rays but better defined on High-Resolution CT (HRCT). The differential diagnosis of GGO is broad and includes image acquisition and other technical factors, a wide variety of lung pathologies such as lung hemorrhage, pulmonary embolism, trauma, and autoimmune vasculitis/capillaritis to name just a few. The appearances are not tissue-specific, but with the input of clinical history, lung function tests and other laboratory data, it is possible to arrive at a more meaningful diagnosis.

Aim: To present the imaging features of GGO, discuss the differential diagnosis and differentiate GGO caused by technical/radiographic factors.

Conclusions: A wide variety of systemic diseases and lung pathologies can present with GGO. An accurate diagnosis can only be achieved with imaging features, lung function tests, and other laboratory parameters.

Keywords: HRCT; GGO; Lung Hemorrhage; Pulmonary Embolism; Trauma; Autoimmune Vasculitis; Sarcoidosis; NHL; Asthma; Infections; Lung Manifestation of Immune-Suppression; Cocaine-Induced Lung Injury; Pre-Invasive Adenocarcinoma of the Lung

Introduction

GGO is caused by the accumulation of pathological products in the alveoli and alveolar septae [1-5]. GGO due to technical/radiographic factors is related to the degree of inspiratory effort, as a consequence of the lack of distension of the air spaces. Therefore, GGO cannot be diagnosed unless confident that the inspiratory effort was adequate. The radiographic factors such as window setting for lung interstitium, with width of $1000 < WW < 1700$ HU, level: $-750 < WL < -600$ are important. Slice thickness: 1 or 2 mm and degree of inspiration. Window settings for lung interstitium: width: $1000 < WW < 1700$ HU, level: $-750 < WL < -600$. Slice thickness: 1 or 2 mm and degree of inspiration [6-8]. There are several causes of increased or decreased lung density; decreased lung density is related to emphysema, lung cysts and bronchial dilatation [9].

Discussion

HRCT is better than a conventional chest radiograph for certain lung pathologies as it provides detail lung pathology detail that may rival or may be better than chest radiography.

HRCT utilizes a conventional CT scanner, but imaging parameters are chosen to enhance spatial resolution. The UCSF protocol of HRCT use (1) a 1 - 2 mm slice width (2) high spatial resolution image reconstruction algorithm (3) minimized field view to reducing the size of pixels (4) optimized focal spot for resolution at the expense of scan speed.

Further changes in protocol may be incorporated dependent on the suspected lung pathology such as scanning in both inspiration and expiration and scanning in both supine and prone positions. HRCT is performed by taking thin sections 10 - 40 mm apart, which minimizes the number sections taken to cover a tenth of the lungs. No intravenous contrast is used because of the high soft tissue/air inherent in HRCT. HRCT is not suitable for assessment of the soft tissues and blood vessels, which is the functionality of intravenous contrast agents.

HRCT identifies emphysema, bronchiectasis, and pulmonary fibrosis, but it may not always be able to categorize specific types of fibrosis with the exception of usual interstitial pneumonitis (UIP), which has very characteristic features, and diagnosed on HRCT alone. And although HRCT cannot always provide a definitive diagnosis, it helps locate a site for tissue diagnosis. Other lung pathologies where HRCT can be useful include Lymphangitis carcinomatosa, fungal, or other atypical, infections, chronic lung disease and Lymphangioleiomyomatosis, Sarcoidosis and organ transplant patients [6-8].

When analyzing the distribution of HRCT abnormalities, it is important that subdivisions of the lungs based on the function and size of airways and vessels is incorporated. Subdivision of the lungs based on the function and size of airways and vessels. Personal communication Klaus Irion Ph.D. (please see Figure 1).

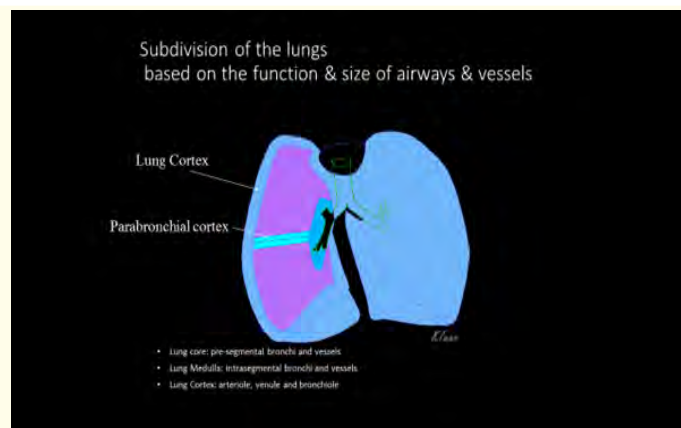


Figure 1: Subdivision of the lungs based on the function and size of airways and vessels.

Reference: Personal communication Klaus Irion Ph.D.

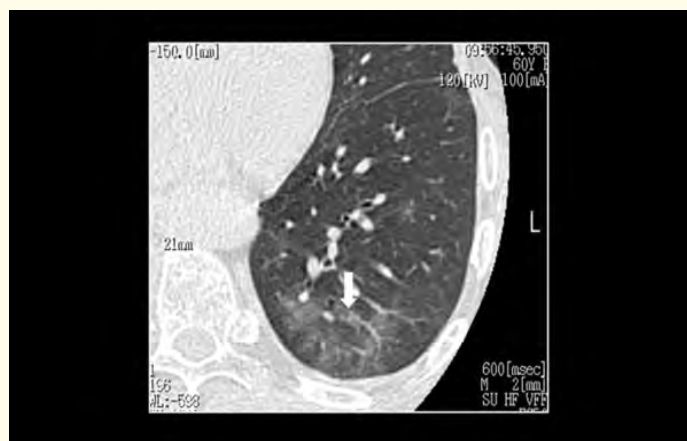


Figure 2: HRCT at the lung base show an example of ground glass opacification.

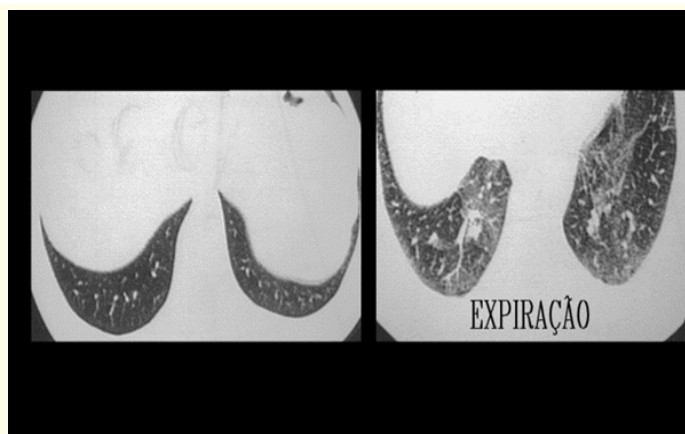


Figure 3: HRCT in inspiration and expiration shows GGO in the expiratory phase; not as a representation of a disease but as a consequence of the lack of distension of the air spaces.

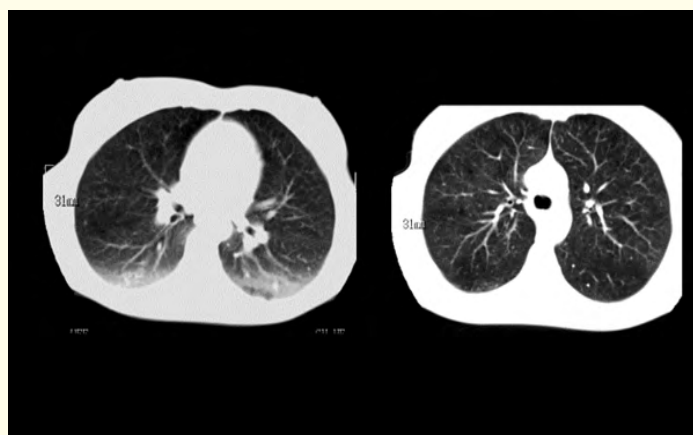


Figure 4: Axial CT scans on the same patient, on the same day in inspiration and expiration, showing how the lack of inspiratory effort can mimic lung disease.

Good Pastures associated GGO

Diffuse alveolar hemorrhage has many causes; most are caused by capillaritis associated with systemic autoimmune diseases such as antineutrophil cytoplasmic antibodies-associated vasculitis, anti-glomerular basement membrane disease, and systemic lupus erythematosus. Pulmonary hemorrhage associated with Anti-GBM antibody is termed Good Pasture's Syndrome. Radiologically the appearance cannot be differentiated from other forms of pulmonary hemorrhage. Both a CXR and CT show diffuse, bilateral, patchy, basal consolidation and alveolar densities with sparing of peripheral lung fields. Early recognition is important as lifesaving treatment can be instituted.

Pulmonary hemorrhage associated with Anti-GBM antibody is termed Good Pasture's Syndrome. Radiologically the appearance cannot be differentiated from other forms of pulmonary hemorrhage. Both a CXR and CT show diffuse, bilateral, patchy, basal consolidation and alveolar densities with sparing of peripheral lung fields. Early recognition is important as lifesaving treatment can be instituted [10-14].

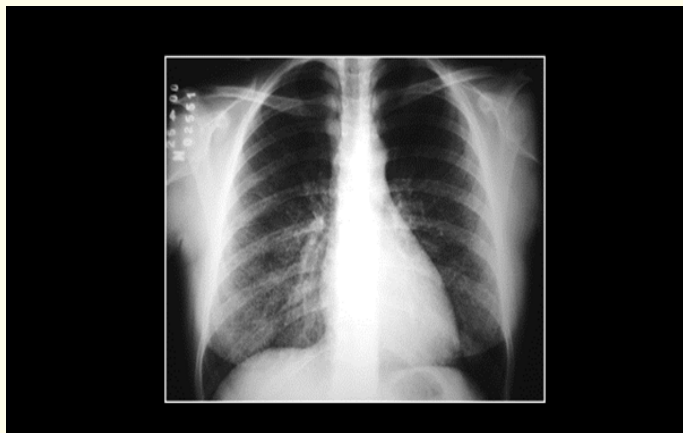


Figure 5: Good pasture's Syndrome: Radiologically the appearance cannot be differentiated from other forms of pulmonary hemorrhage. Both a CXR and a CT show diffuse, bilateral, patchy, basal consolidation and alveolar densities with sparing of peripheral lung fields. Early recognition is important as lifesaving treatment can be instituted.



Figure 6: Good pastures: Axial CT scan shows diffuse, bilateral, patchy, basal consolidation and alveolar densities with sparing of peripheral lung fields.

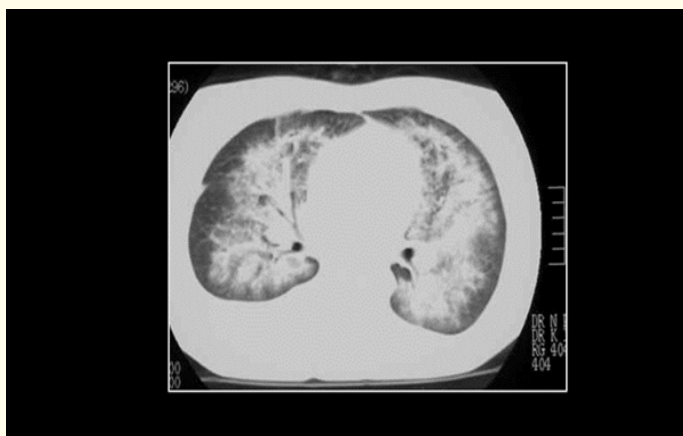


Figure 7: Good pasture's Syndrome: HRCT shows extensive 'bats wing shadowing' associated with an air bronchogram, mimicking pulmonary edema.

Pulmonary hemosiderosis associated GGO

Pulmonary hemosiderosis (PHH) of the lungs occur in two forms: (1) Primary lung disease (2) Secondary to cardiovascular or systemic disease. In adults, the secondary form of PPH is more common in adults. Three variants of the primary type of disease are described

Three variants of primary of PHH are described: (1) PHH associated with antibody to the basement membrane of the lung and kidney as in Goodpasture syndrome (2) PHH associated with hypersensitivity to proteins in cow's milk (Heiner syndrome), and (3) idiopathic pulmonary hemosiderosis (IPH). The diagnosis of isolated PHH and primary PHH is a process exclusion [15-18].



Figure 8: Pulmonary hemosiderosis (PHH) shows extensive air space shadowing and GGO in all the lung lobes.

Cavitating pulmonary infarcts associated GGO

Cavitating pulmonary infarcts have been reported in 4-5% in autopsy series. Cavities may be sterile or septic. Cavitating infarcts are single and often followed by consolidation in the area of infarction [19-21].

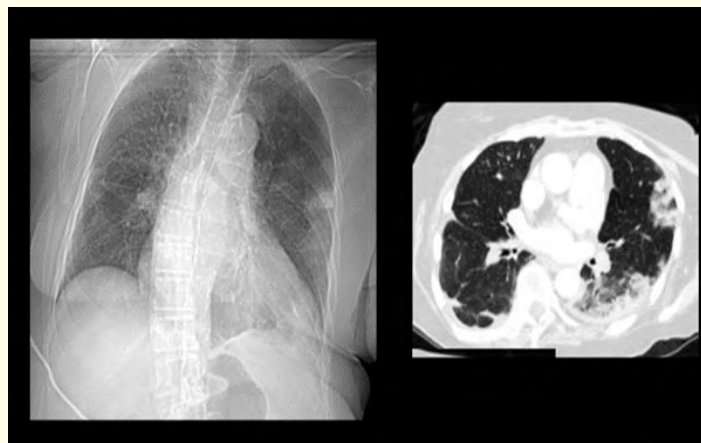


Figure 9: Portable AP chest radiograph in a patient with pulmonary embolism and infarction. Note the segmental pleural based opacity and a cavitating infarct as seen on the axial CT scans. Also, note the GGO.

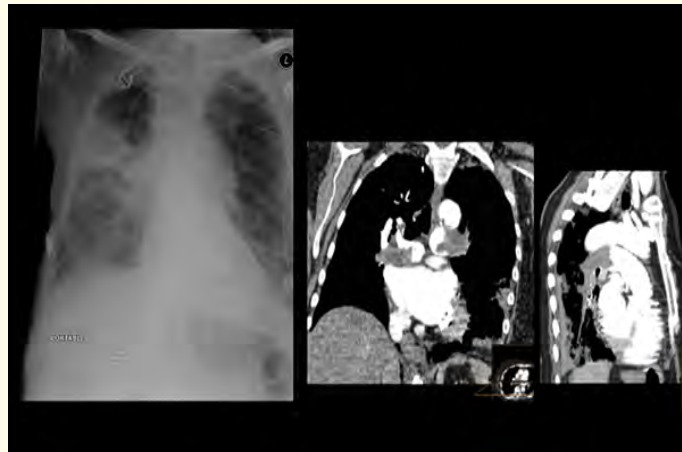


Figure 10: An AP Radiograph on a patient that presented right pleuritic chest pain. Note the segmental pleural-based opacity and loss of volume and GGO at both the lung bases. The coronal and sagittal reconstruction CT scans show extensive pulmonary thrombosis/infarcts.

Lung contusion associated GGO

Lung contusion refers to a non-penetrating lung injury due to blunt thoracic trauma and is associated with interstitial and/or alveolar lung injury without laceration. Blunt trauma may affect any age group. An initial CXR show little indication of the severity lung injury. Lung contusion clear rapidly and usually resolve within 48 hours. The contusion is often of a lobar or segmental distribution.

Computed Tomography typically shows focal lung consolidation usually of crescentic shape, with sub-pleural sparing with smaller contusions. Lung contusions more commonly occur in the lower lobes placed posteriorly [22-25].

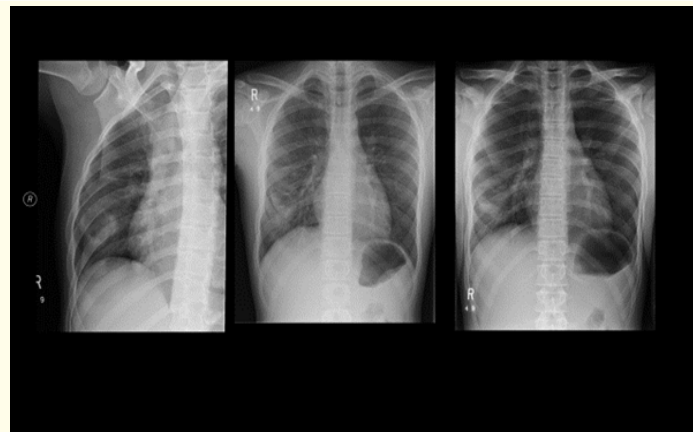


Figure 11: Series of chest radiographs showing a cavitating lung contusion with a right-sided rib fracture and a shallow pneumothorax. A lung contusion develops in a few hours and resolves within a week. Ipsilateral or contra-coup Ill-defined, non-segmental, peripheral GGO are seen adjacent to injured bony.

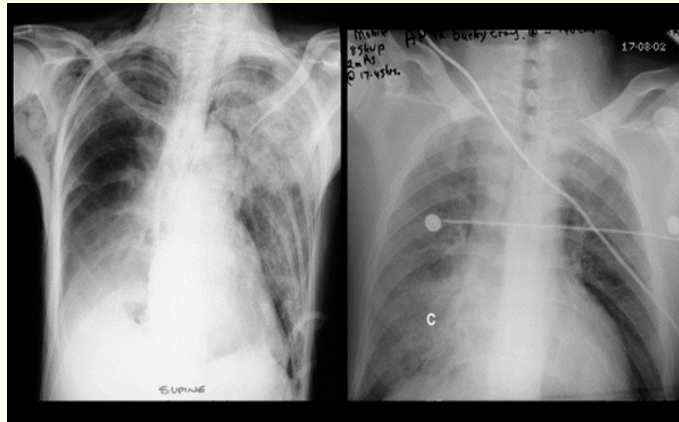


Figure 12: Lung Contusion: A CXR following blunt thoracic trauma showing surgical emphysema and pulmonary haemorrhage, the patient presented with hemoptysis following the injury. Series of chest radiographs showing a cavitating lung contusion with a right-sided rib fracture and a shallow pneumothorax. A lung contusion develops in a few hours and resolves within a week. Ipsilateral or contra-coup ill-defined, non-segmental, peripheral GGO are seen adjacent to injured bony.

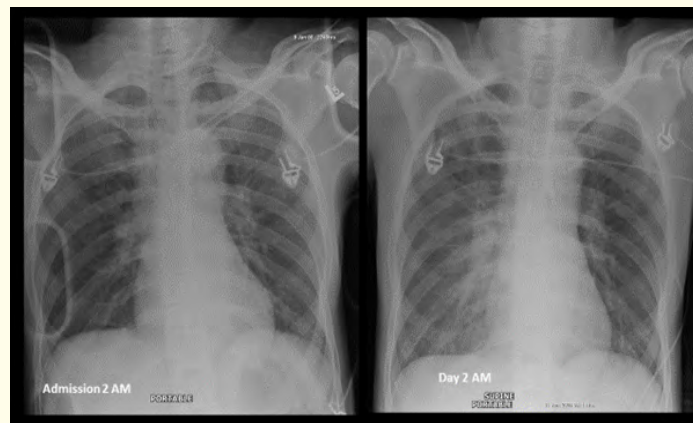


Figure 13: Series of portable chest radiographs and axial CT scans of a young male following a motor vehicle accident (MVA). The images show an evolution of the pulmonary contusion.

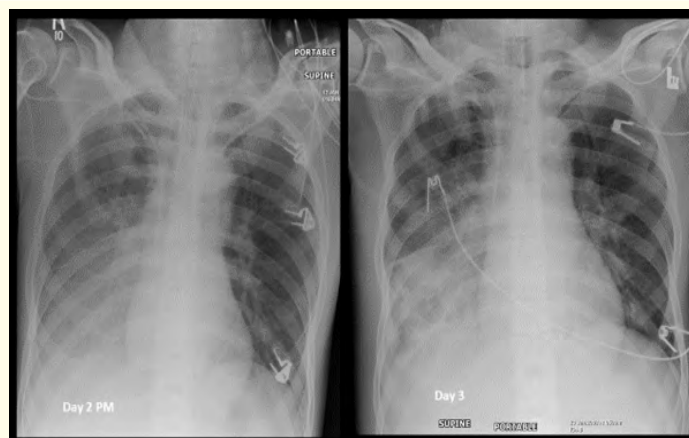


Figure 14: Series of portable chest radiographs and axial CT scans of young male following a motor vehicle accident (MVA). The images show evolution of the pulmonary contusion.

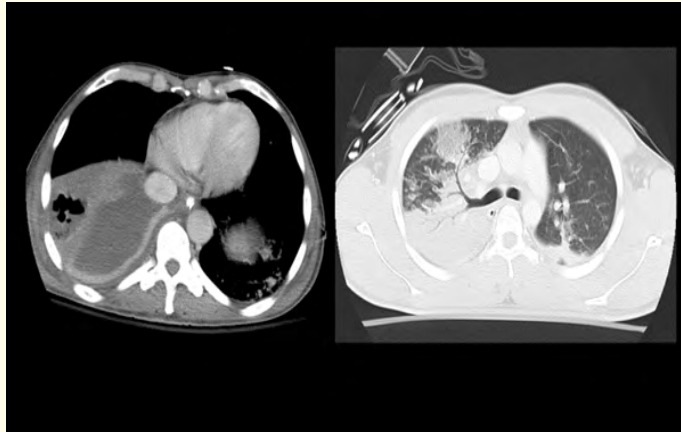


Figure 15: Series of portable chest radiographs and axial CT scans of a young male following a motor vehicle accident (MVA). The images show an evolution of the pulmonary contusion.

Visceral injury/ blunt thoracic trauma associated GGO

The estimated prevalence of liver laceration in polytraumatized patients from blunt trauma is calculated between 1% and 8%. Gerrit Matthes, *et al.* enrolled 218 patients in a cohort of polytraumatized patients who had blunt; undergone contrast-enhanced, whole-body helical CT. The prevalence of Moore III to V lesions was 10.1%, with 99 parenchymal contusions, 15 capsular tears, and two liver fractures. Surgery was required in 15 patients. The authors postulated that the prevalence of liver lacerations among multiple-trauma patients is likely to be underestimated and must be determined by the independent application of reference standards, such as helical CT. High-grade hepatic injuries and the need for surgical repair are associated with poorer survival prognosis [26].

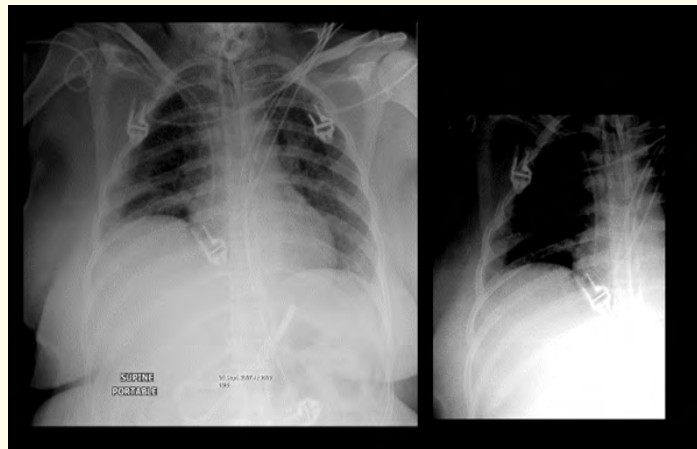


Figure 16: Series of portable chest radiographs and axial CT scans of a young female following MVA. The images show an evolution of pulmonary contusion. Note the elevated right hemidiaphragm. See axial CT scans.

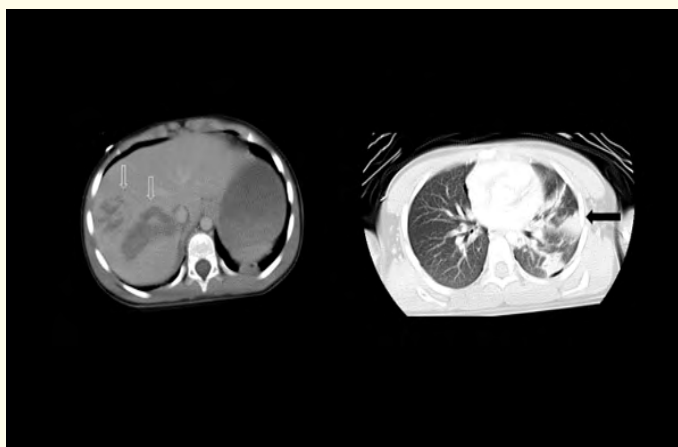


Figure 17: Axial CT scans through the thorax and the liver on a young a female following an MVA. Note the liver laceration (arrows) and countercoup lung contusions (black arrow).

Cocaine-induced lung injury associated GGO

Cocaine-induced lung injury is related to the method of administration and the presence of contaminants and the dose administered. Pulmonary symptoms may be acute or chronic and include asthma, pulmonary edema, pulmonary hemorrhage, and eosinophilic lung disease; BOOP, talcosis, and interstitial lung disease, pulmonary hypertension, emphysema and aspiration pneumonia. Infective pneumonias are also common [27-29].



Figure 18: A CXR and axial CT scans show GGO, interstitial lung disease and bullae in a male intravenous drug abuser (Cocaine) over several years.

Rheumatoid arthritis associated GGO

Chen and associates analyzed HRCT findings in patients with rheumatoid arthritis (RA) that were subsequently classed as RA-ILD or RA-no ILD based on the presence/absence of GGO, and other HRCT findings. Supporting respiratory function tests such as reductions in percent predicted FEV1, FVC, TLC, and/or DLCO were also used in search of occult respiratory defects. The authors found HRCT findings an effective tool in the detection of occult/asymptomatic ILD, which was highly prevalent in unselected, a university-based cohort of RA patients [30].

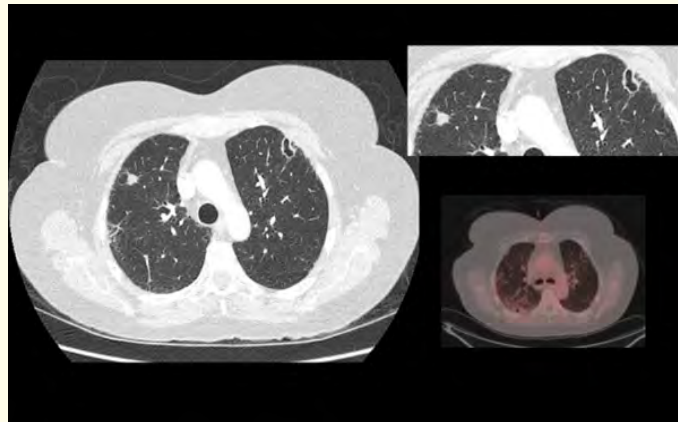


Figure 19: CT and PET/CT on a patient with right upper lobe ground glass nodule and a cavitating left upper lobe rheumatoid nodule, which are not PET/CT avid.

Sjögren disease associated GGO

Ito I, *et al.* retrospectively reviewed lung manifestations 33 cases of primary Sjogren's syndrome (31 surgical lung biopsies and two autopsies) with emphases on the clinical, radiologic, and pathologic manifestations of the disease. The clinicopathologic pulmonary manifestations associated with primary Sjogren's syndrome have yet to be reviewed in an extensive series, none-the-less nonspecific interstitial pneumonia (NSIP) as a distinct and commonest histologic pattern. Among the diverse imaging findings, the authors found NSIP was the most prevalent histologic pattern and had a favorable prognosis [31].

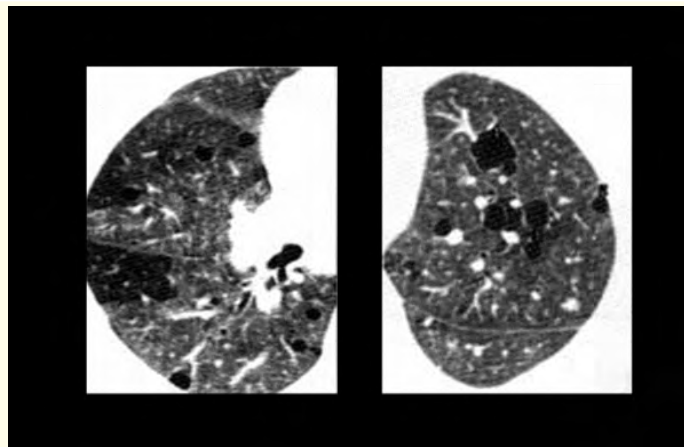


Figure 20: A male patient known to have Sjögren disease shows GGO and multiple lung cysts on HRCT.

Collagen vascular disease associated GGO

Collagen vascular disease (CVD) is a systemic autoimmune pathology. Any organ can be affected, but the intra-thoracic manifestation is frequent. The intrathoracic manifestations are dependent on the type of CVD. One or more of the following of the intra-thoracic components can be involved: the lung parenchyma, the airways, pulmonary vessels, the pericardium, and the pleura. Diffuse interstitial pneumonia and pulmonary hypertension are common and remain the most significant cause of morbidity and mortality in patients with CVD. Therapy and increased susceptibility to infection also contribute to morbidity and mortality. The use of HRCT of the lungs is the most efficient way to characterize the intrathoracic manifestations of CVD and its differential diagnosis [32].

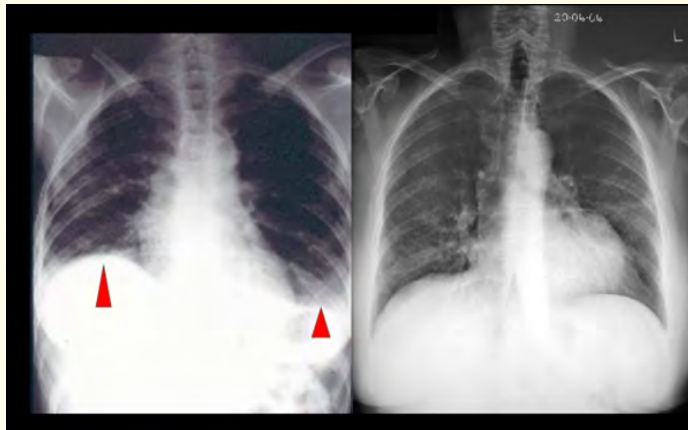


Figure 21: AP and PA CXRs on a patient with known SLE shows GGO at the lung bases, associated with basal pleural effusion (arrow heads).



Figure 22: Axial HRCT scans on a patient with known SLE shows air space shadowing, air-bronchogram, traction bronchiectasis and GGO.



Figure 23: Axial HRCT scan on a patient with known SLE shows GGO, interstitial shadowing and traction bronchiectasis.



Figure 24: Wegner's granulomatosis may present as fleeting opacities/GGOs, appearing in different segments/lobes of the lung.

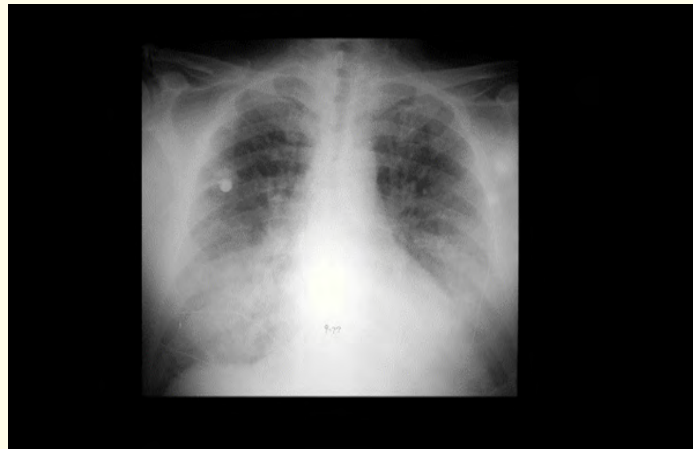


Figure 25: Wegner's granulomatosis may also present as extensive air space shadowing by the CXR.



Figure 26: Wegner's granulomatosis may present as fleeting opacities/GGOs, appearing in different segments/lobes of the lung. Note the cavitating nodules.



Figure 27: Wegner's granulomatosis may present as fleeting opacities/GGOs, appearing in different segments/lobes of the lung associated with a biopsy proved left maxillary antrum Wegner's granuloma.

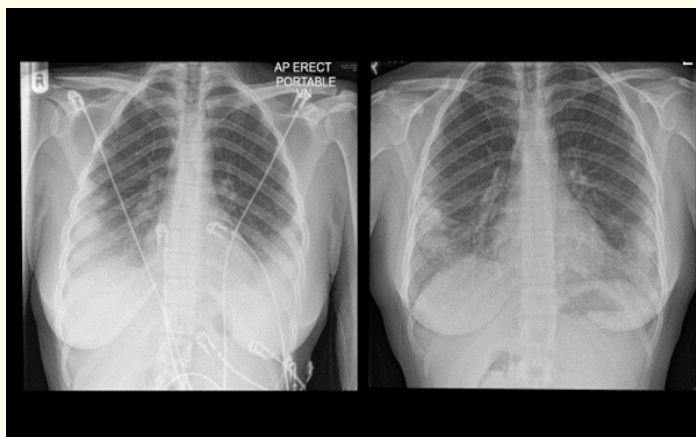


Figure 28: AP and PA CXRs on the same patient shows GGO at the lung bases and the subpleural spaces in a patient with mixed connective tissue disease.

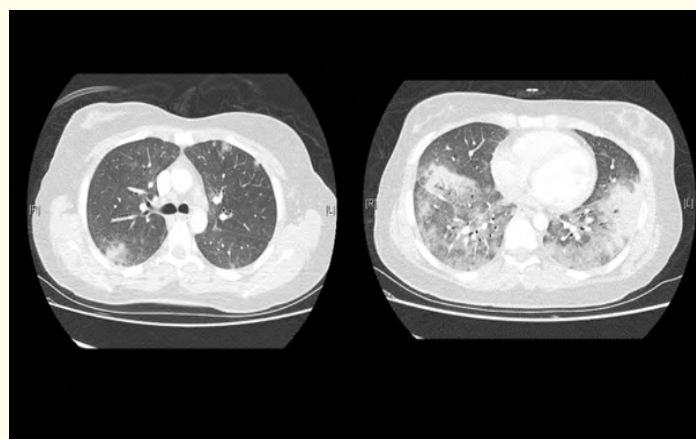


Figure 29: Axial HRCT scans show GGO in Mixed connective tissue disease. The patches of GGO have a peripheral and subpleural distribution. Note the air-bronchogram, traction bronchiectasis, extensive GGO and denser areas of lung consolidation.

Progressive systemic sclerosis associated GGO

Pulmonary manifestations of Progressive Systemic Sclerosis (PSS) include interstitial fibrosis, esophageal dilatation/reflux/aspiration pneumonia, and pulmonary hypertension. PSS patients are more prone to lung infections. Less commonly imaging reveals mediastinal lymphadenopathy, pleural thickening, pleural and pericardial effusions and diffuse alveolar hemorrhage [33]. PSS is associated with skin inflammation, fibrosis, and vascular changes, most pronounced in the fingers, toes, and the nose and around the mouth. There is variable visceral organ involvement including the esophagus, bowel, and the kidneys, but Vasculitis can affect any organ. PSS is classed into 3 subgroups [34]. (1) Classical PSS; (2) CREST syndrome; and (3) Overlap syndromes in which PSS coexists with another connective tissue disease such as rheumatoid arthritis, SLE, or Polymyositis/Dermatomyositis.

Pulmonary involvement has been reported in 74% - 95% in autopsy series in PSS. PSS is a significant cause of morbidity and mortality, with shortness of breath described in a third of the patients [35]. CREST is associated with less common lung findings [36,37].

Pulmonary manifestations of PSS include interstitial fibrosis, esophageal dilatation/reflux/aspiration pneumonia, and pulmonary hypertension. PSS patients are more prone to lung infections. Less commonly imaging reveals mediastinal lymphadenopathy, pleural thickening, pleural and pericardial effusions and diffuse alveolar hemorrhage [33,37-41].

Interstitial fibrosis occurs in 20% - 65% patients with PSS [33,35,38].

Restrictive pulmonary function tests with a decreased diffusing capacity may precede clinical or radiographic changes [33,37].

A CXR show changes of Cryptogenic Fibrosing alveolitis in 65% patients that progress from fine to coarse reticular opacities and honeycombing shadowing [35,38]. Lung cysts may cause a spontaneous pneumothorax [33].

HRCT abnormalities are seen in 60% - 91% of patients [35,37,39]. The signs are those of Cryptogenic Fibrosing alveolitis. Consolidation or masses associated with PSS are uncommon [37].

Pulmonary hypertension is usually secondary to interstitial fibrosis lung disease and occurs in 50% of patients with CREST and 33% of patients with classical PSS at angiography. Chest radiography is less sensitive but is very specific, with enlargement of the main pulmonary arteries and cardiomegaly [42].



Figure 30: A CXR and hand radiographs shows features of systemic sclerosis: The CXR show opacification, GGO and cystic changes at the lung bases and the hand radiographs show loss of the tips of the terminal phalanges due to vasculitis.

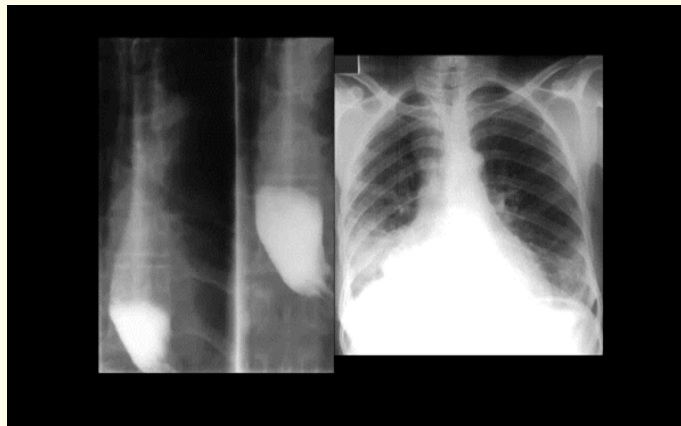


Figure 31: Pulmonary manifestations of PSS include interstitial fibrosis, esophageal dilatation/reflux/aspiration pneumonia, and pulmonary hypertension. PSS patients are more prone to lung infections. Less commonly imaging reveals mediastinal lymphadenopathy, pleural thickening, pleural and pericardial effusions and diffuse alveolar hemorrhage.

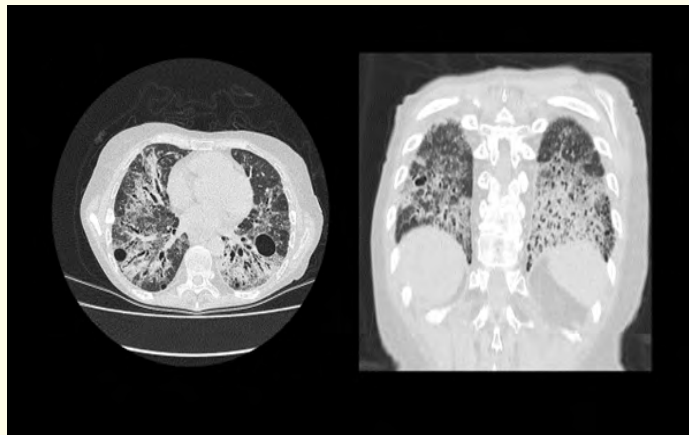


Figure 32: Axial and coronal CT scans on the same patient as in the previous radiographs, showing basal lung fibrosis, cysts, bronchial wall thickening, traction bronchiectasis and GGO. Also, note the pericardial and pleural effusions.

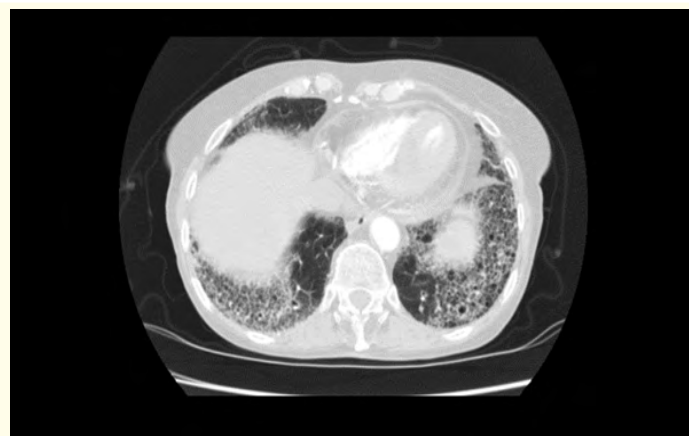


Figure 33: Axial and coronal CT scans on the same patient as in the previous radiographs, showing basal lung fibrosis, cysts, bronchial wall thickening, traction bronchiectasis and GGO. Also, note the pericardial and pleural effusions.

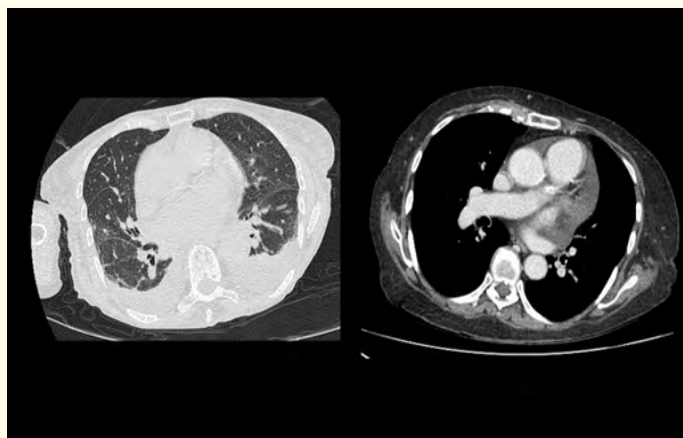


Figure 34: Axial and coronal CT scans on the same patient as in the previous radiographs, showing basal lung fibrosis, cysts, bronchial wall thickening, traction bronchiectasis and GGO. Also, note the pericardial and pleural effusions.



Figure 35: A CXR on a 39-year-old man with known systemic sclerosis that presented with increasing shortness of breath show a normal sized heart with blunting of the left costophrenic angle suggestive of a pleural effusion. The axial CT scan through the heart of the same patient on the same day shows a much larger pleural effusion and a pericardial effusion not depicted on the CXR.

Neurofibromatosis-associated diffuse lung associated GGO

The exact prevalence of neurofibromatosis-associated diffuse lung disease remains unclear, most early studies based on standard CXR with little or no tissue diagnosis. Trisolini R and Associates report on the clinical, functional and HRCT findings in a patient with neurofibromatosis-associated diffuse lung disease and provide a short literature review [43].

Zamora AC and associates retrospectively studied 55 adult patients with a view to defining diffuse lung disease in patients with neurofibromatosis. The medical records including CXRs and HRCT were reviewed. Most of the patients had dyspnea. 16 of the patients gave a history of smoking, 12 patients never smoked. Thirty-seven percent showed GGO on HRCT; half the patients revealed bibasilar reticular opacities and, bullae, cysts, and emphysema changes were seen in a quarter of the patients; no honeycombing was recorded. A group of 14 patients had tissue diagnosis, and all showed interstitial fibrosis and inflammatory interstitial changes were seen in 93%. The authors found that neurofibromatosis with diffuse lung disease is a definable clinical entity, characterized by upper lobe cystic and bullous disease and lower lobe.

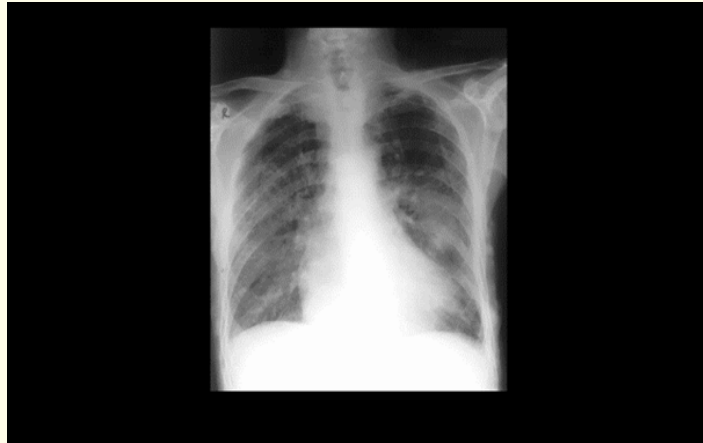


Figure 36: A CXR shows GGO and pulmonary fibrosis in a patient with Neurofibromatosis 1.

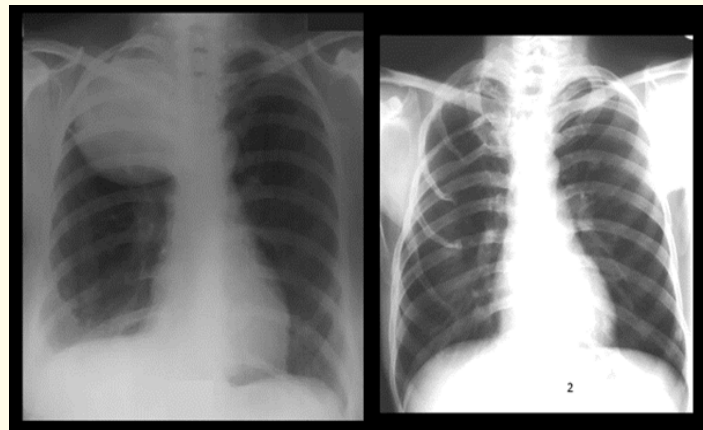


Figure 37: Neurofibromas vary in size and may mimic other benign and malignant tumors. The CXR shows a well-defined mass in the right apical region confirmed neurofibroma on a percutaneous needle biopsy. Note the rib anomaly at the right costophrenic angle. Figure 2 show a CXR on another patient with ribbon ribs characteristic of NF1. Such rib anomalies, when found, may be an indication for HRCT in appropriate clinical setting.

Lung infections associated GGO

Infective Causes of Pneumonia			
bacteria		bacteria	
Localized to the lungs		as part of systemic disease	
Actinomycetes	Fungi	protozoa	
Viruses	Mycoplasma	Chlamydia	Rickettsias
Non-infective Causes of Pneumonia			
Chemicals	Radiation	Allergy	

Table 1 [45]

A large variety of lung infections can present with multifocal consolidations and GGO [45]. Hewitt MG and associates analyzed the causes of widespread GGO in an unselected, consecutive patient population to identify any associated imaging findings that can narrow the differential diagnosis or reorganize the cause. The study group consisted of 234 patients with 124 women and 110 men and a mean age of 53.7 years. The authors established that the most common cause of GGO was hydrostatic pulmonary edema (87.2%). Interstitial lung diseases were the next common cause, most often hypersensitivity pneumonitis, infection accounting for 5%. Technical and radiographic factors such as a poor inspiratory effort accounted for widespread GGO as the next common cause. The authors established a dramatic shift in the relative frequency of the GGO with a change in the clinical setting. Diffuse alveolar disease and widespread lung infection accounted for all of the known diagnoses in an in-patient setting. Interstitial lung disease accounted for 49% in an outpatient setting. When dealing with the immune compromised patients, hydrostatic pulmonary edema was still the most common cause (46%) with diffuse infection (24%) the next most likely diagnosis. The most frequent cause of GGO in patients with bone marrow suppression was an opportunistic viral infection (80%) [45].

Franquet T and associates reviewed the HRCT findings in a hematopoietic stem cell transplant recipients that had human metapneumovirus pneumonia. The authors concluded that the HRCT manifestations of metapneumovirus usually consist of a mixture of patterns, including, most commonly, GGO and nodular opacities [46].

Voloudaki A and associates retrospectively reviewed the radiographic and CT features of acute Q fever pneumonia (QFP). Twelve patients were chosen based the availability of chest CT. The typical features of QFP included multilobar consolidation (MFC), a nodular pattern accompanied by a halo of GGO associated with a vessel connection. In the series above, one patient with MFC, nodular lesions with a vascular connection and a halo of GGO, was suggestive of an angioinvasive pathology. The CT scan on another patient with acute *Coxiella burnetii* infection who abused alcohol revealed necrotizing pneumonia, in the setting of impaired immunity [47].

Pseudomonas aeruginosa is a common lung infection in HIV patients. Traill ZC and associates retrospectively reviewed the chest radiographic appearances of 29 adult HIV patients infected with *Pseudomonas aeruginosa*. The most common radiographic abnormality seen was a diffuse reticular pattern followed by a reticulonodular shadowing. Cavitation and GGO were rare. The authors came to the conclusion that although the radiographic appearances of *Pseudomonas* bronchopulmonary infection in HIV-infected patients are non-specific, an interstitial infiltrate is a common finding. The authors recommend that *Pseudomonas aeruginosa* infection should be considered along with the commoner pathogen *Pneumocystis carinii* in the differential diagnosis of an interstitial infiltrate in this group of patients [48].

In the 19th century, Sir William Osler described pneumonia as ‘the old man’s friend’ because this infection of the lungs was often the final illness which swiftly laid to rest those who were suffering from the ravages of age [49].

The most common causes of lobar pneumonia include *Streptococcus pneumoniae* also called *Pneumococcus*, *Mycoplasma*, Gram-negative organisms and *Legionella*, *Haemophilus influenzae* and *Moraxella catarrhalis*, *Mycobacterium tuberculosis* [50].

Round Pneumonia in an adult is commonly caused by a *Streptococcus*. Round pneumonia is rounded in shape, and while they are well-circumscribed lung parenchymal opacities, they tend to have irregular margins. They are most commonly located in the superior segments of lower lobes; the majority (98%), are solitary. Air bronchograms are often present, and helpful in arriving at a diagnosis, but seen only in 17% round pneumonia in adults. Round pneumonia in children tends to be solitary and occur at a mean age of 5 years. Commonly located in the superior segment of the lower lobes and are often misdiagnosed [51-53].

Primary pulmonary tuberculosis is seen in patients not previously exposed to *Mycobacterium tuberculosis*. It is most common in infants and children and has the highest prevalence in children under 5 years of age, but may occur in adults. The radiological manifestation includes lung parenchymal consolidation in any part of the lung, but there is a predilection sub-pleural space of the lower and middle lobes, particularly in adults. There is associated hilar/mediastinal lymphadenopathy, usually unilateral, pleural effusion and may be complicated by miliary TB. In approximately two-thirds of cases, the parenchymal focus resolves without sequelae on a routine CXR. However, a calcified scar persists called Ghon Focus in 15%, and 10% of patients may develop calcified tuberculomas [54].

Post-primary TB (reactivation TB/secondary tuberculosis TB) occurs in patients 1 - 2 years following primary TB. Post-primary TB usually affects the lung apices in patients with decreased immune status. Radiologically Post-primary TB appears as patchy consolidation, cavitation usually within consolidation, fibro proliferative disease with coarse reticulonodular densities. Endobronchial spread leads to a ‘tree-in-bud’ appearance, on HRCT. Eventual healing leads to loss of lung volume and traction bronchiectasis. Lymphadenopathy is rare and occurs in 5% patients. Pleural effusion, pleural thickening, and pleural calcification has been reported in 18% patients. Extension to the chest wall is rare and cause bone and/or cartilage destruction and fistula formation. CXR and axial CT show consolidation left upper lobe associated with an air-bronchogram due to post-primary pulmonary tuberculous pneumonia [54,55].

Atypical mycobacteria as *Mycobacterium malmoense*, which are Gram-positive, non-motile, acid-fast and coccoid to short rods, can be indistinguishable from *Mycobacterium tuberculosis* on imaging [56,57].

The overall prevalence pulmonary nontuberculous mycobacteria (PNTM) is increasing, worldwide. The accepted mode of transmission remains an inhalation from the environment, with recent reports of person-to-person transmission. PNTM predominantly develops in immunocompetent patients. In order of frequency, PNTB infections include *Mycobacterium avium*, *Mycobacterium abscesses*, *Mycobacterium chelonae*, and *Mycobacterium fortuitum* [56,57].

Immune suppression, whatever the etiology increase the risk of nontuberculous mycobacterial disease. Extrapulmonary NTM disease, including disseminated, skin, and catheter-related disease, is more common in immunosuppressed than immunocompetent patients [56,57].



Figure 38: GGO in bronchiectasis: 31-y-o-f presented with weight loss, was unwell and had been coughing for several weeks. The scanogram and axial CT show consolidation in the superior segment of the right lower lobe.

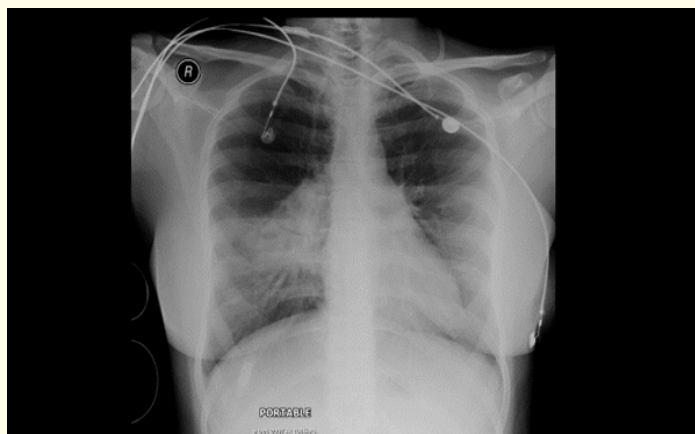


Figure 39: GGO in bronchiectasis: 31-y-o-f presented with weight loss, was unwell and had been coughing for several weeks. The AP portable radiograph show consolidation in the right lower lobe associated with an air-bronchogram and GGO.

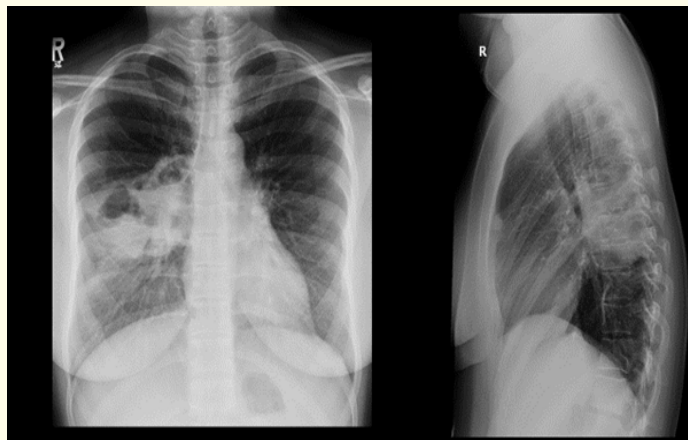


Figure 40: GGO in bronchiectasis: 31-y-o-f presented with weight loss, was unwell and had been coughing for several weeks. A PA and right lateral radiograph show consolidation and cavitation in the superior segment of the right lower lobe.

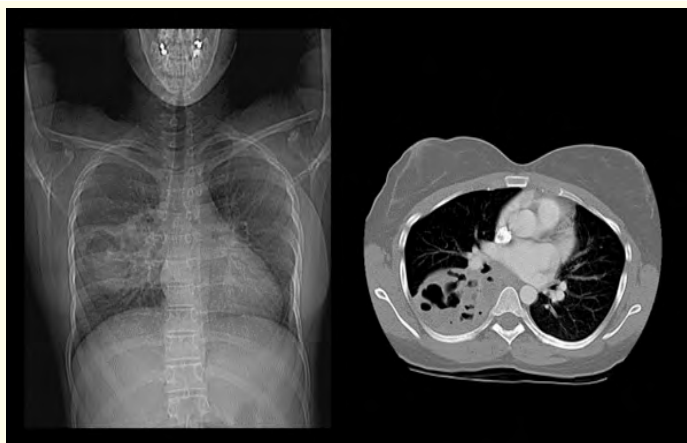


Figure 41: GGO in bronchiectasis: 31-y-o-f presented with weight loss, was unwell and had been coughing for several weeks. A scanogram and axial CT show cavitation and GGO in the apical segment of the right lower lobe.



Figure 42: GGO in bronchiectasis: 31-y-o-f presented with weight loss, was unwell and had been coughing for several weeks. A scanogram and axial CT show cavitation and GGO in the apical segment of the right lower lobe.

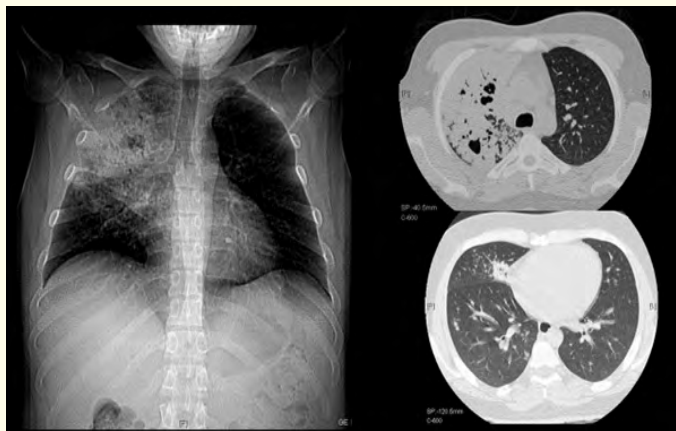


Figure 43: A CXR and axial CT scan of a patient with Pneumonia with an Air-bronchogram with underlying bronchiectasis.

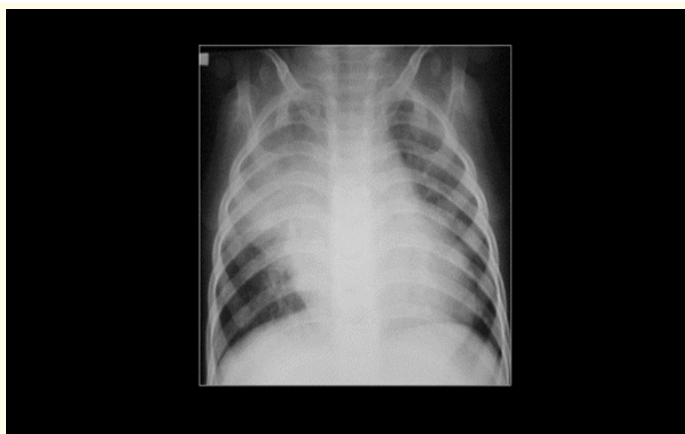


Figure 44: An AP CXR showing lobar consolidation the right upper lobe, due to Pneumococcal pneumonia with supporting laboratory evidence.



Figure 45: A CXR show lobar consolidation in the right lobe due to Mycoplasma pneumoniae. The slide on the left show filamentous Mycoplasma pneumoniae cells from the sputum.

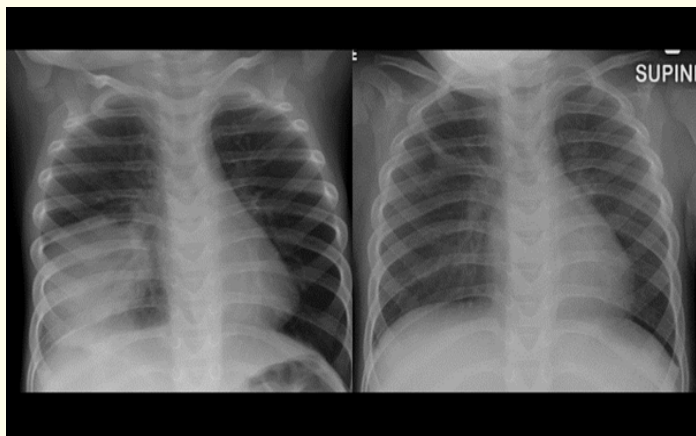


Figure 46: AP chest radiographs on a child with Down's syndrome showing round pneumonia before and following treatment that presented with a cough and fever.

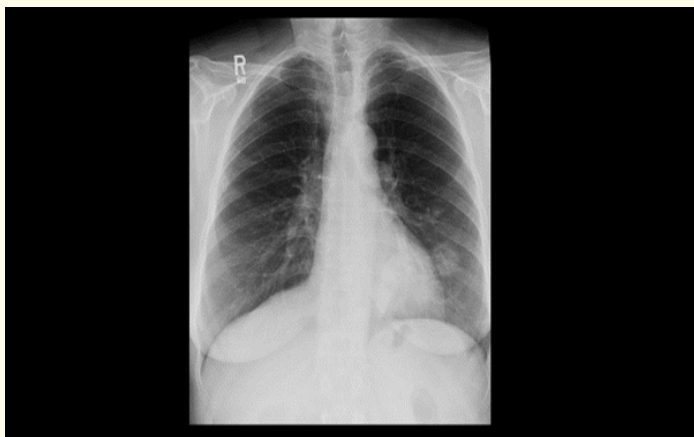


Figure 47: Round pneumonia has a rounded shape, and while this pneumonia is well-circumscribed parenchymal opacities, they tend to have irregular margins.



Figure 48: Staph. Pneumonia: There is consolidation at the left base and with a thick-walled cavity with fluid levels and basal pleural effusion.

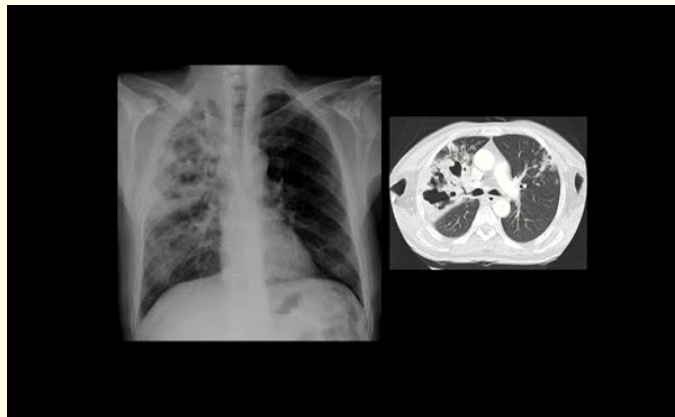


Figure 49: *Staph. Pneumonia: CXR and axial contrast-enhanced axial CT scans multiple cavitating lesions in the right upper and midzone with air-fluid levels and sub-segmental consolidation in the left upper lobe. The patient was immune compromised. Sputum cultures grew Staphylococcal aureus.*

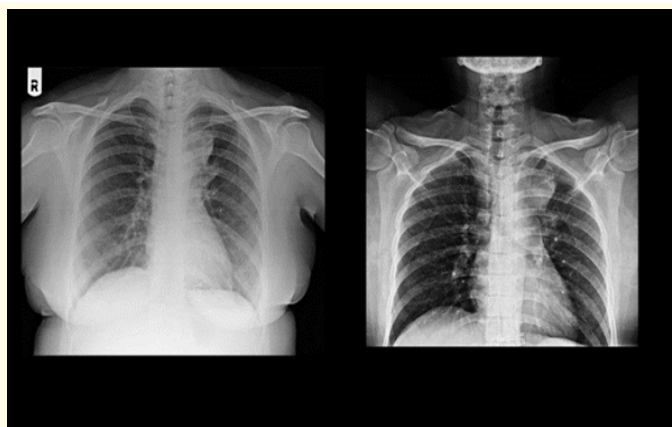


Figure 50: *Series of Chest Radiographs and CT scans showing features of Primary Pulmonary Tuberculosis.*

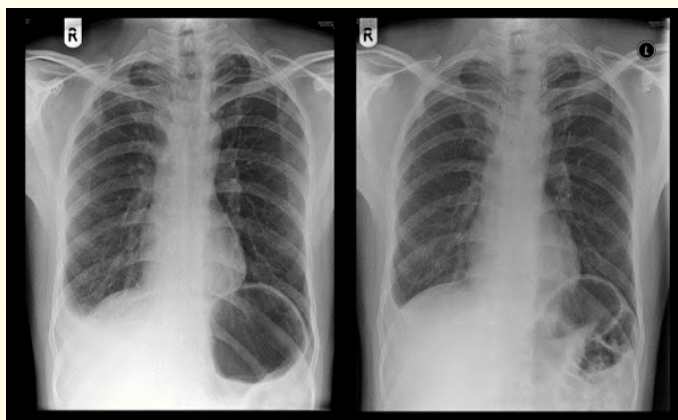


Figure 51: *Series of Chest Radiographs and CT scans showing features of Primary Pulmonary Tuberculosis.*

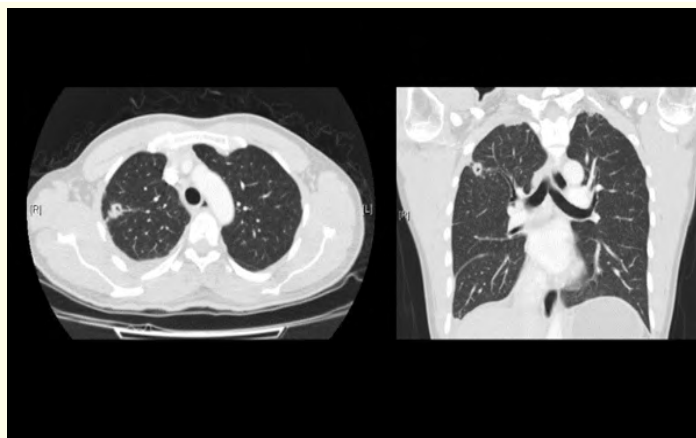


Figure 52: Series of Chest Radiographs and CT scans showing features of Primary Pulmonary Tuberculosis.



Figure 53: Series of Chest Radiographs and CT scans showing features of Primary Pulmonary Tuberculosis.

Primary pulmonary tuberculosis is seen in patients not previously exposed to *Mycobacterium tuberculosis*. It is most common in infants and children and has the highest prevalence in children under 5 years of age, but may occur in adults. The radiological manifestation includes lung parenchymal consolidation in any part of the lung, but there is a predilection sub-pleural space of the lower and middle lobes, particularly in adults. There is associated hilar/mediastinal lymphadenopathy, usually unilateral, pleural effusion and may be complicated by miliary TB. In approximately two-thirds of cases, the parenchymal focus resolves without sequelae on a conventional CXR.

Post-primary TB (reactivation TB/secondary tuberculosis TB) occurs in patients 1 - 2 years following primary TB. Post-primary TB usually affects the lung apices in patients with decreased immune status. Radiologically Post-primary TB appears as patchy consolidation, cavitation usually within consolidation, fibro proliferative disease with coarse reticulonodular densities. Endobronchial spread leads to a 'tree-in-bud' appearance, on HRCT.



Figure 54: Series of Chest Radiographs and CT scans showing features of post-Primary Pulmonary Tuberculosis.

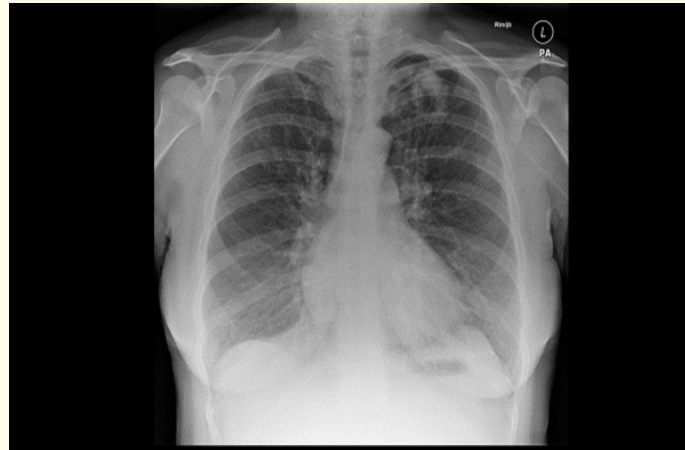


Figure 55: Series of Chest Radiographs and CT scans showing features of post-Primary Pulmonary Tuberculosis.

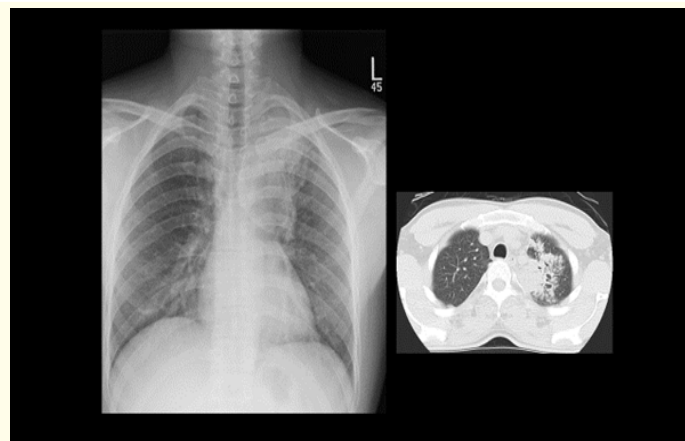


Figure 56: Series of Chest Radiographs and CT scans showing features of post-Primary Pulmonary Tuberculosis.

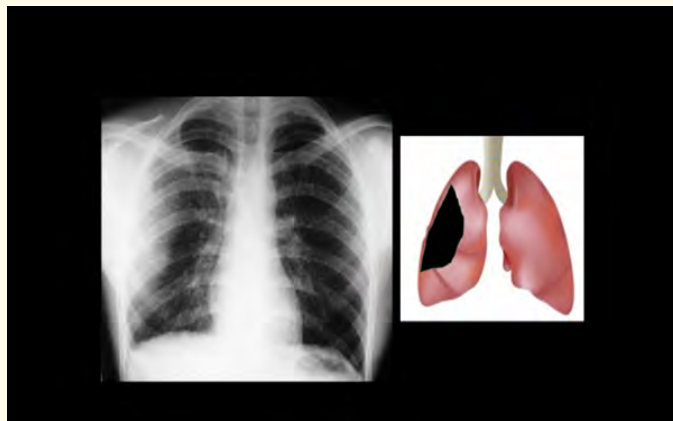


Figure 57: Miliary TB, showing miliary shadowing both lung fields. A right-sided pleural effusions and miliary spread to the brain, shown on CT and MR brain scans. A CXR following treatment shows complete resolution following treatment. The miliary shadowing is more profuse in the sub-pleural region as shown by the line diagram.

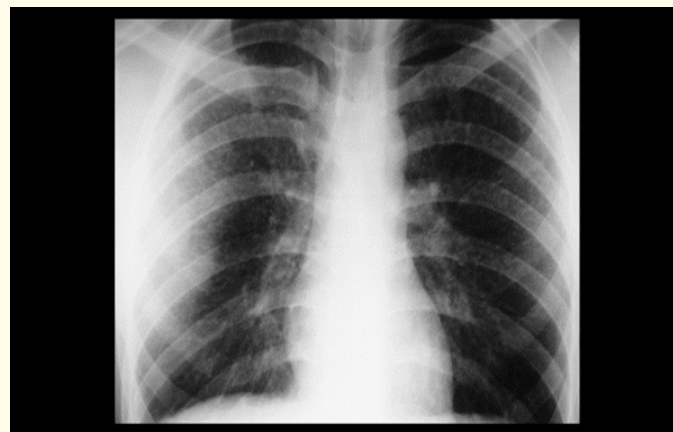


Figure 58: Miliary TB, showing miliary shadowing in both lung fields. A right-sided pleural effusion and miliary spread to the brain, shown on the CT and MR brain scans. A CXR following treatment shows complete resolution following treatment.



Figure 59: Miliary TB, showing miliary shadowing in both lung fields. A right-sided pleural effusion and miliary spread to the brain, shown on the CT and MR brain scans. A CXR following treatment shows complete resolution.



Figure 60: A CXR and coronal reconstruction of CT shows extensive miliary nodules in both the lung fields. The patient presented with neck rigidity and ophthalmoscopy revealed choroidal tubercles.

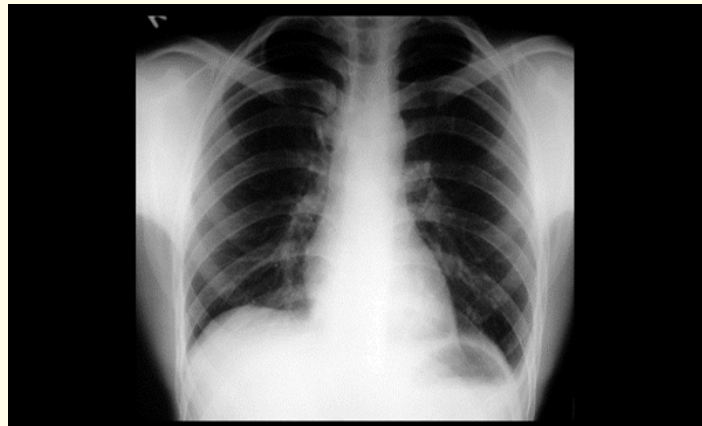


Figure 61: Miliary TB, showing miliary shadowing both the lung fields. A right-sided pleural effusion and miliary spread to the brain, shown on the CT and MR brain scans. A CXR following treatment show complete resolution.

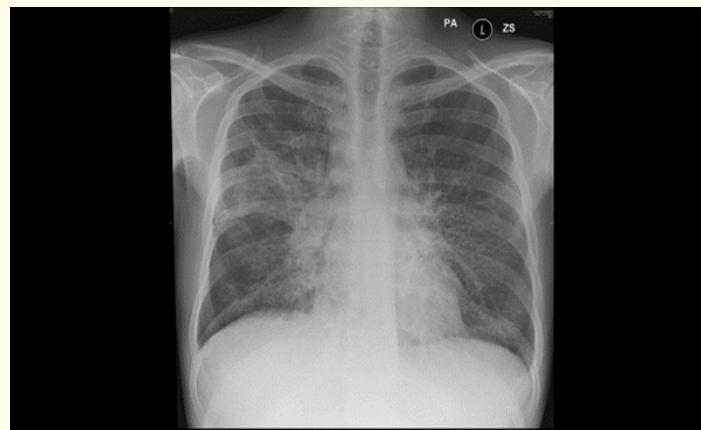


Figure 62: Atypical mycobacteria such as *Mycobacterium malmoeense*, which are Gram-positive, non-motile, acid-fast and coccoid to short rods, can be indistinguishable from *Mycobacterium Tuberculosis* on imaging. Note the consolidation, loss of volume, pleural effusion and GGO.



Figure 63: Atypical mycobacteria such as *Mycobacterium mageritense*, which are Gram-positive, non-motile, acid-fast and coccoid to short rods, can be indistinguishable from *Mycobacterium Tuberculosis* on imaging. Note the consolidation, loss of volume, pleural effusion and GGO.

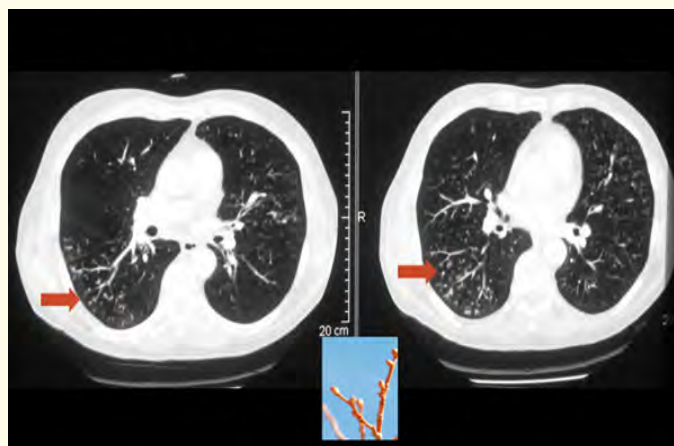


Figure 64: Tree-in-bud sign or pattern describes the CT appearance of multiple areas of centrilobular nodules with a linear branching pattern. Although initially described in patients with endobronchial tuberculosis it is now recognized in some other conditions.

Histoplasmosis associated GGO

Histoplasmosis is caused by the fungus *Histoplasma capsulatum*. Histoplasmosis primarily affects the lungs, with variable symptoms but the systemic disease can occur and can be fatal if untreated. Histoplasmosis is common among AIDS patients because of immune suppression. Immunocompetent individuals that have a history of past infection acquire in partial protection against re-infection. *Histoplasma capsulatum* is found in soil, contaminated by bird and bat droppings. Disturbance of contaminated soil for excavation or construction can release infectious material that when inhaled can cause histoplasmosis [58,59].

Citation: Ali Nawaz Khan., *et al.* "A Pictorial Assay of Ground Opacification of the Lungs". *EC Pulmonology and Respiratory Medicine* 5.2 (2017): 53-134.

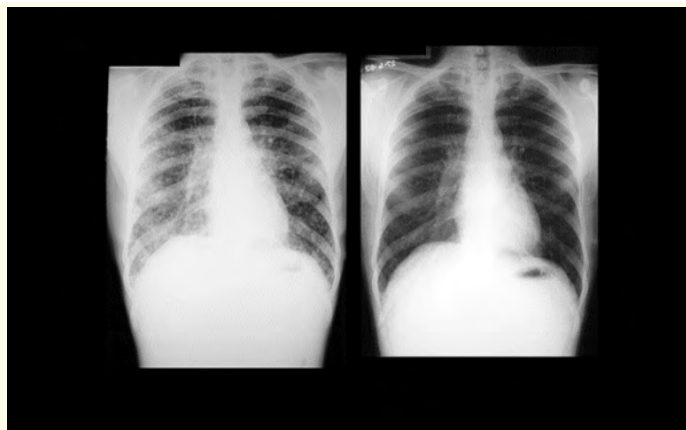


Figure 65: The PA CXR shows miliary type of histoplasmosis before and after treatment. Histoplasmosis is caused by the fungus *Histoplasma capsulatum*.

Pneumocystis pneumonia (PCP) associated GGO

Pneumocystis pneumonia (PCP) is caused by the yeast-like fungus *Pneumocystis jirovecii*. Although PCP is not commonly found in the lungs of healthy people, it is a cause of opportunistic infection in the immune compromised in people with HIV/AIDS, cancer, and patients undergoing chemotherapy. Patients usually present with pyrexia, non-productive cough, dyspnea, weight loss and night sweats. A pneumothorax is a known complication of PCP and may present with an acute chest pain and dyspnea. PCP infection may become systemic and affect other visceral organs such as the spleen, liver, and kidneys.

There is an increased of PCP risk to patients when the CD4 positive T-cell level falls to < 200 cells/ μ L. The diagnosis can be established by characteristic findings on CXR with widespread pulmonary infiltrates, and a low arterial oxygen level.

Gallium 67 scans are a useful adjunct to the diagnosis. The diagnosis can be definitively established by histological identification PCP in the sputum or a broncho-alveolar lavage. Pneumocystis infection can also be diagnosed by immunofluorescent or histochemical staining of the specimen, and molecular analysis of polymerase chain reaction products comparing DNA samples [60-63].



Figure 66: A basal section of a PA CXR shows bilateral basal reticular shadowing in a patient with an HIV secondary to PCP infection. An HRCT through the upper mediastinum show GGO and reticular shadowing in a patient with a PCP post liver transplant.

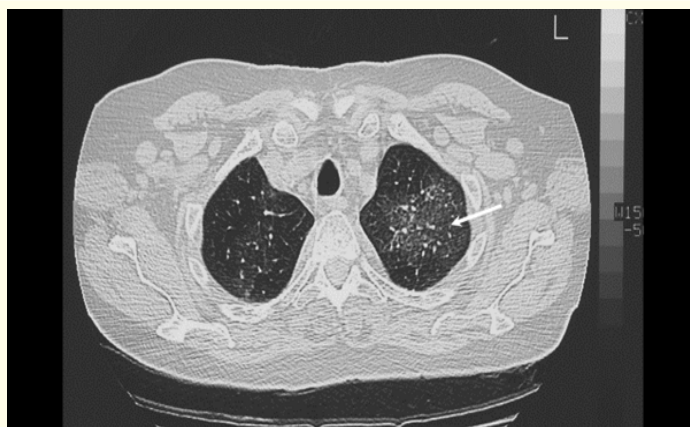


Figure 67: An HRCT on an HIV-positive male patient with PCP shows GGO in the left upper zone.

***Klebsiella pneumoniae*/Friedländer's pneumonia associated GGO**

Klebsiella pneumoniae/Friedländer's pneumonia is caused by a Gram-negative, non-motile, encapsulated, lactose-fermenting, facultative anaerobic, rod-shaped bacterium. The bacterium is found in the normal body flora, but if inhaled can cause inflammatory in the lungs resulting in blood-stained sputum [64]. The bacterium is naturally found in the soil, and about 30% of strains can fix nitrogen in anaerobic conditions [65].

Klebsiella infections affect middle-aged and older men with underlying impaired immunity due to chronic debilitating illness, such as diabetes, alcoholism, malignancy, liver disease, chronic obstructive pulmonary diseases, glucocorticoid therapy, renal failure, and certain occupational dust exposure. Most of these infections are contacted in patients who are in the hospital for some other reason (a nosocomial infection). Feces and contact with contaminated instruments are the most common source of infection. *Klebsiella* pneumonia, which usually affects patients outside the hospital, and is typically seen as bronchopneumonia and bronchitis. There an increased tendency towards developing lung abscess, cavitation, empyema, and pleural adhesions. It has a death rate of about 50%, even with antimicrobial therapy. The mortality rate can be nearly 100% for people with alcoholism and bacteremia [66,67]. The most common condition caused by *Klebsiella* bacteria outside the hospital is pneumonia, typically in the form of bronchopneumonia and also bronchitis. These patients have an increased tendency to develop lung abscess, cavitation, empyema, and pleural adhesions. It has a 50% mortality despite antimicrobial therapy. A mortality rate of a 100% has been reported in patients with a history of alcoholism and bacteremia [66,67].

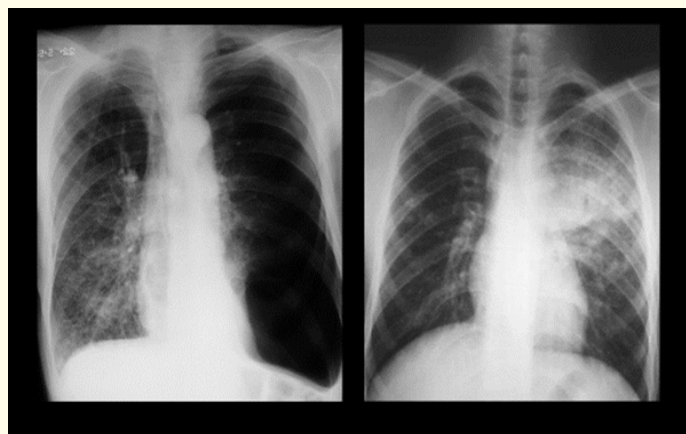


Figure 68: Friedlander's pneumonia associated with emphysema: *Klebsiella pneumoniae* is a Gram-negative, non-motile, encapsulated, lactose-fermenting, facultative anaerobic, rod-shaped bacterium. Widespread consolidation occurs with small areas of translucency. There is an element of collapse at the right lung, indicated by mediastinal shift. A small pleural effusion is present. *Klebsiella pneumoniae* is a Gram-negative, non-motile, encapsulated, lactose-fermenting, facultative anaerobic, rod-shaped bacterium.

Legionnaires’ disease/pneumonia associated GGO

Legionnaires’ disease/pneumonia is caused by the *Legionella* bacteria *Legionella*. Patients present with signs and symptoms of a systemic illness such as a cough, shortness of breath, fever, muscles pains, and headaches. Occasionally nausea, vomiting, and diarrhea may occur. The incubation period is 2 - 10 days. *Legionella* bacteria is found naturally in fresh water, but more importantly can contaminate hot water tanks, hot tubs, and cooling towers of large air conditioners. Legionnaires’ disease/pneumonia is spread by inhaling a mist that contains the bacteria. It can also occur when contaminated water is aspirated. No person to person spread occurs. Risk factors that predispose to *Legionella* infection include older age, smoking, chronic lung disease, and depressed immunity. Any patient with severe pneumonia following recent travel should be tested for *Legionella*. Diagnosis is made by testing for urinary antigen test and sputum culture. The disease is named after the outbreak where it was first identified, the 1976 American Legion convention in Philadelphia. Treatment of Legionnaires’ disease is with antibiotics. Patients are often hospitalized. Mortality in those infected is about 10% [68-75].

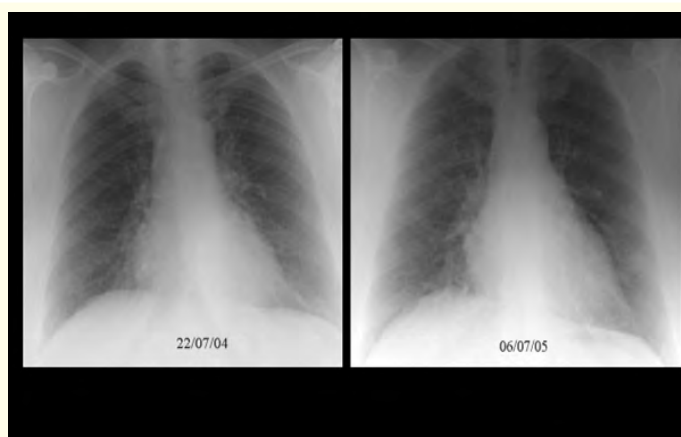


Figure 69: Sequential CXRS on a patient with Legionnaires pneumonia.

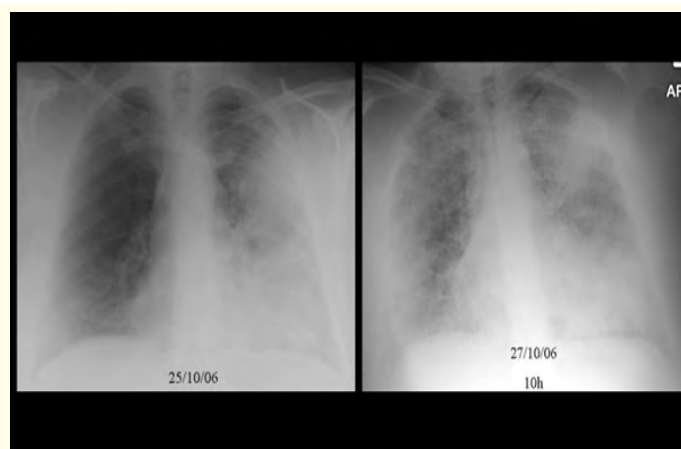


Figure 70: Sequential CXRS on a patient with Legionnaires pneumonia.



Figure 71: Sequential CXRS on a patient with Legionnaires pneumonia.

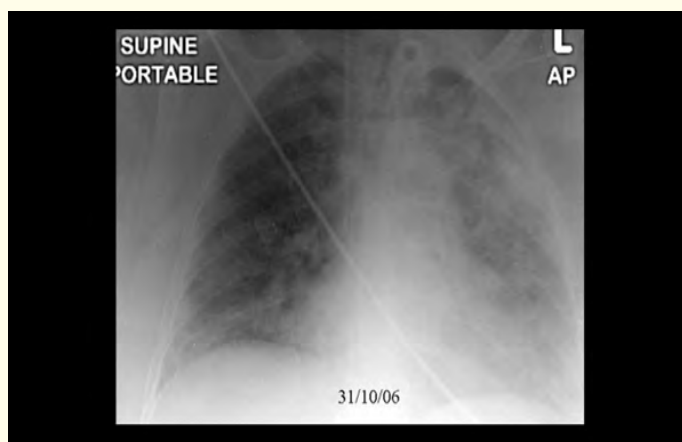


Figure 72: Sequential CXRS on a patient with Legionnaires pneumonia.

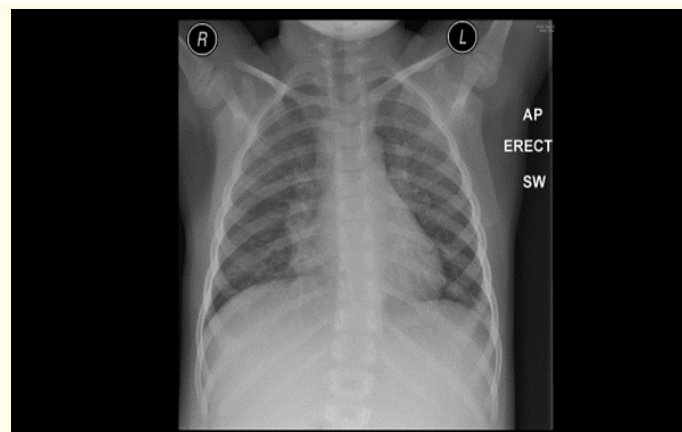


Figure 73: Influenza Virus Pneumonia: Non-segmental, poorly defined areas of opacification are present predominantly in the middle lobe and lingula. A complement fixation test revealed a 4-fold rising titre to influenza A.



Figure 74: Axial CT scans on a patient with *Varicella pneumonia* in an immunosuppressed patient with pancreas and renal transplant that presented with acute pulmonary symptoms. The patient died from the infection and diagnosed on a Post-mortem.

Cavitating lung lesion associated GGO

Pulmonary cavities represent a lung nodule/lung mass/lung consolidation that is gas filled and as such readily seen on a CXR and CT. These cavities are thick walled greater than 2 - 5 mm. The cavity may demonstrate air-fluid level. The Fleischner Society define a pulmonary cavity as a “gas-filled space, seen as a lucency or low-attenuation area, within pulmonary consolidation, mass, or a nodule”. A Cavitating pneumonia can be associated with a severe necrotizing pneumonia. The complication is rare. A variety of organisms can cause cavitation. Cavitation is associated with *Mycobacterium tuberculosis*, *Streptococcus pneumoniae* which other less frequently being *Aspergillus* spp., *Legionella* sp. and *Staphylococcus aureus*. The actual incidence is not known necrotizing pneumonia, but in one study by Pande A., et al. 6.6% of adults with pneumococcal pneumonia. *Klebsiella pneumoniae* is also another organism that is known to cause cavitation. Rare infections that may cavitate include; pulmonary coccidioidomycosis pulmonary actinomycosis/thoracic actinomycosis, pulmonary nocardiosis, melioidosis, pulmonary, cryptococcosis [76-81].

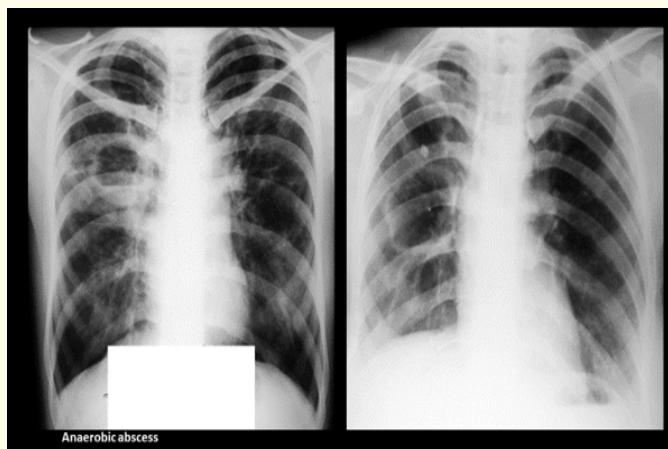


Figure 75: Anaerobic abscess: *Bacteriodes fragilis*: There is a 3cm abscess cavity with fluid level and some patchy surrounding consolidation in the anterior segment of the RUL and the middle lobe; easily be mistaken for a carcinoma. Note the image on the left taken 8 weeks later shows considerable improvement in the wall thickness and the surrounding inflammatory changes.

Bronchiolitis obliterans organizing pneumonia (BOOP) associated GGO

Bronchiolitis obliterans organizing pneumonia (BOOP) is a clinicopathologic syndrome characterized symptomatically by subacute or chronic respiratory illness. Histologically BOOP is marked by the presence of granulation tissue in the bronchiolar lumen, alveolar ducts, and some alveoli, associated with a variable degree of interstitial and airspace infiltration by mononuclear cells and foamy macrophages. All ages can be affected; patients usually present with a dry cough and shortness of breath of 2 weeks to 2 months in duration; symptoms persist despite antibiotic therapy. On imaging, air space consolidation can be indistinguishable from chronic eosinophilic pneumonia (CEP), interstitial pneumonitis (acute, nonspecific and usual interstitial pneumonitis, neoplasm, inflammation, and infection). The definitive diagnosis is achieved by tissue biopsy. Patients with BOOP respond favorably to treatment with steroids [82-90].

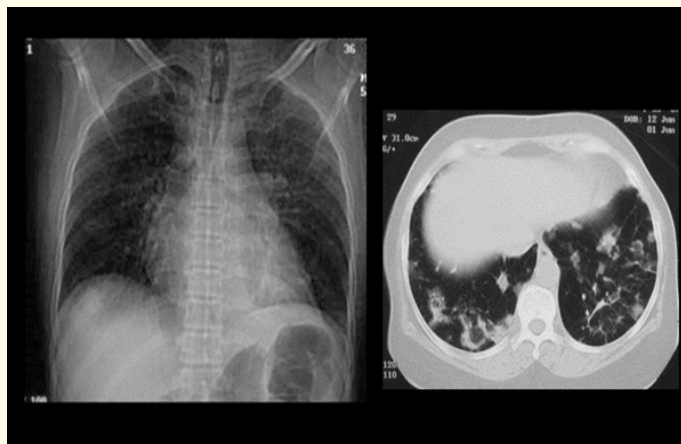


Figure 76: BOOP can present with a variety of lung parenchymal shadowing that includes consolidation, nodules of varying size or shadowing presenting like pneumonia as shown by the digital radiograph and axial CT.

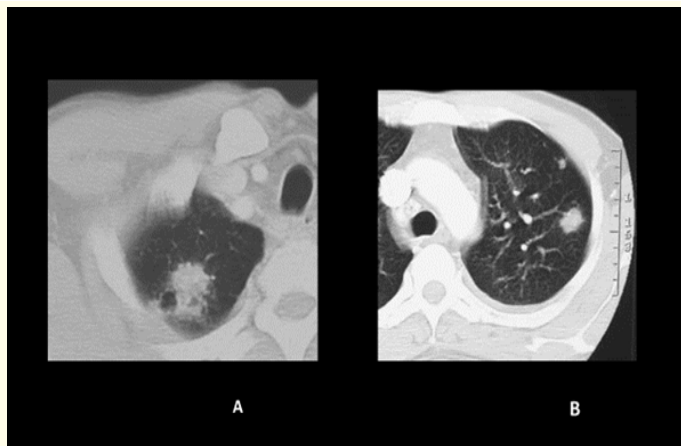


Figure 77: (A) BOOP presenting as a nodule with partial speculation. (B) Peripheral and Central nodules.

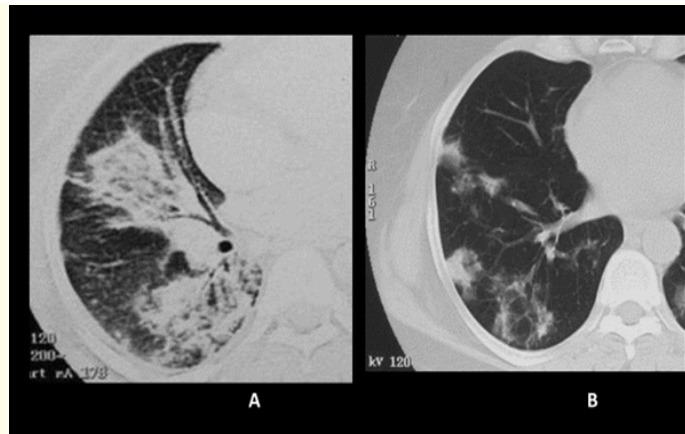


Figure 78: (A) BOOP presenting as airspace and nodular opacities (L) Typical picture of BOOP with peripheral bilateral airspace opacities, predominantly at the bases (R). Note the GGO, micronodules, and air-bronchogram. There are an incidental cardiomegaly and small basal pleural effusions. (B) Multiple bilateral airspace and interstitial patchy opacities.

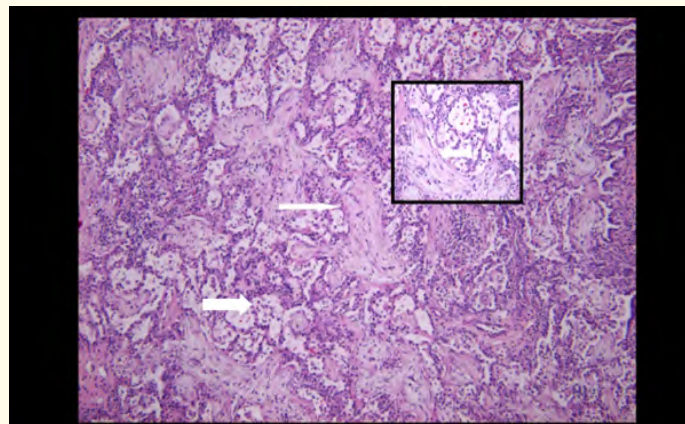


Figure 79: Histopathological slide on a patient with idiopathic BOOP shows [magnification X 10] pale staining areas of elongated branching fibrosis, involving bronchiolar lumen and peribronchial airspaces [solid arrow]. The alveolar septae [inset] show mild chronic inflammation.

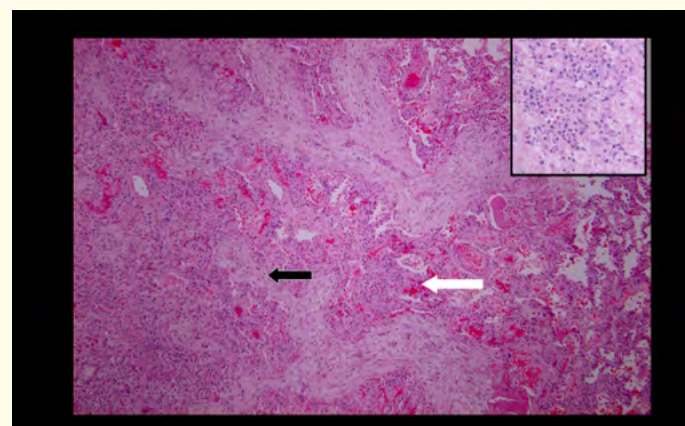


Figure 80: Histopathological slide of a patient of BOOP with associated abscess, the pale, elongated, serpiginous branching fibrous plugs in the alveolar spaces is demonstrated by the solid arrows. The abscessed area is displayed by transparent arrow magnified X 40 in the inset. HandE stain, magnification X 10.

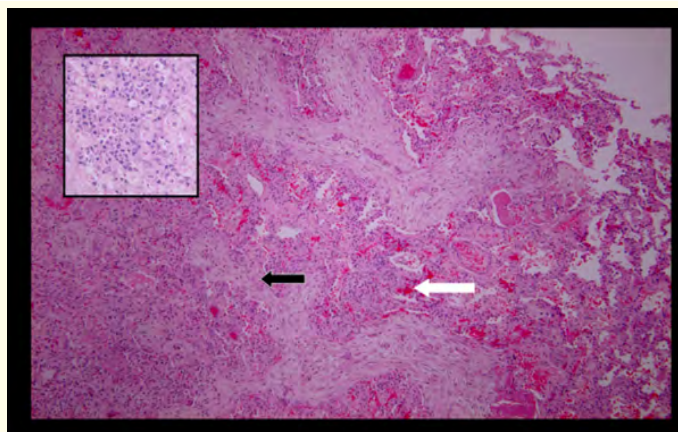


Figure 81: A histopathological slide of a patient with BOP with associated abscess, the pale, elongated, serpiginous branching fibrous plugs in the alveolar spaces is demonstrated by the solid arrow. The abscessed area is displayed by transparent arrow magnified X 40 in the inset. HandE stain, magnification X 10.

Invasive pulmonary aspergillosis associated GGO

Pulmonary aspergillosis is a spectrum of mycotic diseases caused by *Aspergillus* species, usually *Aspergillus fumigatus*. This intensely antigenic and ubiquitous soil fungus is commonly found in the sputum of healthy individuals. However, in susceptible hosts, its ability to invade the arteries and veins facilitates its hematogenous spread.

The development of disease and its histologic, clinical, and radiologic manifestations depend on the virulence and number of spores inhaled and, more importantly, on the patient’s immune status. Pulmonary aspergillosis may take any of 4 forms: (1) Allergic bronchopulmonary aspergillosis (ABPA) is caused by a hypersensitivity reaction to the fungus and most commonly occurs in those with asthma. (2) Saprophytic aspergillosis, or aspergilloma, is the most common form. This form is non-invasive and involves colonization of pre-existing cavities. (3) Chronic necrotizing aspergillosis, also called airway-invasive or semi-invasive aspergillosis, is a chronic cavitary pneumonic illness that often affect patients with pre-existing chronic lung disease. (4). Angioinvasive aspergillosis affects immunocompromised patients and is often fatal [91-94].

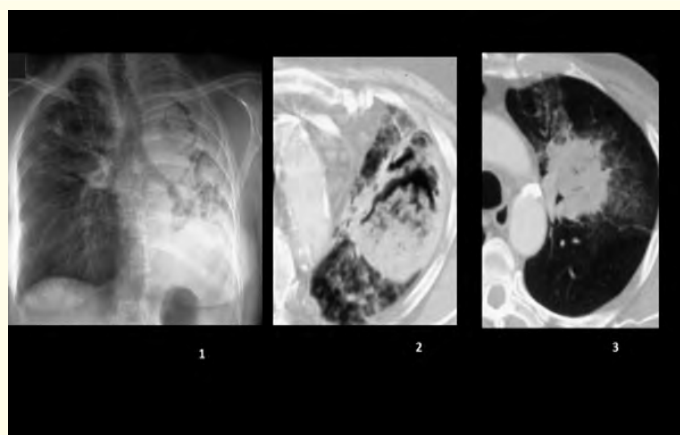


Figure 82: Images showing (1) saprophytic aspergilloma (2) saprophytic aspergilloma and (3) invasive aspergilloma, See next image for bacteriological/histological slides.

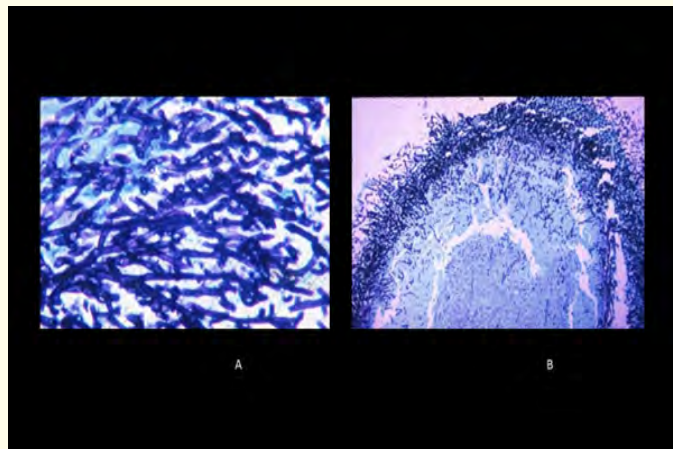


Figure 83: Invasive pulmonary aspergillosis: Microscopic features of *A. fumigatus*. (A) High-power photomicrograph demonstrates conidiophores with the characteristic head appearance and minute spores. (B) The Slide shows lung tissue in invasive aspergillosis. Microscopic slide of lung tissue shows broad hyphae, which branch at acute angles. Section of a blood vessel shows branching fungal hyphae that invade the vessel wall.

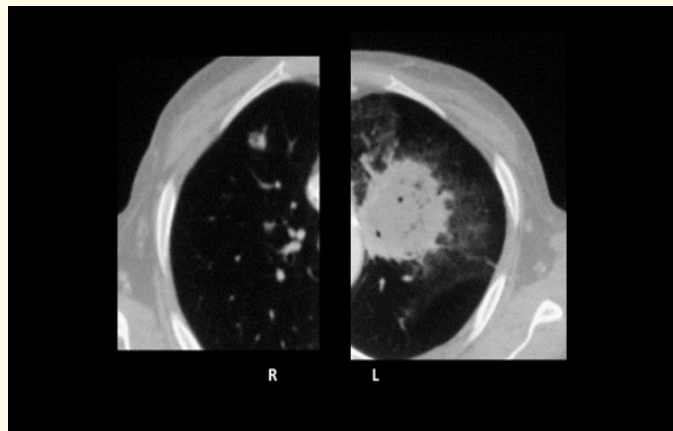


Figure 84: Axial CT scans show features of invasive aspergilloma; R- small cavitating nodule L-hilar mass with whiskery margins and associated surrounding GGO.

Aspiration pneumonia associated GGO

Aspiration pneumonia of foreign material into the bronchial tree usually oral or gastric contents is a cause of bronchopneumonia. Depending on the PH of the aspirate a chemical pneumonitis can develop, and bacteria add to the lung inflammation. There are many predisposing causes [95-97].

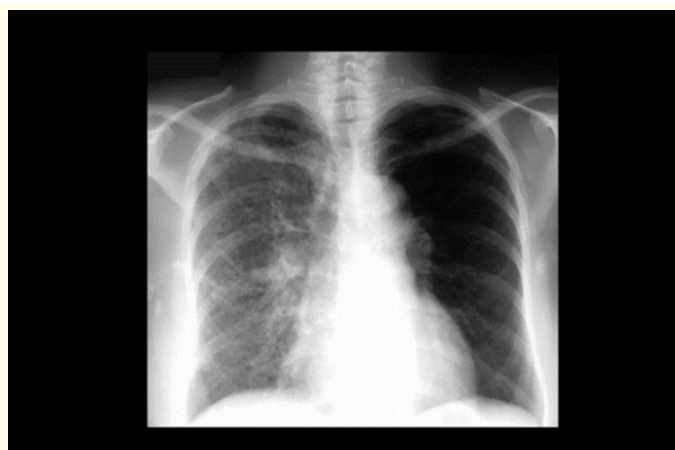


Figure 85: CXR shows a right-sided opacification and GGO due to aspiration pneumonia. The patient was found unconscious on the floor at home.



Figure 86: A CXR on a patient with swallowing difficulty presented with shortness of breath, fever, and leucocytosis due to aspiration pneumonia. Note the lung basal opacification/GGO.



Figure 87: A CXR and axial CT scan through the lower esophagus in a patient with aspiration pneumonia, showing GGO, note the thickened lower esophagus/gastro-esophageal junction and the open lower esophagus due to gastroesophageal reflux.

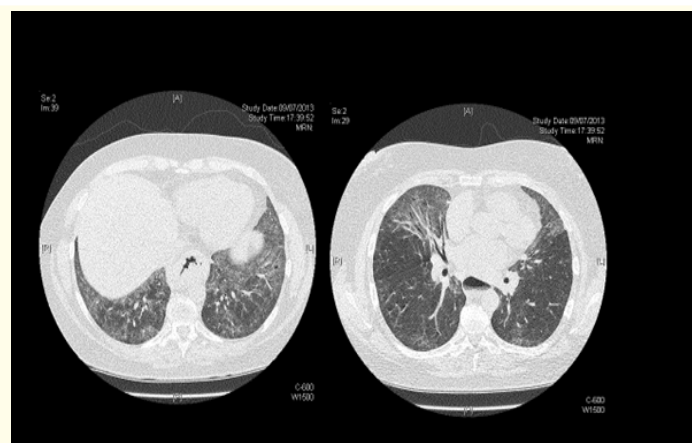


Figure 88: Axial CT scans through the lower esophagus in a patient with aspiration pneumonia, showing GGO, note the thickened lower esophagus/gastro-esophageal junction and the open lower esophagus due to gastroesophageal reflux.

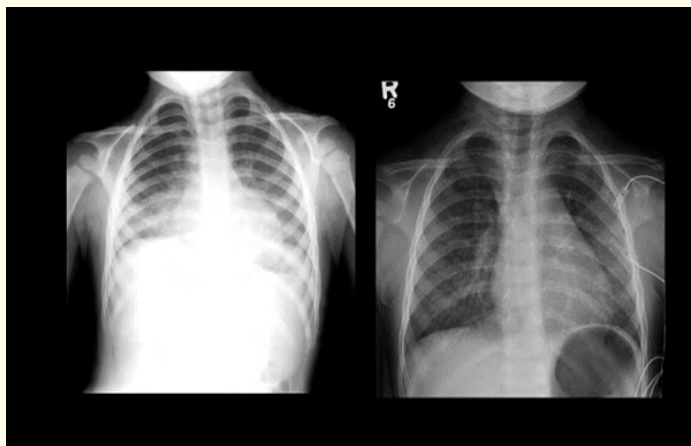


Figure 89: Chest Radiographs on two separate children showing aspiration pneumonia due to paraffin aspiration.

Pulmonary edema associated GGO

Interstitial edema results from a fluid collection in the lung interstitial space and usually develops when the pulmonary venous pressure rises to 25-30 mm Hg. Alveolar pulmonary edema develops when the pulmonary venous pressure exceeds 30 mm Hg [98,99].

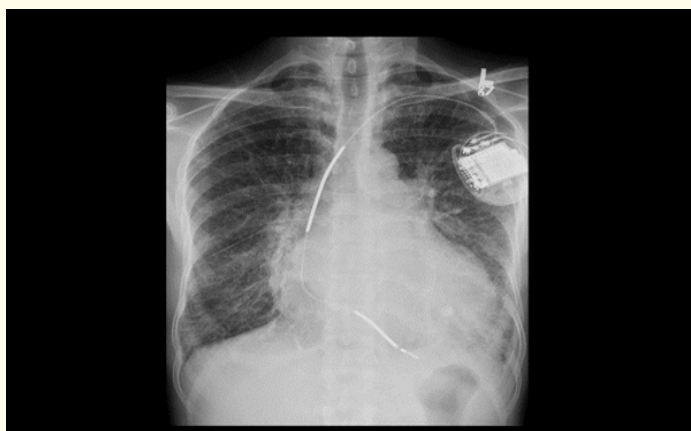


Figure 90: A CXR shows interstitial pulmonary edema. Note the cardiomegaly and the septal lines.



Figure 91: CXR and HRCT show interstitial pulmonary edema with a Honeycomb lung pattern.

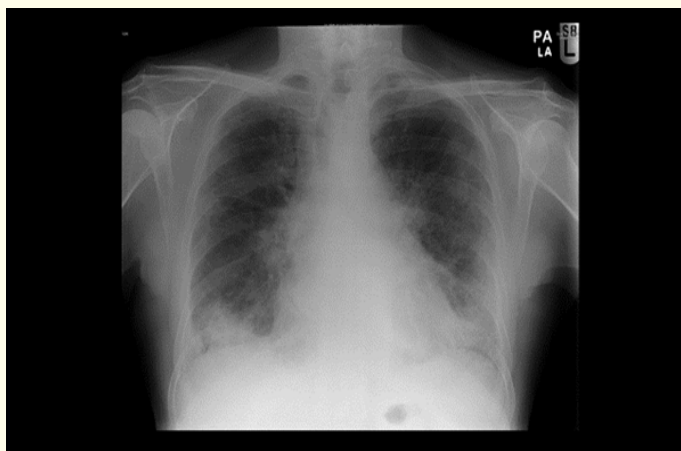


Figure 92: A CXR shows GGO and interstitial shadowing in a patient with congestive heart failure.



Figure 93: An Axial HRCT scan shows interstitial shadowing associated with reticular shadowing, cysts and GGO in a patient with congestive cardiac failure.

Bat wing pulmonary edema associated GGO

Batwing pulmonary opacities: Has been classically described in association with pulmonary edema; classically seen on a CXR, but the appearance is also seen on a CT scan. Similar shadowing can occur with pneumonia, inhalation injury, pulmonary alveolar proteinosis, pulmonary hemorrhage and lymphoma/leukemia and bronchoalveolar carcinoma [100-103].



Figure 94: A CXR shows perihilar shadowing due to a combination of alveolar and interstitial pulmonary (Batwing pulmonary edema).

Cardiogenic pulmonary edema associated GGO

Cardiogenic unilateral pulmonary edema (UPE) is a rare entity, and represents 2.1% of UPE and frequently misdiagnosed on initial imaging. UPE usually appears as opacification of the right lung and is always associated with severe mitral regurgitation. UPE is an independent risk factor for mortality and morbidity, and prompt recognition is necessary to avoid a delayed diagnosis and treatment. It is postulated that the regurgitation jet is directed towards the right superior pulmonary vein, which preferentially increase the hydrostatic pressure in the right upper lobe. Besides, mitral regurgitation UPE is associated with re-expansion pulmonary edema, pulmonary vein occlusion and a right to left pulmonary shunt (congenital or surgical). UPE with perfusion abnormality in the contralateral lung is associated with a unilateral pulmonary embolism, unilateral pulmonary artery hypoplasia, Swyer-James syndrome and unilateral emphysema or lung bullae [104-106].

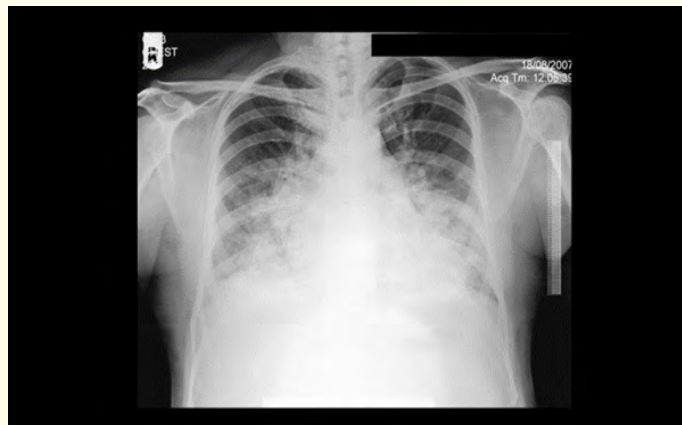


Figure 95: A PA CXR shows cardiomegaly, cephalization of upper lobe blood vessels, basal and midzone shadowing, septal lines and GGO in an alveolar pulmonary edema.

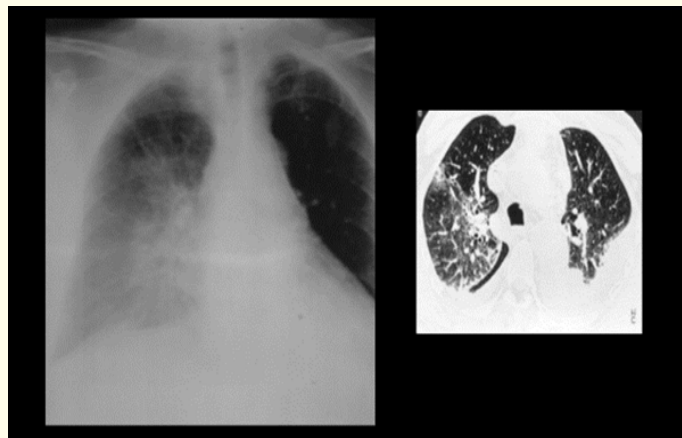


Figure 96: CXR and an axial CT scan show unilateral pulmonary edema and GGO.

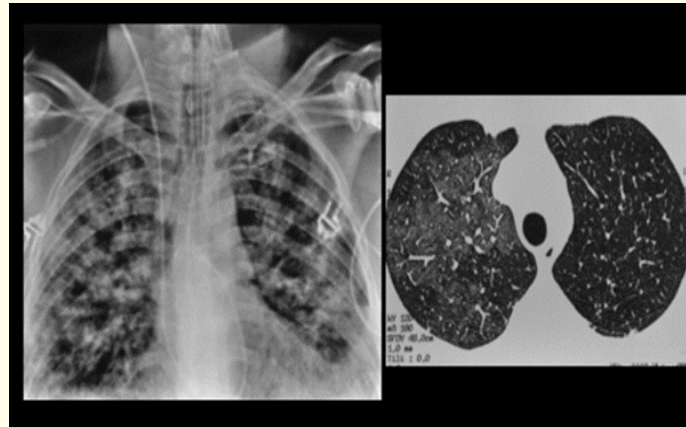


Figure 97: An AP CXR shows extensive air space shadowing due to pulmonary edema in a patient known to have a veno-occlusive disease. The HRCT show unilateral pulmonary edema due to right-sided thromboembolism.

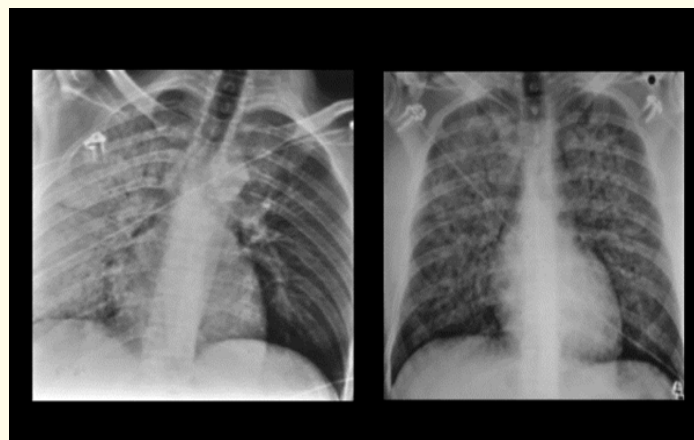


Figure 98: AP CXR on the same patient admitted to the intensive care unit following heroin overdose with heroin induced pulmonary edema.

High-altitude pulmonary edema associated GGO

High-altitude pulmonary edema is a non-cardiogenic pulmonary edema, which occurs in otherwise healthy mountaineers typically above 2,500 meters but can happen at lower altitudes between 1,500 - 2,500 meters in some susceptible climbers. It is a leading cause of death related to high-altitude exposure. Early recognition is vital to institute and prompt emergency treatment. Cerebral dysfunction due to cerebral edema is considered a component of acute mountain sickness. Asymptomatic high-altitude retinal hemorrhage also occurs. This spectrum of pathological events is initiated by an exaggerated vascular response to hypoxia. Except the retinopathy, high-altitude illness can be prevented by slow ascent. Early recognition and immediate descent will prevent serious complications in non-acclimatized climbers that are acutely exposed to hypobaric environments [107].

Citation: Ali Nawaz Khan., *et al.* "A Pictorial Assay of Ground Opacification of the Lungs". *EC Pulmonology and Respiratory Medicine* 5.2 (2017): 53-134.

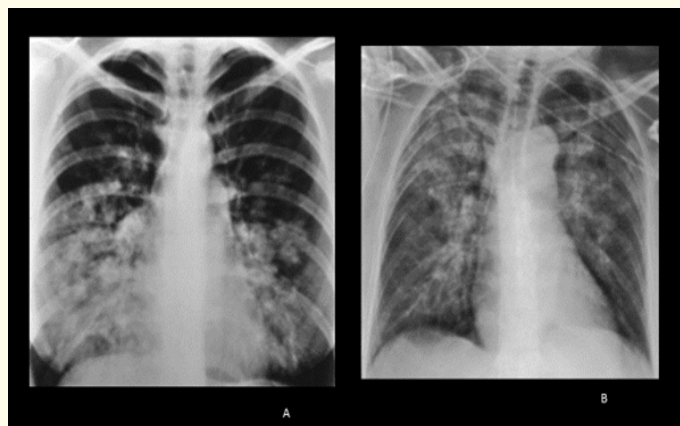


Figure 99: A CXR on a high altitude climber show pulmonary edema. High-altitude pulmonary edema is a non-cardiogenic pulmonary edema, which occurs in otherwise healthy mountaineers typically above 2,500 meters but can happen at lower altitudes between 1,500 - 2,500 meters in some susceptible climbers.

Pulmonary edema following lung transplantation associated GGO

Pulmonary edema following lung transplantation occurs in 57% post- lung transplant patients. The lung edema is non-cardiogenic and occurs in the lung allografts in the first few days following transplantation. The pathogenesis is speculative. The use of cardiopulmonary bypass during surgery is associated with increased incidence and severity. The reported pulmonary edema is said to be heterogeneous and perihilar and lower lobes. Severe pulmonary edema results in primary graft failure in 15% patients. The pulmonary edema peaks a few days following transplantation, and then begin to resolve in most patients. Treatment involves the use of steroids and IL-2 antagonists [108-111].

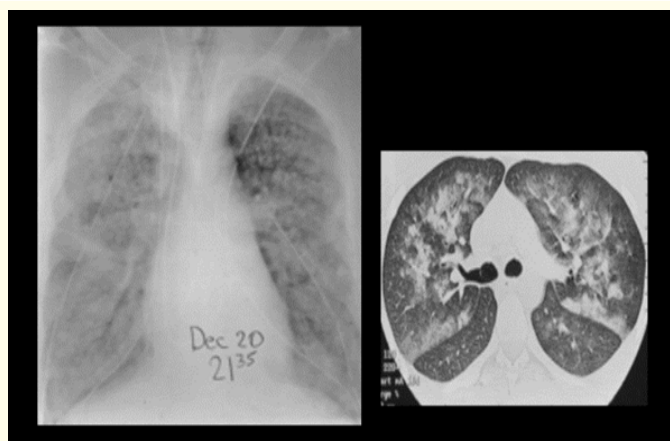


Figure 100: A CXR and Axial HRCT show mainly perihilar pulmonary edema in an allograft lung transplant.

Near drowning pulmonary edema associated GGO

Near drowning pulmonary edema; classed as non-cardiogenic pulmonary edema can occur with either salt or fresh water drowning. Inhaled water can damage the air sacs and cause a ventilation-perfusion mismatch. Three stages are described; stage I acute laryngospasm with inhalation of a small amount of water, stage II: victim presents with laryngospasm but may begin to swallow water into the stomach, stage III 10 - 15% of patients persist with laryngospasm. In 85 - 90% of patients, the laryngospasm relaxes secondary to hypoxia and large amounts of water are aspirated. A CXR and CT show varying degrees of GGO [103,112-113].

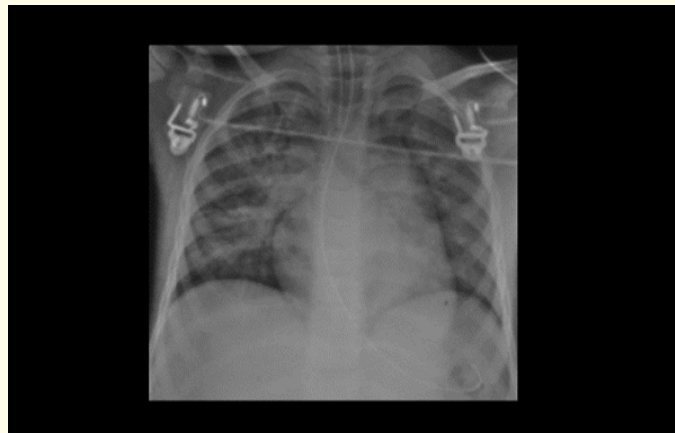


Figure 101: AP CXR shows pulmonary edema secondary to fresh water near drowning.

Acute respiratory distress syndrome (ARDS) associated GGO

Acute respiratory distress syndrome (ARDS) or shock lung, is an inflammatory condition of the lungs, but is not a specific pathology, but nevertheless, the result is the same whatever the cause. ARDS occurs in the critically ill and triggered by trauma, severe respiratory infections, and sepsis.

The pathologic characteristic of ARDS is a diffuse injury to cells that form an alveolar barrier, surfactant and immune dysfunction and abnormal coagulation. ARDS is associated with mortality reported between 20 and 50%.

The syndrome is associated with a high mortality rate between 20 and 50%. The mortality is dependent on associated co-morbidity such as the patient's age, and the severity of ARDS.

All ages are affected with ARDS [114-116].



Figure 102: A supine radiograph on a 10-year-old boy with severe ARDS, following a road traffic accident. Note the extensive GGO/consolidation, associated with an air-bronchogram.

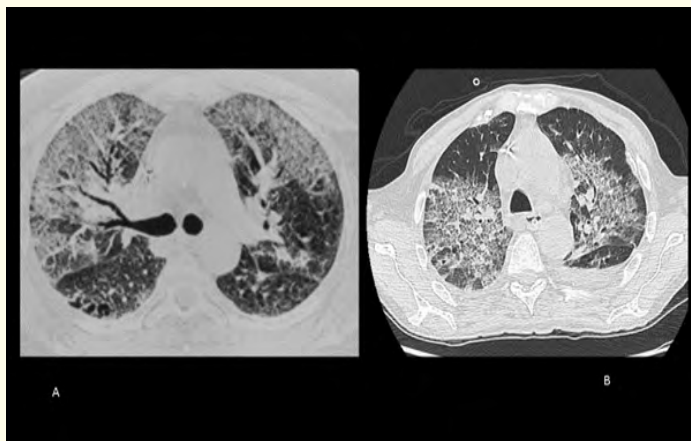


Figure 103: A: An Axial HRCT shows features of atypical ARDS; note the peripheral/subpleural GGO, air bronchogram, and relative sparing of the lower lobes. B: Axial HRCT scan GGO in a man with adult respiratory distress syndrome (ARDS). Note the lower lobes and perihilar GGO, associated with small bilateral pleural effusions.

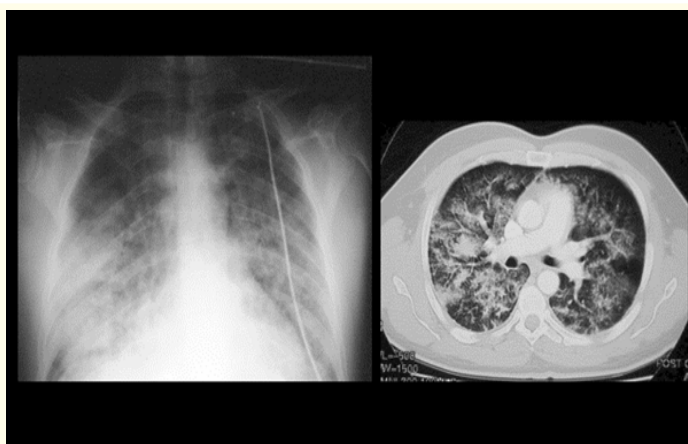


Figure 104: CXR and an axial CT scan show GGO in a patient with ARDS.

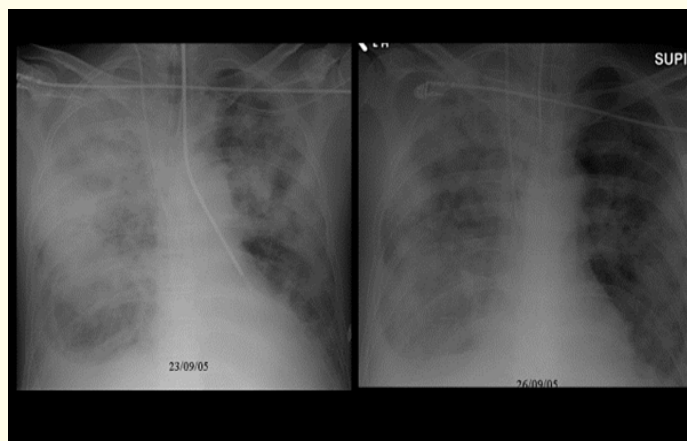


Figure 105: Series of portable chest radiographs with complicated ARDS.

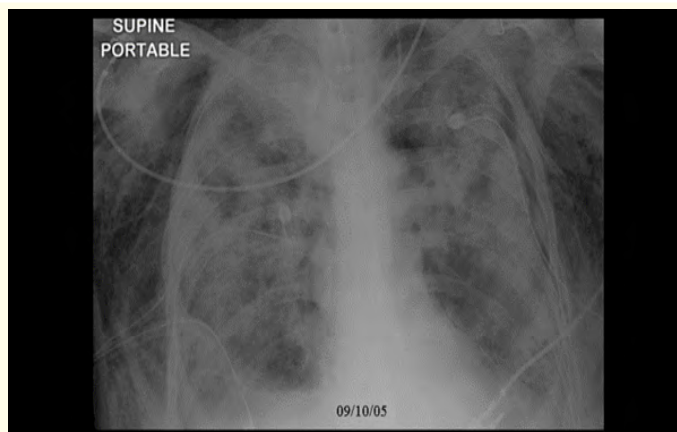


Figure 106: Series of portable chest radiographs with complicated ARDS.

Eosinophilic pneumonia (EP) associated GGO

Eosinophilic pneumonia (EP) is a disease process in which eosinophils, accumulate in in the lungs, causing of alveolar space oxygen absorption. Several types of EPs are described. Patients may present with a cough, fever, shortness of breath, and night sweats. EP is diagnosed by patient history, physical examination and laboratory tests such as a full blood count and blood biochemistry aided by radiology such as a CXR and CT where needed. Once diagnosed EP responds to corticosteroids.

EP is called Idiopathic when no cause is found, which can be further sub-divided into acute eosinophilic pneumonia and chronic eosinophilic pneumonia depending on the patient’s symptoms.

EP can be triggered by certain medications or environmental factors, parasitic infections, and cancer. EP can also present as an autoimmune disease of the lungs such in Churg-Strauss syndrome [117].



Figure 107: Eosinophilic pneumonia in 21-year female that presented to ER with asthma, hypoxia, and shortness of breath. The CXR and coronal CT scan show GGO and lung cysts.

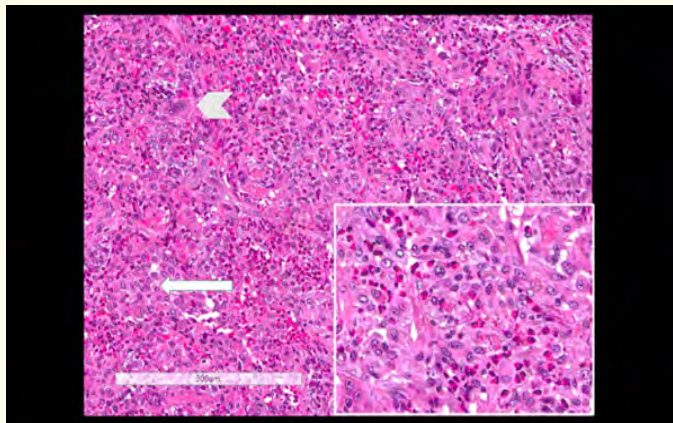


Figure 108: A wedge biopsy shows lung tissue with an accumulation of intra-alveolar eosinophils and macrophages (Arrow). Some giant cells are also seen (Arrowhead). The inset shows higher power of mixed eosinophils with red granular cytoplasm and macrophages. The image is HandE section X 300.

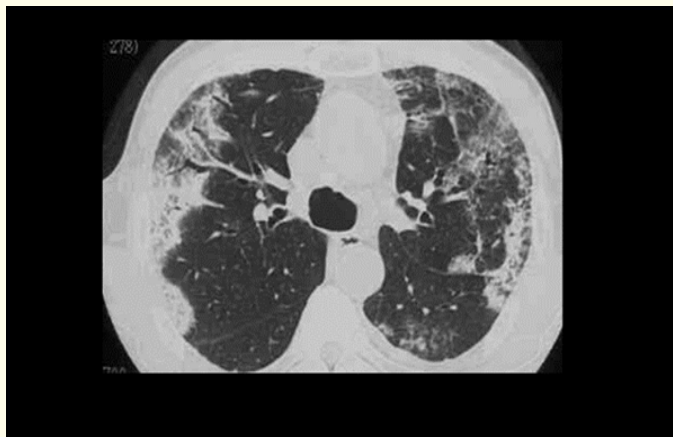


Figure 109: Axial CT scan shows features of Chronic Eosinophilic Pneumonia. It is an idiopathic condition and is characterized by chronic and progressive clinical features. Note the non-segmental peripheral airspace consolidation GGO, nodules, and reticulation.

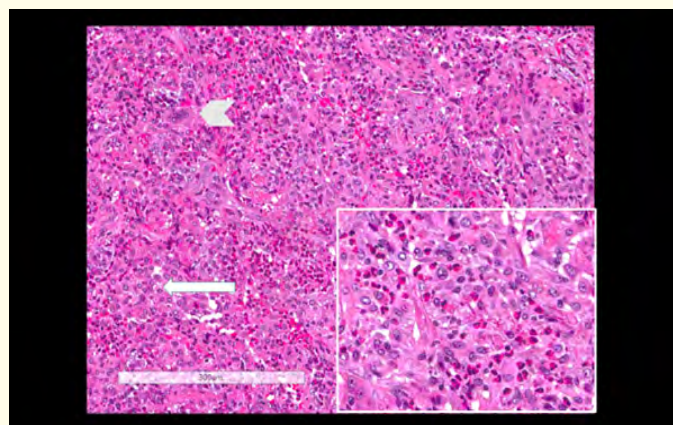


Figure 110: A wedge biopsy shows lung tissue with accumulation of intra-alveolar eosinophils and macrophages (Arrow). Some giant cells are also seen (Arrowhead). The inset shows higher power of mixed eosinophils with red granular cytoplasm and macrophages. The image is HandE section X 300.

Non-specific interstitial pneumonia (NSIP) associated GGO

Non-specific interstitial pneumonia (NSIP) is a common interstitial lung disease with two subtypes: (1) The less common cellular type, with a better prognosis and (2) The more common fibrotic type with a poor prognosis. The imaging features of NSIP include GGO associated with fine reticulations, lung volume loss, and traction bronchiectasis. Subpleural sparing is considered characteristic when present for NSIP. Nevertheless, diagnosis of NSIP remains challenging with correct diagnosis amongst chest radiologist varies between 65 - 85%. NSIP affects adults, 40 - 50 years of age with a higher prevalence in a woman. Symptoms are not specific; presenting with a slow onset of shortness of breath, dry cough, and restrictive pattern lung function and reduced gas exchange capacity. There is a strong association with connective tissue disorders and a variety of autoimmune diseases [3,118-122].

A CXR is normal in the early phase of the disease. Later in the course of NSIP GGO with lower lobes predominance, or patchy consolidation, a reticulonodular or mixed pattern may develop.

HRCT chest provides more specific features, which include GGO, reticular opacities, thickened bronchovascular bundles, traction bronchiectasis, and consolidation [3,118-122].

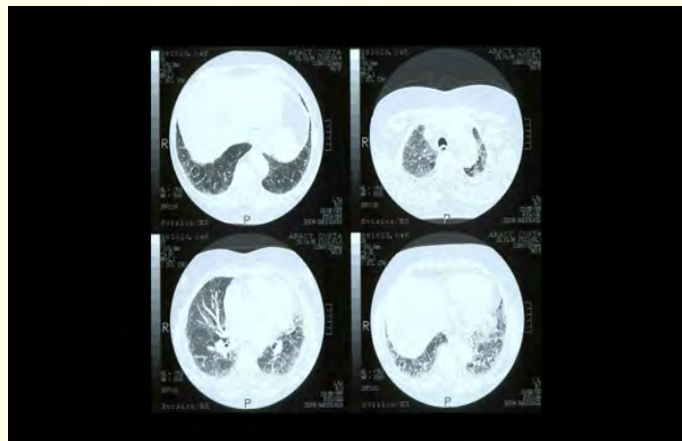


Figure 111: The figure shows an example of diffuse interstitial lung disease with NSIP pattern. Note that the assessment of the severity of the illness is impaired when the patient has not performed an adequate inspiration. The configuration of the posterior wall of the trachea is bending towards the lumen and the shape of the vessels which are wider and tortuous in the periphery of the lungs, revealing that the inspiratory effort was inadequate. The images on the left side are from the same patient, on the same day, asking the patient to repeat a better inspiratory effort.

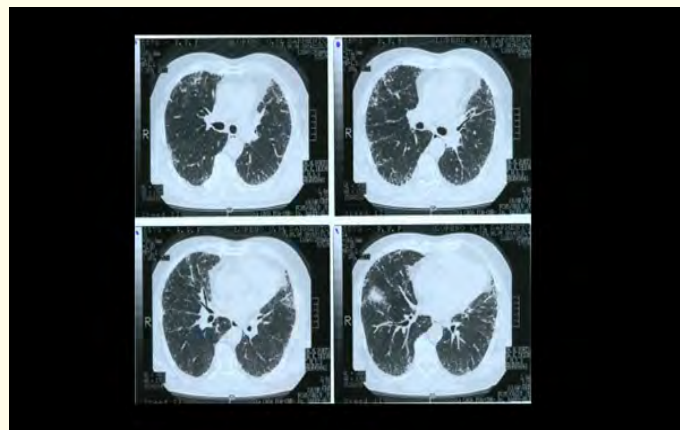


Figure 112: Fibrotic NSIP interstitial septal thickening with distortion of the acinar anatomy. There is also ground-glass, but the distortion of the acinar anatomy is the clue for inferring that the subacute lesion is fibrotic NSIP.

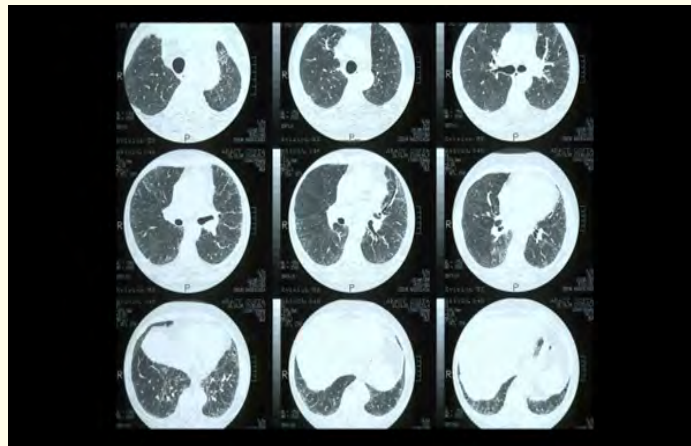


Figure 113: NSIP diffuse lung disease manifested by areas of ground-glass, predominant in the caudal zones (lower thirds) also with a subpleural or cortical predominance. Note that in NSIP, the cortex itself does not necessarily will be affected and a certain number of the cases the predominance is in the cortico-medullary transition.

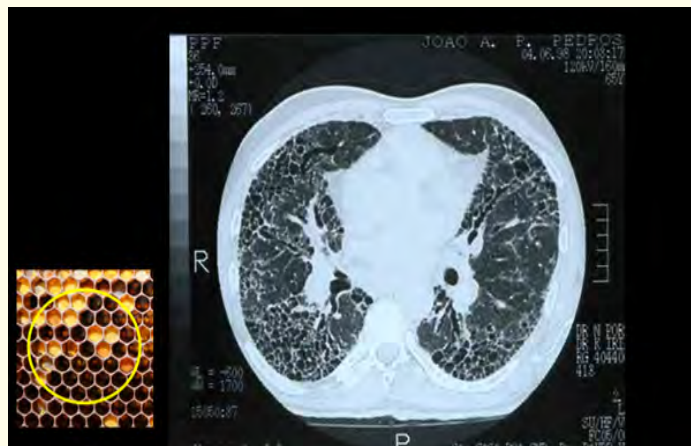


Figure 114: The figure shows a classical pattern of UIP. Note the interstitial disease with a significant distortion of the acinar anatomy with the development of cystic spaces which have well-defined walls and are organized in such a way which to resemble honeycombing. In the classical pattern, the lesions are reasonably symmetric affecting both lungs, with a predominance in the caudal regions and also with dominance in the cortex or the periphery medullary regions. Note the 'honeycomb' shadowing.

Pulmonary sarcoidosis associated GGO

Interstitial lung disease is usually seen as reticulonodular interstitial shadowing in sarcoidosis; usually bilateral and symmetrical predominantly in the upper and mid zones [123]. The nodular opacities can become confluent and coalesce forming bilateral perihilar shadowing with irregular borders extending outward from the hila [124,125]. Resolution of sarcoid granulomas is common but in 20 - 25% of patients, fibrosis eventually develops. Fibrosis associated with sarcoidosis is seen as volume loss, linear opacities, traction bronchiectasis, and architectural distortion [124]. Fibrosis is seen primarily in the upper and mid zones although a generalized pattern with relative basal sparing is also common. Atypical features are rare such as an isolated unilateral hilar lymph node enlargement (usually right) seen in < 5% of cases.

Patchy airspace consolidation, usually referred to as "Alveolar sarcoidosis", is seen in approximately 4% of plain films. It is usually ill-defined, peripheral and associated with air bronchograms. It is typically bilateral but if solitary then it can mimic a lung mass [124].

Other described uncommon appearances include miliary opacities, cavitation, and pleural disease. Cavitation is rare and found in less than 1% of sarcoid patients. It is mainly found in association with necrotizing sarcoid granulomatosis, but TB and fungal infections need to be ruled out [125,126].



Figure 115: A CXR and HRCT on the 26-year-old male of North African descent known to have Pulmonary Sarcoidosis with an ACE level of 71 shows GGO on CT and HRCT.



Figure 116: An Axial CT scan on a patient with known Sarcoidosis showing an area of GGO.

Pulmonary alveolar proteinosis (PAP) associated GGO

Pulmonary alveolar proteinosis (PAP) is a rare diffuse lung disease characterized by the alveolar and interstitial accumulation of a periodic acid-Schiff (PAS) stain-positive phospholipoprotein derived from the surfactant and is clinically associated with increased work of breathing and derangement of gas exchange. The alveolar air spaces are filled with a dense proteinaceous-lipid fluid mix. Typically, both the pulmonary interstitium and airways are relatively spared. PAP may affect infants, children as well as adults.

The classic chest radiographic finding is bilateral symmetric air-space opacity, appearing either as ground glass or frank consolidation, with a perihilar or basilar predominance. An air bronchogram is not a feature. Radiographic opacities often are vaguely nodular and may be accompanied by fine linear opacities or reticulation. Serial radiographs may demonstrate the persistence of this pattern over time. The heart size is usually normal and pleural effusions, and lymphadenopathy is not a feature.

Conventional CT may reveal bilateral areas of consolidation and reticulation.

Occasionally, an underlying linear abnormality that represents thickened interlobular septa may be appreciated. HRCT better demonstrates the morphologic characteristics of PAP. Crazy paving is the characteristic finding of and consists of patchy, bilateral, geographic areas of ground-glass opacity associated with interlobular septal thickening. The disease is often distributed uniformly from lung apex to base. Interlobular septal thickening may be encountered more frequently in the lower lung zones.

Although findings of the interlobular septa commonly are abnormal on pathologic specimens from patients with PAP, septa findings occasionally may be pathologically normal despite a thickened appearance on HRCT.

Pleural effusions and adenopathy are rare in PAP and should suggest superimposed infection or malignancy. Occasionally, pleural effusions may be encountered in uncomplicated cases of PAP shortly following bronchoalveolar lavage [100,127-135].

HRCT demonstrates crazy paving consisting of patchy, bilateral, geographic areas of ground-glass opacity associated with interlobular septal thickening due to pulmonary alveolar proteinosis.

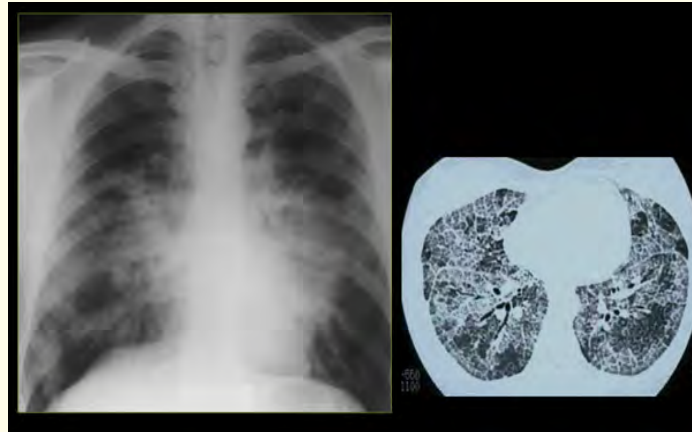


Figure 117: A PA chest radiograph shows bilateral symmetric air-space opacification, appearing as frank consolidation, with a perihilar predominance.

Non-Hodgkin's Lymphoma associated GGO

Qin L., *et al.* reviewed six cases of pulmonary non-Hodgkin's lymphoma (NHL) with diffuse GGO on chest CT over a two year period. The authors retrospectively analyzed the clinical, pathological and imaging characteristics, misdiagnosis and treatment of pulmonary non-Hodgkin's lymphoma with diffuse ground-glass opacities (GGO). The study included 5 males and 1 female with an average age of 52 years. The patients presented with dyspnea and weight loss. Two patients had superficial adenopathy, and two had hepatosplenomegaly. The CT scan showed diffuse GGO in two patients and GGO with consolidations in 3 patients and mediastinal lymphadenopathy in two patients. The diagnosis was achieved by tissue sampling in 6 patients. The final tissue diagnosis showed intravascular lymphoma (n = 2), diffuse large B-cell lymphoma (n = 2) and T-cell lymphoma (n = 2). The authors concluded that diffuse GGO on chest CT scan in NHL was rare, but its misdiagnosis common due to a lack of specific clinical feature. Lung tissue sampling is required for an early diagnosis [136].

Tokuyasu H., *et al.* reported 2 rare cases of NHL associated with pulmonary with diffuse GGO in the lungs. Histological examination of the lung tissue revealed a diffuse large B-cell-type lymphoma within the bronchiolar wall and alveolar septum. The authors concluded that this is a rare presentation and diffuse large B-cell-type NHL should be considered in the differential diagnosis of diffuse pulmonary GGO seen on a chest CT scan [137].

M. Yc and associates retrospectively analyzed 32 patients with NHL and Richter's syndrome with lung involvement (age 10 - 82, men 26 and woman 6). The authors concluded that pulmonary involvement in lymphoma is characterized by GGO, lung nodules of varying sizes and ill-defined consolidation, peribronchial disease. Thoracic wall involvement mediastinal adenopathy and extra nodal lymphomatous soft tissue masses provide further supporting evidence to the diagnosis of NHL. When a mass like consolidation is seen in association with chest wall involvement of acute onset chronic lymphocytic leukemia the diagnosis of Richter's syndrome should be considered [138].

Punch biopsies were taken from the skin nodule. The biopsy showed a normal surface basket-weave keratin and epidermis. The superficial, mid and deep dermis showed a diffuse, as well as perivascular, infiltrate of the dyscohesive population of large cells with single

to multiple nucleoli. The morphological was highly suggestive of NHL. The immuno-chemistry revealed diffuse lymphoid infiltrate with positivity with CD20, CD79a, BCL2, and BCL6 and MUM1. The specimen was negative for CD3, CD5, CD10, CD23, Cyclin D1, and CD30 and EBV-LMP. The Ki-67 proliferation index approached 95%. Further characterization classed the lymphoma as Diffuse Large B-cell lymphoma (DLBCL) MYCnormalalpha-8normal, with no evidence of MYC gene rearrangement (Dako probe) FISH on FFPE sections. Unfortunately, the patient expired before treatment could be instituted.

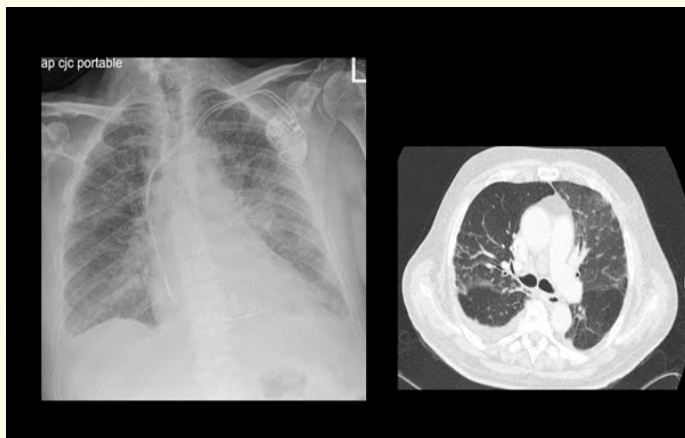


Figure 118: Non-Hodgkin’s lymphoma: the patient presented with shortness of breath, with peripheral lymphadenopathy, scrotal swelling and cutaneous nodules particularly in the groins, Punch biopsies were taken from the skin nodule. Note the GGO, and micronodules, GGO, and bilateral pleural effusions more pronounced on the left.



Figure 119: Non-Hodgkin’s lymphoma: scrotal ultrasound scan on the same patient as in Figure 118 showing solid multifocal lesions in both testes.

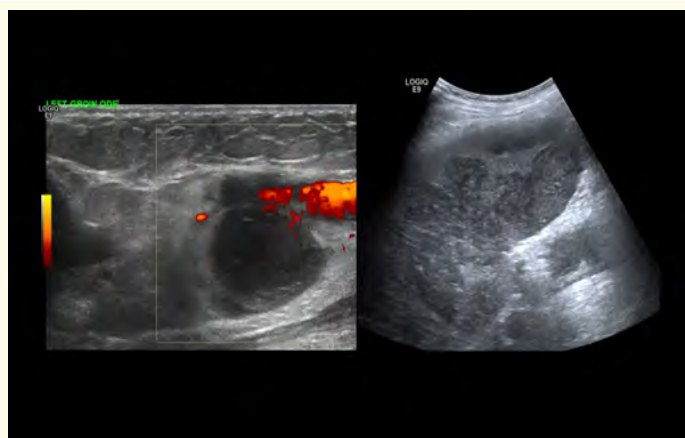


Figure 120: Non-Hodgkin’s lymphoma: Ultrasound scan of the right groin and the liver on the same patient as in Figures 118 and 119 showing a large necrotic lymph gland and multiple mixed echogenicity masses in the liver due to metastases.

Testicular Choriocarcinoma metastatic to lung associated GGO

Arana S and associates described a metastatic lung choriocarcinoma in a 24-year-old man that presented with left scrotal swelling and subsequently underwent orchiectomy for a germ cell testicular tumor. A CXR showed multiple well-defined lung nodules, associated with GGO. Testicular germ cell tumors are the most common solid tumors in men between 15 and 35 years of age. Choriocarcinoma is the most aggressive and characteristically secrete of large amounts of HCG. A CXR and CT show multiple lung nodules with surrounding GGO [139,140].



Figure 121: Testicular choriocarcinoma metastatic to the lungs. Note the multiple lung nodules and surrounding GGO.

Immune Compromise Related Lung Disease associated GGO

Cytomegalovirus (CMV) can remain in a latent state in humans with the potential for reactivation in the immune-compromised. CMV is a well-known cause viral pneumonia in the immune-compromised such as AIDS and allogenic bone marrow transplantation. An incidence of CMV infection as high 20-35% has been described in recipients of hematopoietic cell transplantations.

The imaging features of pulmonary infection with CMV are non-specific on conventional radiograph and vary from air-space consolidation, interstitial shadowing, CGO, Tree-in-bud appearance, bronchiectasis, and micronodules [141-148].

HRCT findings are also non-specific and do not differentiate between AIDS and non-AIDS patients. HRCT findings include GGO, micronodules, larger lung masses, confluent consolidation, reticulation, bronchiectasis, a tree in bud appearance and thickening of the bronchovascular bundles. The differential diagnosis includes *Pneumocystis jirovecii* pneumonia and other forms of viral pneumonia [141-148]. Gallbladder wall thickening is associated with CMV and other viral infections [149].

Invasive aspergillosis HIV/AIDS: Aspergillosis is caused by the fungus, *Aspergillus*, which can present with a wide range of manifestations including Allergic Aspergillosis, semi-invasive, and invasive disease. The infection is particularly important in immunocompromised such as in AIDS. *Aspergillus* infection can lead to disseminated disease with high rates of morbidity and mortality in patients that are immune compromised [150].

Kaposi Sarcoma (KS) is the most common AIDS-related malignancy [151]. Pulmonary involvement in 50% and is almost always preceded by cutaneous or visceral disease [151].

Bilateral perihilar and lower zone reticulonodular shadowing is characteristic associated septal lines and flamed shaped opacities associated with a halo [151]. Endobronchial lesions are identified in 75% patients on bronchoscopy but are not apparent in CT [151,152]. Thickened bronchovascular bundles are seen on HRCT. Pleural effusions occur in 30% patient [151-153].

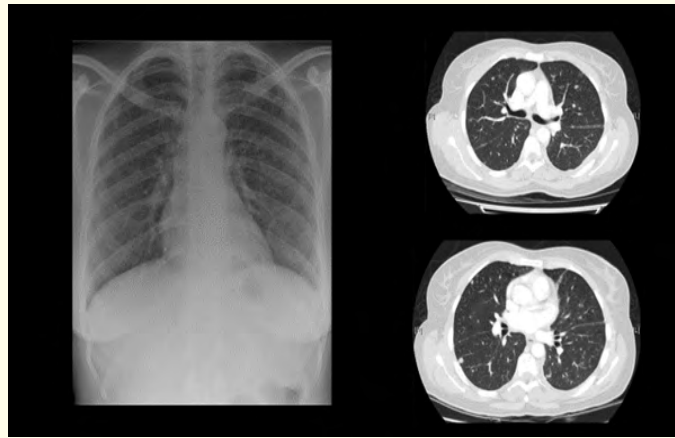


Figure 122: Cytomegalovirus pulmonary infection: The imaging findings are non-specific on conventional radiographs. HRCT findings do not differentiate between AIDS and non-AIDS patients. The findings described include GGO, small nodules, confluent consolidation, interstitial reticulation, bronchiectasis, a tree in bud appearance and thickened bronchovascular bundles. Pleural effusions may also occur.

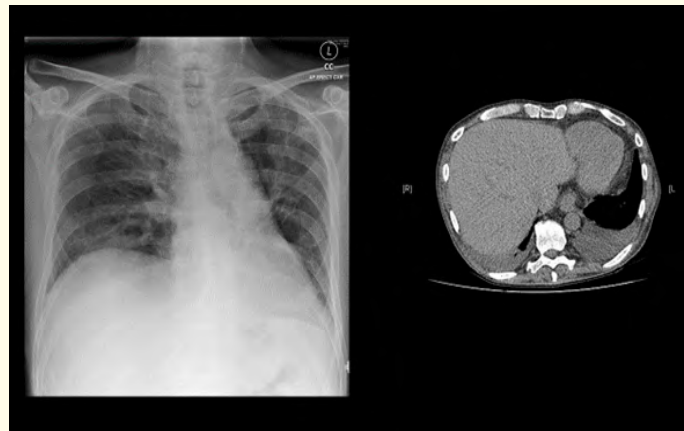


Figure 123: Cytomegalovirus pulmonary infection: The imaging findings are non-specific on conventional radiographs. HRCT findings do not differentiate between AIDS and non-AIDS patients. The findings described include GGO, small nodules, confluent consolidation, interstitial reticulation, bronchiectasis, a tree in bud appearance and thickened bronchovascular bundles. Pleural effusions may also occur.

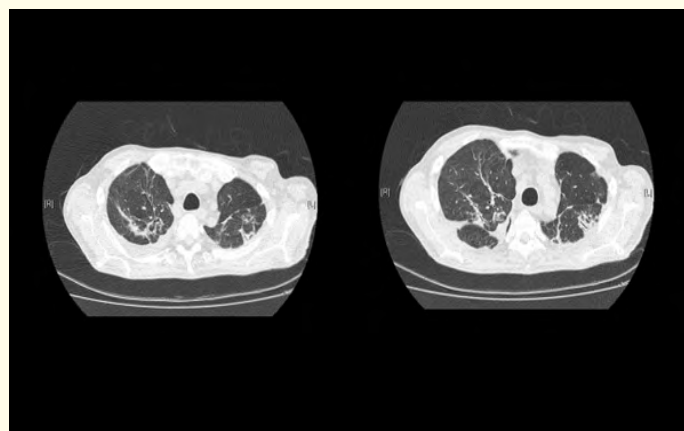


Figure 124: Cytomegalovirus pulmonary infection: The imaging findings are non-specific on conventional radiographs. HRCT findings do not differentiate between AIDS and non-AIDS patients. The findings described include GGO, small nodules, confluent consolidation, interstitial reticulation, bronchiectasis, a tree in bud appearance and thickened bronchovascular bundles. Pleural effusions may also occur.

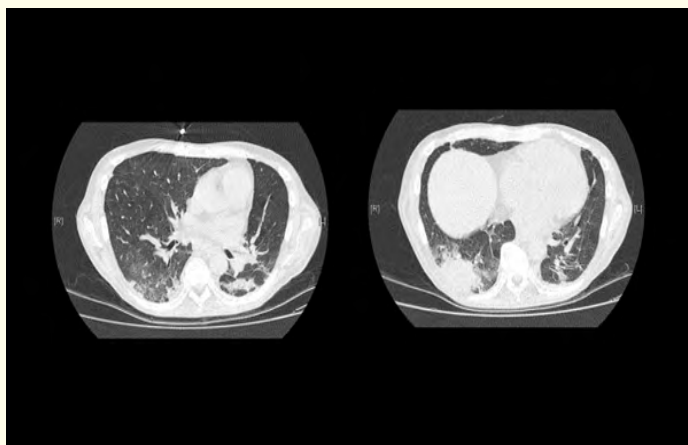


Figure 125: Cytomegalovirus pulmonary infection: The imaging findings are non-specific on conventional radiographs. HRCT findings do not differentiate between AIDS and non-AIDS patients. The findings described include GGO, small nodules, confluent consolidation, interstitial reticulation, bronchiectasis, a tree in bud appearance and thickened bronchovascular bundles. Pleural effusions may also occur.

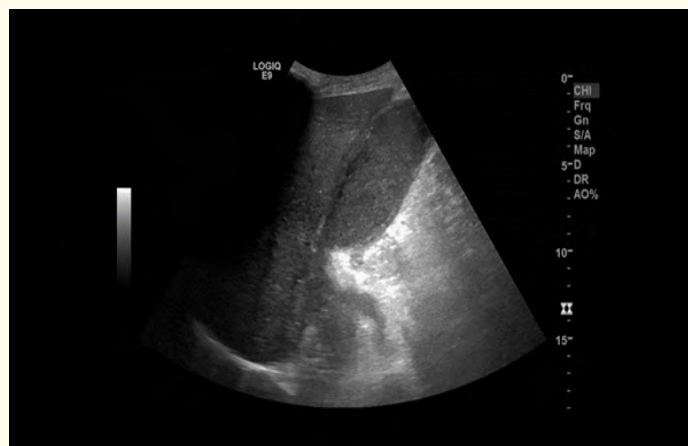


Figure 126: Gallbladder wall thickening is associated with CMV and other viral infections.



Figure 127: CMV: Axial HRCT scan show micronodules of varying sizes in a patient with HIV/AIDS.

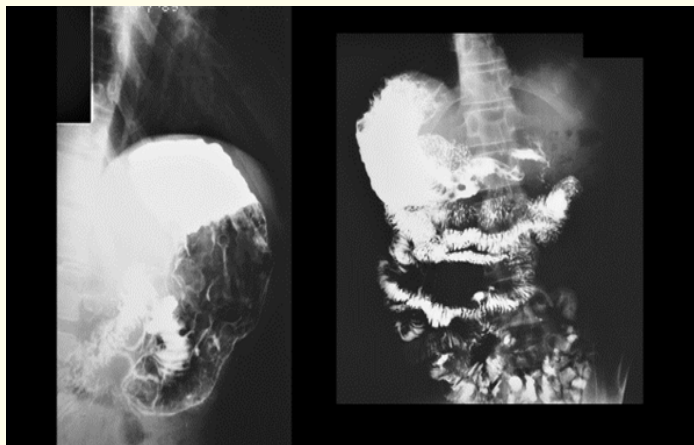


Figure 128: An upper GI barium series on 22-Y-O HIV-positive patient that presented with facial swelling, skin nodules and dyspepsia. A biopsy taken from one of the stomach nodules showed Kaposi sarcoma. See lung changes on the same patient in the next figure.

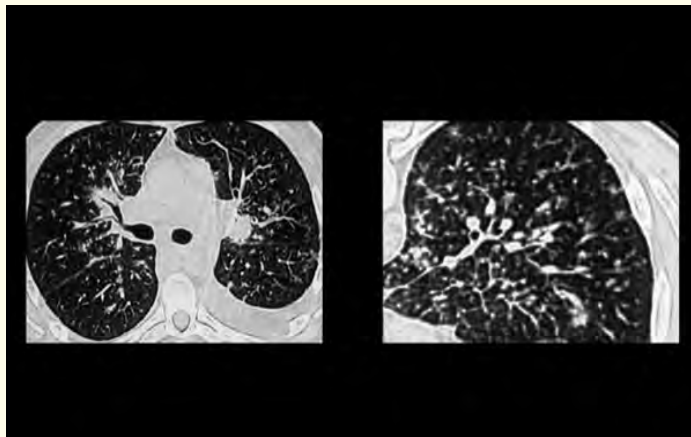


Figure 129: HRCT on HIV patient with Kaposi sarcoma shows GGO, nodules and a tree in bud appearance.



Figure 130: A CXR shows flame-shaped ill-defined opacities in an HIV patient associated with GGO in a biopsy proved Kaposi sarcoma. Note the perihilar and subpleural distribution.

Smoking-related lung disease associated GGO

Recent reviews on smoking-related lung disease are not only confined to chronic obstructive pulmonary disease and lung cancer. The current focus is on the association smoking and development of interstitial lung diseases, namely respiratory bronchiolitis-associated, desquamative interstitial pneumonia and pulmonary Langerhans cell histiocytosis [154-157].

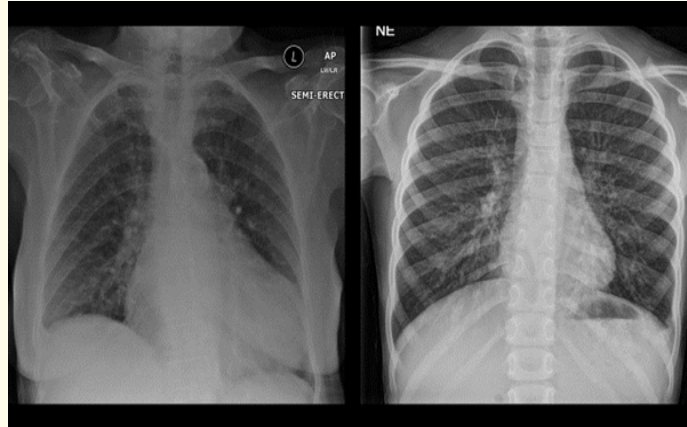


Figure 131: 'Dirty chest'- chronic bronchitis in a 70-year old woman and an 8 -year-old girl with asthma. Both parents were heavy smokers.

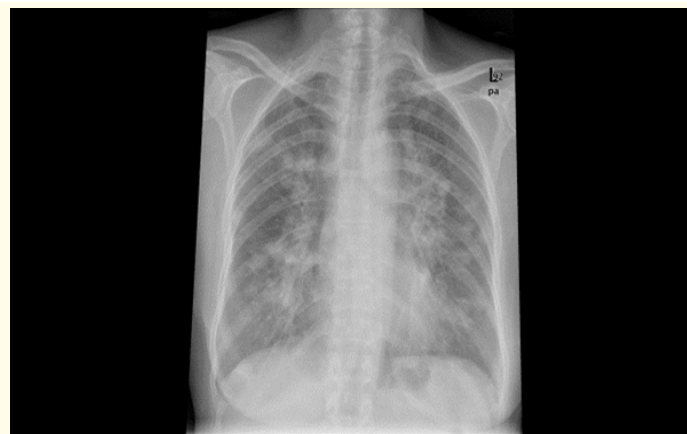


Figure 132: Langerhans cell histiocytosis (LCH) is a rare systemic disease that has been called by several names including Hand-Schüller-Christian disease, Letterer-Siwe disease, and histiocytosis X. As pathologically it is one disease but affecting different organs, in 1985 the disease was renamed by the Histiocyte Society as Langerhans cell histiocytosis (LCH).

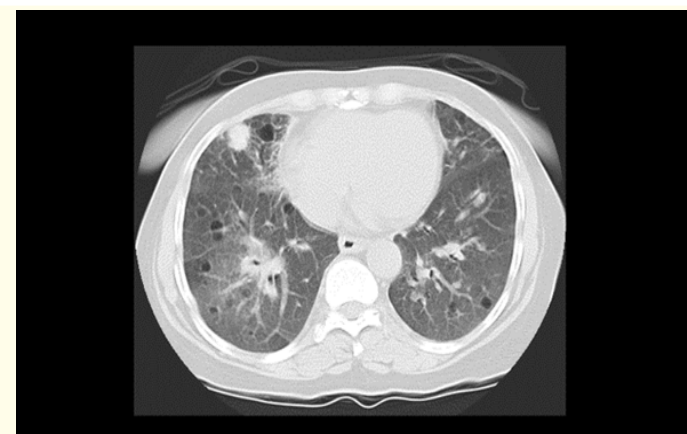


Figure 133: A variant of Langerhans histiocytosis called Pulmonary Langerhans Cell Histiocytosis exclusively occur in adults that smoke a cigarette. The lungs show GGO and interstitial lung pattern. Some patients recover completely after cessation of smoking, but others progress to long-term sequelae such as pulmonary fibrosis and pulmonary hypertension.

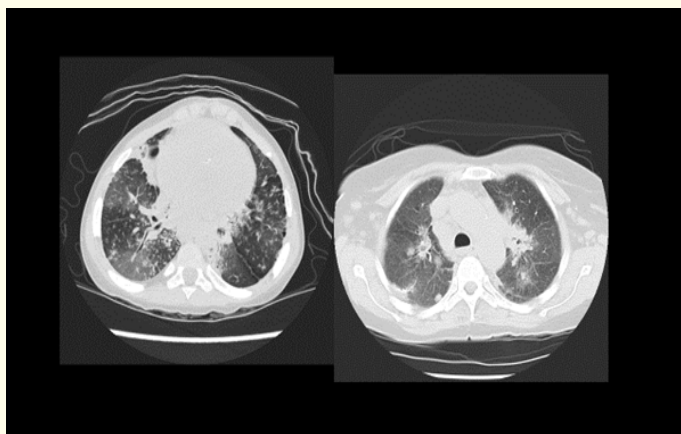


Figure 134: Pulmonary Langerhans Cell Histiocytosis show GGO and interstitial lung pattern. Some patients recover completely after cessation of smoking, but others progress to long-term sequelae such as pulmonary fibrosis and pulmonary hypertension.

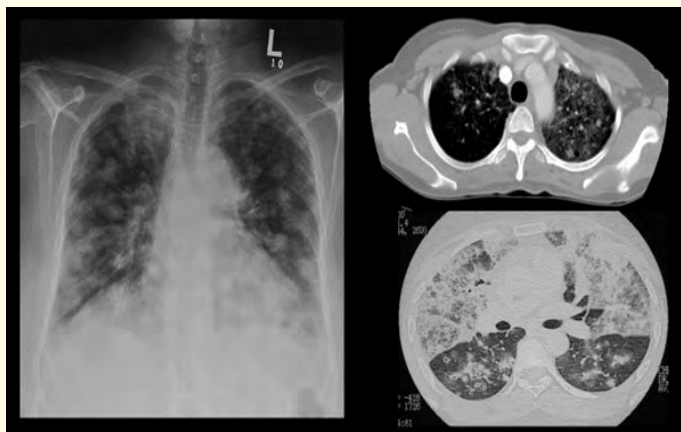


Figure 135: A PA CXR and axial CT/HRCT scans show multiple lung nodules and GGO associated with of a biopsy proved Bronch-Alveolar Carcinoma.



Figure 136: A CXR and contrast enhanced axial CT show consolidation, reticular shadowing, an air-bronchogram and GGO in a biopsy proved Multi-centric adenocarcinoma of GI origin.



Figure 137: An axial CT scans on a 54-year-old woman that was being followed-up at regular interval for a colon cancer. The scan show a 1 cm GGO, which was not PET/CT avid. The GGO remained stable for 3 years. However, the opacity was excised, which revealed a primary adenocarcinoma of the lung.

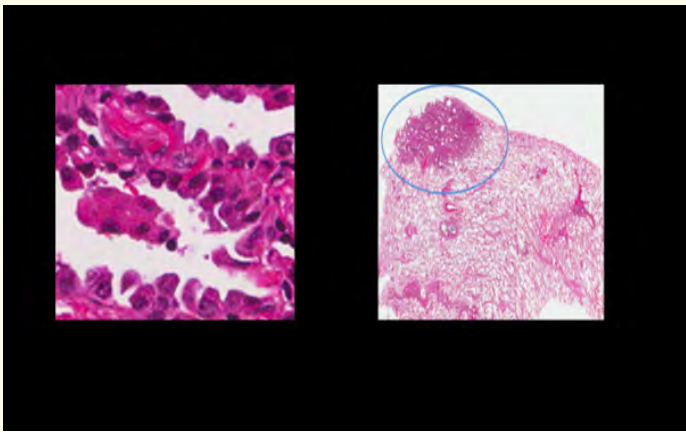


Figure 138: Haematoxylin and Eosin section at X400 shows hyperchromatic cells lining thin septa. A lung biopsy shows a well-demarcated 1 cm sub-pleural lesion.

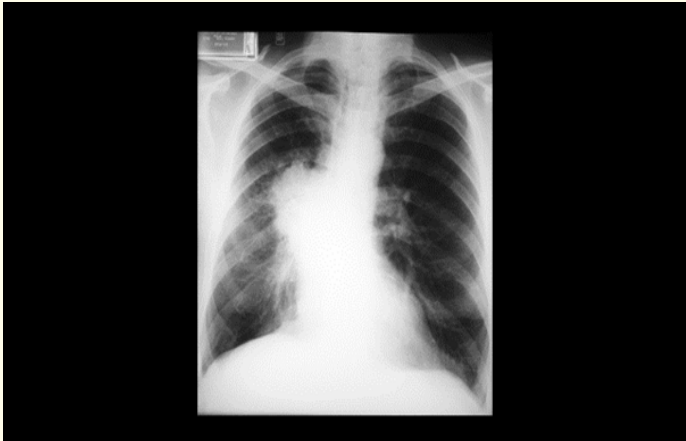


Figure 139: A CXR shows GGO distal to hilar adenocarcinoma.

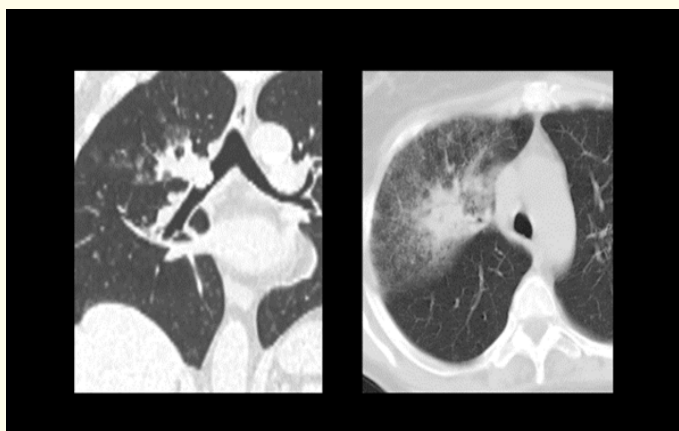


Figure 140: A coronal reconstruction CT in a patient with an endoluminal biopsy proved adenocarcinoma of the right main bronchus. The CT scans show GGO distal to the bronchial obstruction.

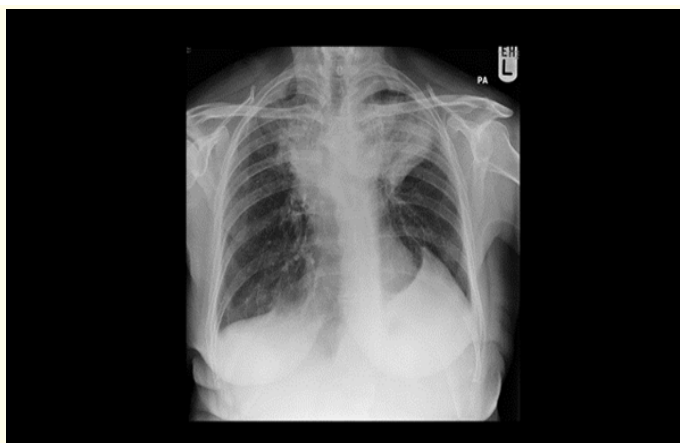


Figure 141: A CXR shows GGO in post- irradiation pneumonitis.

Hypersensitivity pneumonitis associated GGO

Hypersensitivity pneumonitis has been traditionally classified into acute, subacute, and chronic phases. However, there are only 2 clinical phases or syndromes: acute and subacute/chronic. Most affected patients present acutely with flulike illness with a cough. Patients can also present subacutely with recurrent pneumonia or chronically with exertional dyspnea, productive cough, and weight loss. Most patients recover completely after exposure to the inciting antigen ceases [158,159].

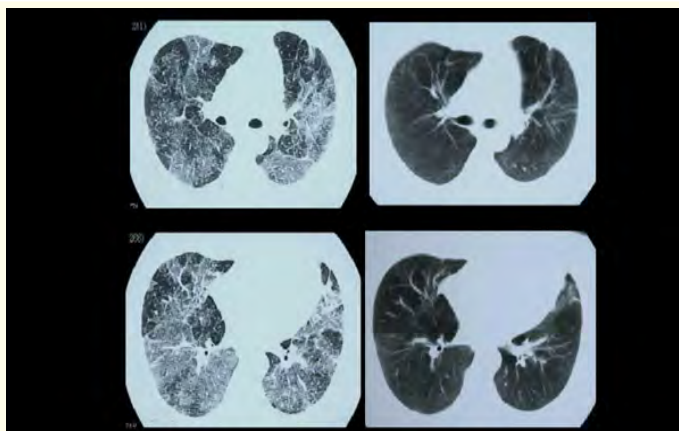


Figure 142: HRCT scans on a patient with hypersensitivity pneumonitis due to mouldy hay; images before and after the allergen was removed. Note the extensive GGO at exposure.

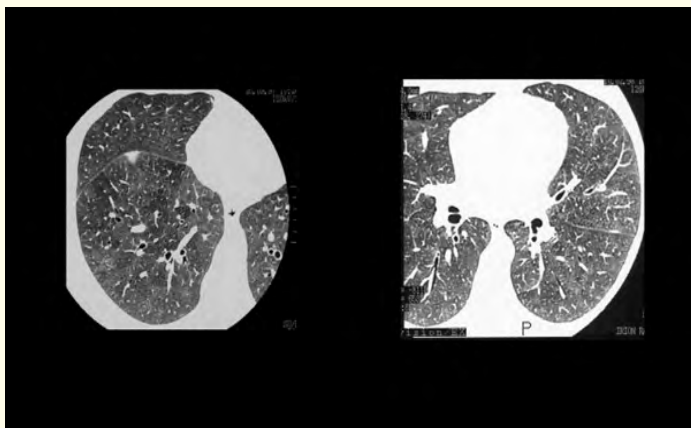


Figure 143: Axial HRCT scans show GGO, traction bronchiectasis in a patient with hypersensitivity pneumonitis.

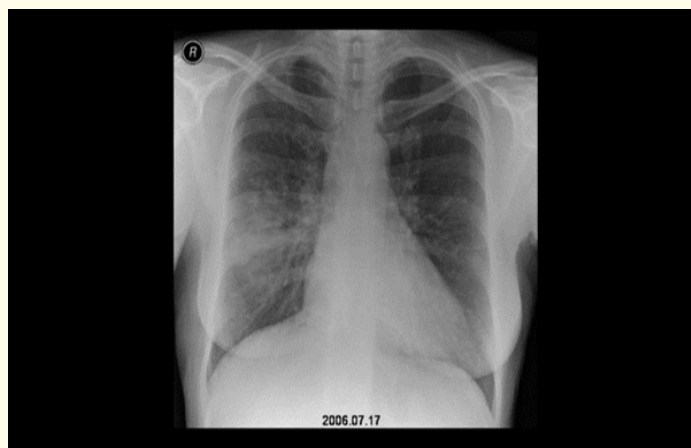


Figure 144: Allergic aspergillosis is a hypersensitivity pneumonitis. The PA CXR shows airspace shadowing, reticular opacities, and GGO.

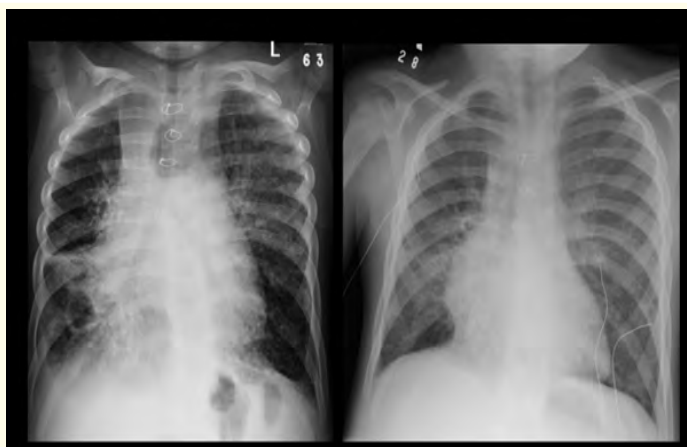


Figure 145: PA CXRs in a patient with allergic aspergillosis before and after corticosteroid treatment.

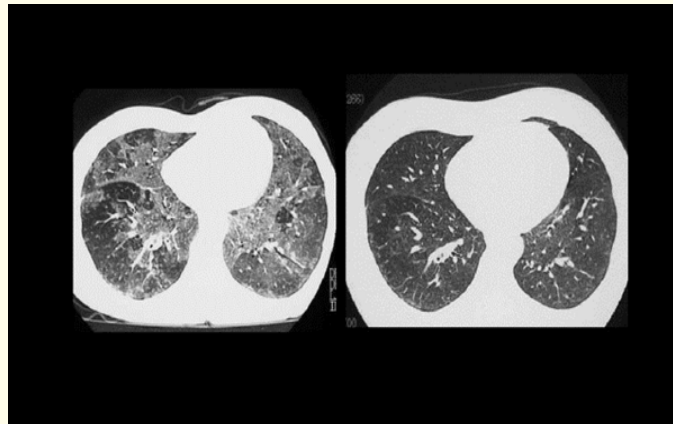


Figure 146: HRCT in allergic aspergillosis before and after treatment. Note the air-space shadowing and GGO.



Figure 147: HRCT scan demonstrates, peripheral tree-in-bud appearance shown as centrilobular opacities, which represent mucoid impaction of the small bronchioles due to allergic bronchopulmonary aspergillosis. In some individuals, exposure to these fungi also can lead to asthma or a lung disease resembling severe inflammatory asthma. This latter condition, which occurs only in a minority of people with asthma, is characterized by wheezing, low-grade fever, and coughing up of brown-flecked masses or mucus plugs.

Drug related pneumonitis related GGO

The number of drugs that adversely affect the respiratory system continues to increase and their effects poses a great challenge to all physicians. A review in 1972 identified only 19 drugs with the potential to cause pulmonary disease; now, more than 350 (and counting) have been identified. Awareness of drug-induced pulmonary disease is increasing. The sole purpose of one clinical study group, the Groupe d'Etudes de la Pathologie Pulmonaire Iatrogene (GEPI), is to provide information regarding individual cases, to collect and update literature on drug-induced lung disease, to publish updated lists of offending compounds, and to provide warnings when adverse effects of drugs are recognized. Drug-related lung disease can virtually give rise to a variety of lung patterns from interstitial fibrosis, honeycombing, pleural.

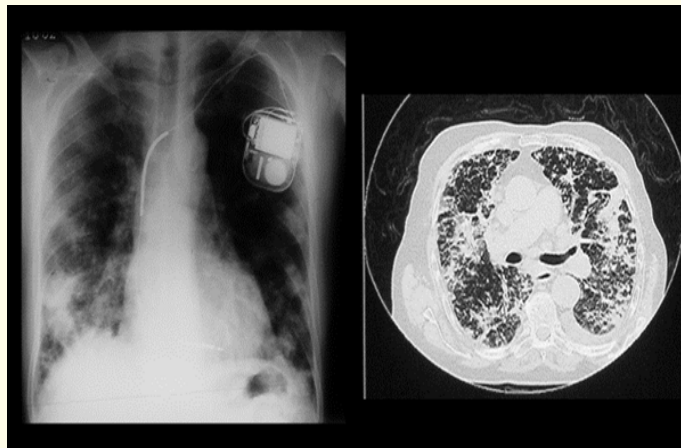


Figure 148: PA CXR and axial CT scan toxicity to Amiodarone, note the interstitial fibrosis, flame shaped opacities, left basal pleural effusion and GGO.

Sickle cell disease related GGO

Sylvester KP and associates studied 33 patients with sickle cell disease (SCD) with HRCT findings and to whether the HRCT findings correlated with coexistent lung function test abnormalities. The authors concluded that HRCT assessment of hemolysis might be useful to identify SCD disease patients with respiratory function impairment [160-170].

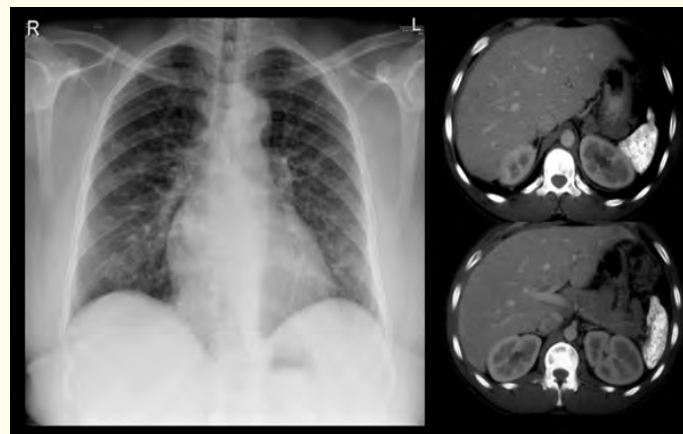


Figure 149: CXR in a patient with Sickle cell crises shows GGO. Axial CT scans show heavily calcified spleen, in keeping with auto splenectomy.

Cryptogenic organizing pneumonia and GGO

Lee JW and associates analyzed the HRCT findings in 22 patients with Cryptogenic organizing pneumonia and concluded that the prognosis in 73% was good but in the remaining patients follow-up CT scans results, resemble a fibrotic nonspecific interstitial pneumonia pattern [171].

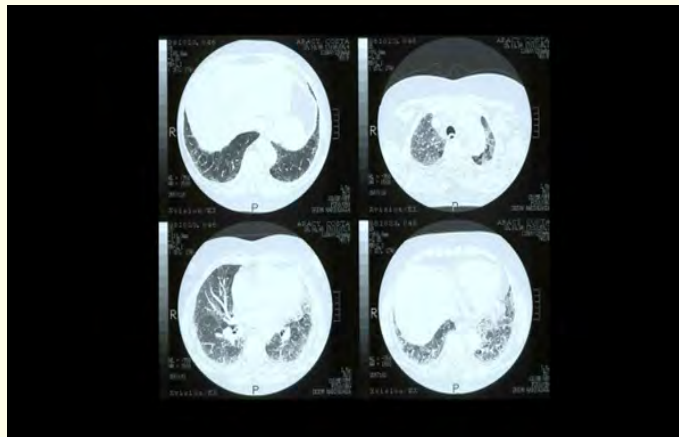


Figure 150: Axial HRCT scans show an example of diffuse interstitial lung disease with NSIP pattern. Note that the assessment of the severity of the disease is impaired when the patient has not taken an adequate inspiration (make note of the images on the right with the posterior wall of the trachea bending towards the lumen and the configuration of the vessels which are wider and tortuous in the lung periphery). The images on the left are from the same patient, the same day, with the patient making an adequate inspiratory effort.

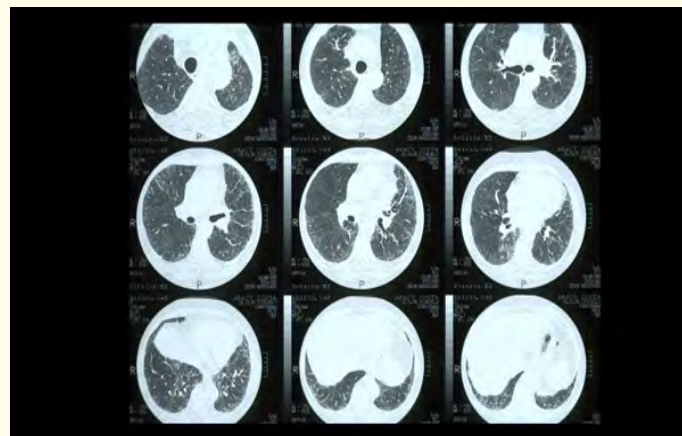


Figure 151: NSIP manifests by areas of GGO, predominantly in the lower thirds, with a subpleural or cortical predominance. Note that in NSIP, the cortex itself is not necessarily affected.

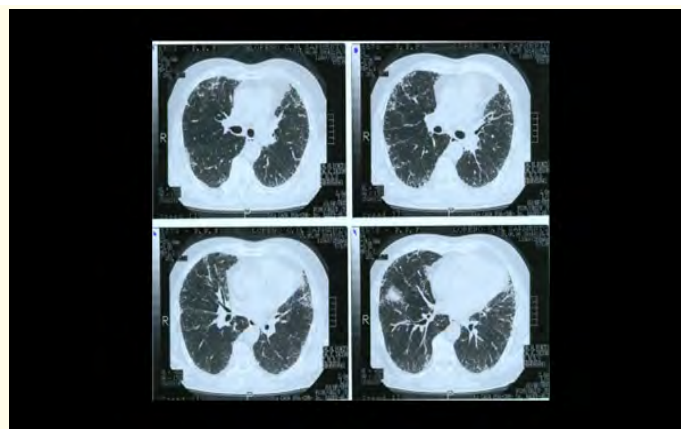


Figure 152: Fibrotic NSIP interstitial septal thickening with distortion of the acinar anatomy. There is also, GGO but the distortion of the acinar anatomy is the clue for inferring that the subjacent lesion is fibrotic NSIP.



Figure 153: An Axial HRCT shows features of a Fibrosing Interstitial pneumonia following lung transplantation.

Fibrotic idiopathic interstitial pneumonia with little honeycombing: serial changes and prognostic implications

Lee HY and associates in a retrospective study clarified the prognostic determinants on HRCT findings in fibrotic idiopathic interstitial pneumonia with little honeycombing. The authors also found that even in cases with little honeycombing, the extent of honeycombing and reticulation showed a decrease in the extent of GGO. The overall extent of lung fibrosis on the baseline HRCT examination appears predictive of survival in fibrotic idiopathic interstitial pneumonia with little honeycombing [172].



Figure 154: HRCT in Fibrosing Interstitial pneumonia- Desquamative type, note the GGO, interstitial fibrosis, amounting to a honey-comb pattern and traction bronchiectasis.

Acute lung transplant rejection and GGO

Acute lung transplant rejection occurs within one year following transplantation, but can occur as early as five days following a lung transplant. Transplant rejection peak around two months following transplant surgery. The event is rare after six months. Histopathologically rejection is characterized Perivascular or peribronchiolar mononuclear inflammation and may affect up to 55% of lung transplant recipients within the first year after a transplant.

There are no characteristic findings on HRCT. A variety of results has been reported including GGO, consolidation, nodules, interlobular septal thickening and pleural effusions with no associated signs of left ventricular failure.

A further complication is the occurrence of bronchiolitis obliterans with progressive airflow obstruction that limits survival to only 50% at five years following transplantation 2.

Similar HRCT findings can occur pulmonary edema as a reimplantation response and lung infections [111,173-178].

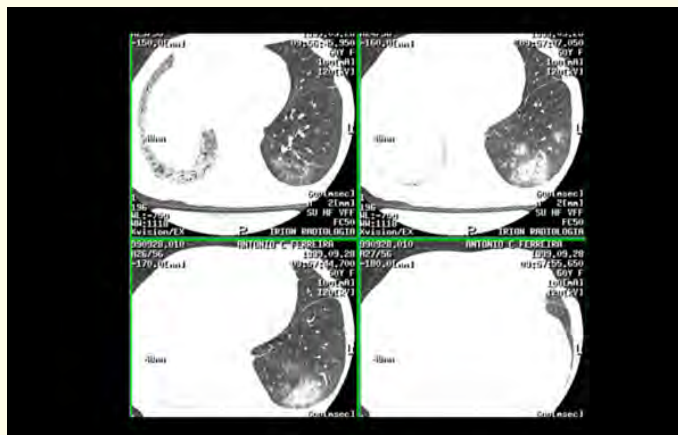


Figure 155: Acute rejection (transbronchial diagnosis).

Acute lung transplant rejection occurs within one year following transplantation, but can occur as early as five days following a lung transplant. Transplant rejection peak around two months following transplant surgery. The event is rare after six months. Histopathologically rejection is characterized Perivascular or peribronchiolar mononuclear inflammation and may affect up to 55% of lung transplant recipients within the first year after a transplant.

There are no characteristic findings on HRCT. A variety of results has been reported including GGO, consolidation, nodules, interlobular septal thickening and pleural effusions with no associated signs of left ventricular failure.

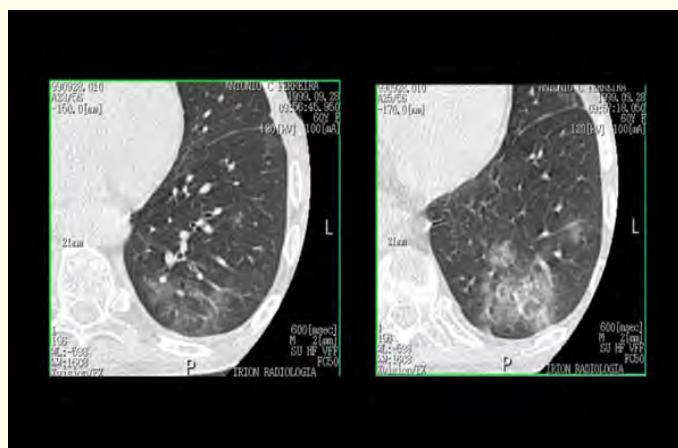


Figure 156: Acute lung transplant rejection: There are no characteristic findings on HRCT. A variety of results has been reported including GGO, consolidation, nodules, interlobular septal thickening and pleural effusions with no associated signs of left ventricular failure.

A further complication is the occurrence of bronchiolitis obliterans with progressive airflow obstruction. Similar HRCT findings can occur pulmonary edema as a reimplantation response and lung transplant rejection.

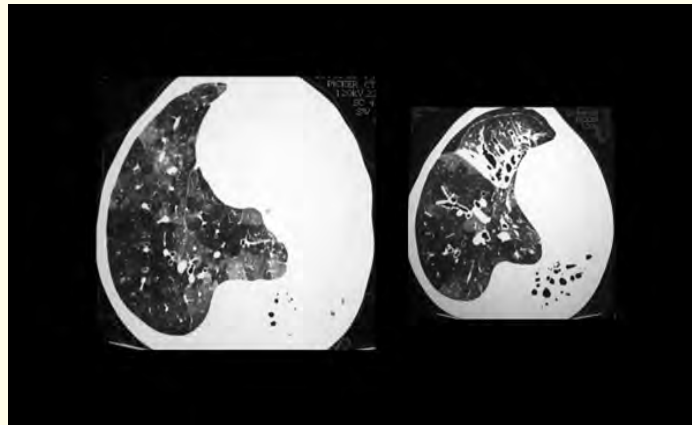


Figure 157: Lung transplant rejection, showing features of bronchiolitis, associated with bronchial dilatation and GGO.

Asthma

Asthma is a common disorder of bronchial airways and is defined as 'a state of bronchial hyperreactivity resulting from a persistent inflammatory process in response to a number of stimuli in a genetically susceptible individual'. The key pathophysiological features include mucosal edema, secretion of mucus, epithelial damage and bronchoconstriction.

Although the causes of asthma are separated into allergic and nonallergic ones, a considerable crossover is observed in the features of both types of asthma, and treatment varies little between them [179-185].

While asthma has been considered a disorder of the airways, a number of conditions have a presentation similar to that of bronchial asthma. These conditions originate, often silently, in organ systems other than the lungs, and they either provoke airway responses equivalent to those found in asthma or mimic the clinical findings of asthma [179-185].



Figure 158: PA chest radiograph demonstrates a pneumomediastinum in bronchial asthma. Note the crisp outline of the mediastinum and air trapping extending into the neck. Note the perihilar GGO.

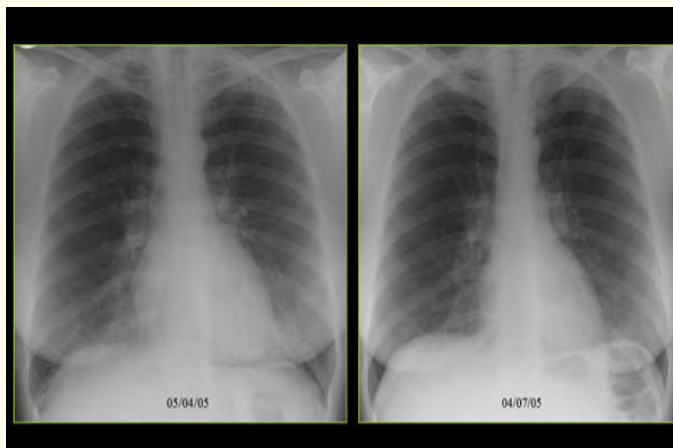


Figure 159: CXR in asthma: note subtle bronchial wall markings, flattening of diaphragm and hyperinflation see also digital radiographs and HRCT.

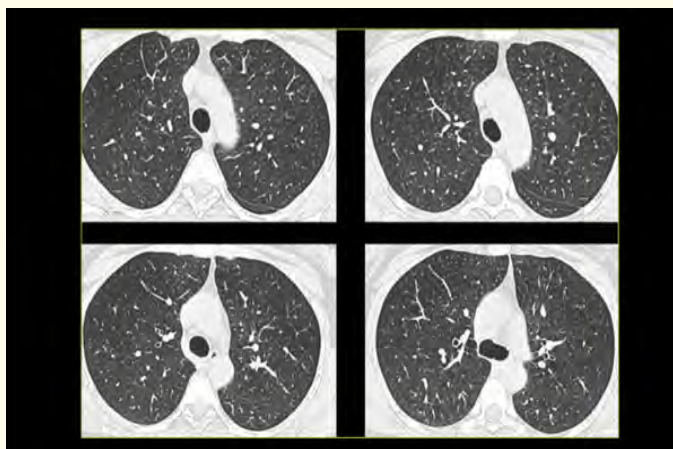


Figure 160: HRCT show mild bronchial wall thickening, including small airways and some restricted areas of reduced vascularity, presumably indicating some degree of air-trapping, especially in the middle lobe, anterior segment of the right upper lobe and lingula.

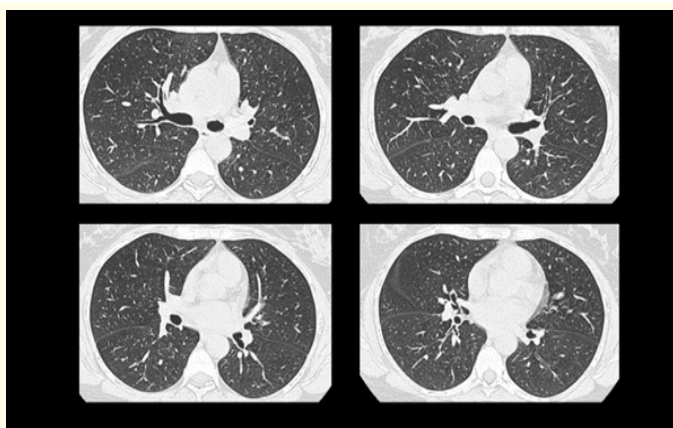


Figure 161: HRCT show mild bronchial wall thickening, including small airways and some restricted areas of reduced vascularity, presumably indicating some degree of air-trapping, especially in the middle lobe, anterior segment of the right upper lobe and lingula.

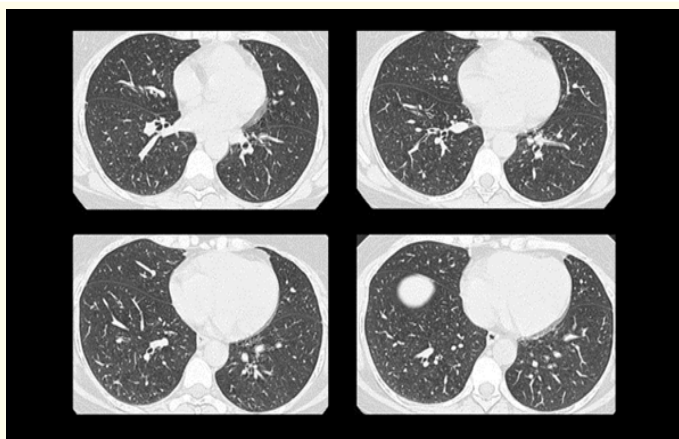


Figure 162: HRCT show mild bronchial wall thickening, including small airways and some restricted areas of reduced vascularity, presumably indicating some degree of air-trapping, especially in the middle lobe, anterior segment of the right upper lobe and lingula.

Emphysema

Emphysema is defined as abnormal permanent enlargement of the airspaces distal to the terminal bronchioles, accompanied by destruction of alveolar walls, without obvious fibrosis. The disease is irreversible and affects about 14 million people; being considered the 4th most common cause of death in the United States. Emphysematous patients will only reveal symptoms when lungs are severely affected. Once symptoms are manifested, treatment options are limited and addressed to symptomatic relief. Lung transplantation and lung volume reduction surgery (LVRS) are indicated in more advanced cases. A significant percentage of heavy smokers will develop emphysema, and the disease should ideally be detected in an early phase to avoid progression to an incapacitating condition. Since pulmonary emphysema is defined on an anatomical basis, computed tomography (CT) is ideal for *in vivo* analysis of emphysema. HRCT and helical CT can detect and quantify emphysema showing good correlation with histopathology [186]. It is known that CT can be more sensitive and accurate than pulmonary function tests. Sanders demonstrated that up to 69% of smokers with emphysema could show normal functional tests [187-224]. Recently, Newell and colleagues reported a workshop in quantitative CT where it has been concluded that CT is superior to the decline of forced expiratory volume in 1 second (FEV1) in the evaluation of progression of emphysema [187-224].

Three-dimensional computed tomography (3DCT) densito-volumetry is a technique that uses post-processing tools applied on data acquired by helical CT. The method allows measuring volumes of zones with different densities. It can be used to quantify emphysema on information obtained from any helical chest CT in which the total lung extension has been scanned during a single breath hold, preferably with the patient in the total lung capacity (end of a maximum inspiratory effort). Some acquisition parameter scan improves accuracy and precision when quantifying emphysema.

Previous studies comparing pulmonary function tests and volumetric CT quantification of patients with emphysema and without emphysema have been reported [187-224]. In these studies, elderly and smokers had been included in the non-emphysematous controls groups. Establishing reference values of the ideal lung condition is a necessity if we want to differentiate normal subjects from subjects already presenting signs of ageing-lungs or from patients with emphysema. In analogy to densitometry bone TScore, we are suggesting the name Emphysema T-Score. The aim of this study is to create an emphysema T-score or reference parameters of the ideal lung condition in CT densito-volumetry for the threshold -950HU [187-224]. Kinsella M and associates have used a 'density mask' depicting regions of attenuation $< -910\text{HU}$ to show areas of emphysema in 85 patients. The authors demonstrated a significant correlation between severity of emphysema on a CT scan and lung function tests. Low attenuation areas on a CT density thus provides a useful method for quantitating emphysema in life [191].

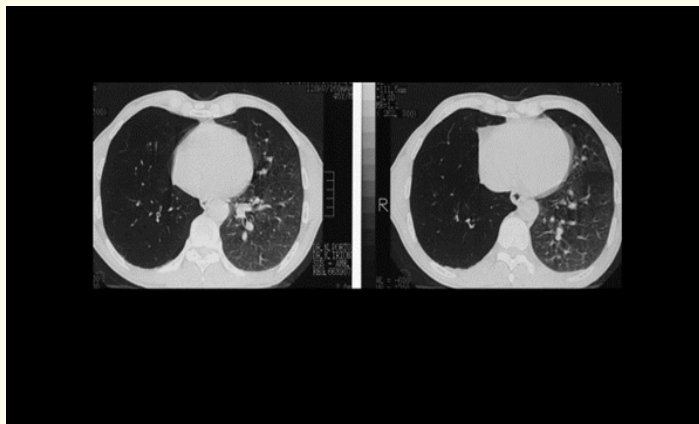


Figure 163: Axial CT scans show a Panacinar emphysema associated with GGO on the uninjured side.

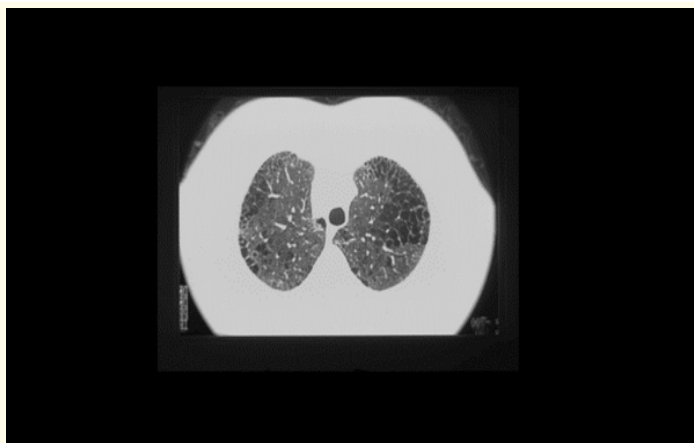


Figure 164: HRCT show a Para septal and Centriacinar Emphysema with Associated GGO.

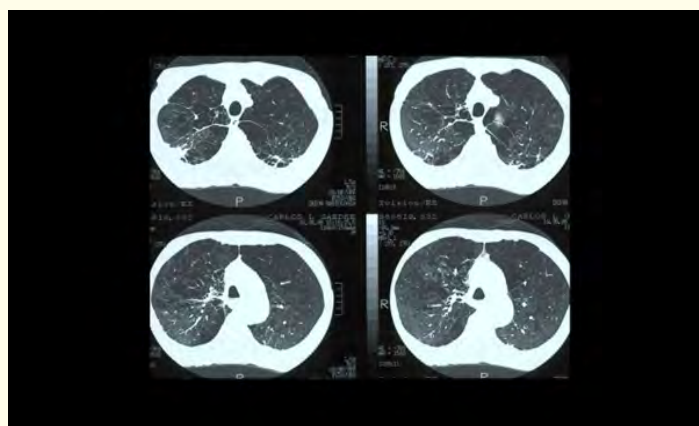


Figure 165: Axial CT scans show Irregular emphysema (scar emphysema) with associated GGO.



Figure 166: Kinsella and associates have used a 'density mask' depicting regions of attenuation < -910 HU to show regions of emphysema in 85 patients. The authors showed a significant correlation between severity of emphysema on a CT scan and lung function tests. Low attenuation areas on a CT density thus provides a useful method for quantitating emphysema in life [191].

Conclusion

GGO of the lungs is caused by an accumulation of pathological products in the alveoli and alveolar septae. GGO is detectable on Chest-X-rays but better defined on HRCT. The differential diagnosis of GGO is extensive and besides radiographic acquisition and other technical factors, a wide variety of lung pathologies such as lung hemorrhage, pulmonary embolism, trauma, and autoimmune vasculitis/capillaritis to name just a few. Infections such as CMV, P. carinii pneumoniae, *Mycoplasma pneumoniae*, Early resolving bacterial pneumonia, BOOP, pulmonary edema various types, smoking-related disease, hypersensitivity pneumonia and different types of interstitial pneumonia also enter the differential diagnosis. The appearances are not tissue-specific, but with the input of clinical history, lung function tests and other laboratory data, it is possible to arrive at a more meaningful diagnosis. The ultimate diagnosis is achieved by tissue sampling.

Bibliography

1. Austin JH., et al. "Glossary of terms for CT of the lungs: recommendations of the Nomenclature Committee of the Fleischner Society". *Radiology* 200.2 (1996): 327-331.
2. Jeong YJ., et al. "Eosinophilic lung diseases: a clinical, radiologic, and pathologic overview". *Radiographics* 27.3 (2007): 617-637.
3. Mueller-mang C., et al. "What every radiologist should know about idiopathic interstitial pneumonias". *Radiographics* 27.3 (2007): 595-615.
4. Park CM., et al. "Nodular ground-glass opacity at thin-section CT: histologic correlation and evaluation of change at follow-up". *Radiographics* 27.2 (2007): 391-408.
5. Miller WT and Shah RM. "Isolated diffuse ground-glass opacity in thoracic CT: causes and clinical presentations". *American Journal of Roentgenology* 184.2 (2005): 613-622.
6. Sylvia Worthy. "High resolution computed tomography of the lungs". *British Medical Journal* 310 (1995): 616.
7. Naidich W., et al. "High-resolution CT of the lung (Fifth edition)" (2014).
8. The University of California, San Francisco HRCT Protocol.
9. Hansell DM. "Thin-Section CT of the Lungs: The Hinterland of Normal". *Radiology* 256.3 (2010): 695-711.

10. Goodpasture EW. "The significance of certain pulmonary lesions in relation to the etiology of influenza". *American Journal of the Medical Sciences* 158.6 (1919): 863-870.
11. Salama AD., et al. "Goodpasture's disease". *Lancet* 358.9285 (2001): 917-920.
12. Kathuria P., et al. "Goodpasture Syndrome Clinical Presentation". In: Schwarz MI. Goodpasture Syndrome: Diffuse Alveolar Hemorrhage and Pulmonary-Renal Syndrome". Merck Manual Professional (2013).
13. Kathuria P., et al. "Goodpasture Syndrome". Medscape Reference (2013).
14. Kathuria P., et al. "Goodpasture Syndrome Workup". Medscape Reference. WebMD (2013).
15. Boitsios G., et al. "Diffuse pulmonary nodules". *American Journal of Roentgenology* 194.5 (2010): W354-W366.
16. Parker BR. "Idiopathic pulmonary hemosiderosis". *American Journal of Roentgenology* 136.5 (1981): 1031-1032.
17. Rubin GD., et al. "Diagnosis of pulmonary hemosiderosis by MR imaging". *American Journal of Roentgenology* 152.3 (1989): 573-574.
18. Woolley K and Stark P. "Pulmonary parenchymal manifestations of mitral valve disease". *Radiographics* 19.4 (1999): 965-972.
19. Butler MD., et al. "Pulmonary resection for treatment of cavitory pulmonary infarction". *Annals of Thoracic Surgery* 63.3 (1997): 849-850.
20. Morgenthaler TI., et al. "Cavitory pulmonary infarct in immunocompromised hosts". *Mayo Clinic Proceedings* 70.1 (1995): 66-68.
21. Wilson AG., et al. "The radiology of aseptic cavitation in pulmonary infarction". *Clinical Radiology* 37.4 (1986): 327-333.
22. Wagner RB., et al. "Classification of parenchymal injuries of the lung". *Radiology* 167.1 (1988): 77-82.
23. Kaewlai R., et al. "Multidetector CT of blunt thoracic trauma". *Radiographics* 28.6 (2008): 1555-1570.
24. Kerns SR and Gay SB. "CT of blunt chest trauma". *American Journal of Roentgenology* 154.1 (1990): 55-60.
25. Van hise ML., et al. "CT in blunt chest trauma: indications and limitations". *Radiographics* 18.5 (1998): 1071-1084.
26. Matthes G., et al. "Blunt liver injuries in Polytrauma: results from a cohort study with the regular use of whole-body helical computed tomography". *World Journal of Surgery* 27.10 (2003): 1124-1130.
27. Guillaume Chassagnon., et al. "Tracheobronchial Branching Abnormalities: Lobe-based Classification Scheme". *RadioGraphics* 36.2 (2016): 358-373.
28. Almeida RR., et al. "Cocaine-induced pulmonary changes: HRCT findings". *Jornal Brasileiro de Pneumologia* 41.4 (2015): 323-330.
29. Baldwin GC., et al. "Evidence of chronic damage to the pulmonary microcirculation in habitual users of alkaloidal ("crack") cocaine". *Chest* 121.4 (2002): 1231-1238.
30. Chen J, et al. "Asymptomatic preclinical rheumatoid arthritis-associated interstitial lung disease". *Clinical and Developmental Immunology* (2013): 406927.
31. Ito I., et al. "Pulmonary manifestations of primary Sjogren's syndrome: a clinical, radiologic, and pathologic study". *American Journal of Respiratory and Critical Care Medicine* 171.6 (2005): 632-638.

32. C Isabela, *et al.* "Intrathoracic manifestations of collagen vascular diseases on high-resolution chest computed tomography". *Radiologia Brasileira* 41.3 (2008).
33. Hunninghake GW and Fauci AS. "Pulmonary involvement in the collagen vascular diseases". *American Review of Respiratory Disease* 119.3 (1979): 471-503.
34. Medsger TA Jr, *et al.* "Survival with systemic sclerosis (scleroderma). A life-table analysis of clinical and demographic factors in 309 patients". *Annals of Internal Medicine* 75.3 (1971): 369-376.
35. Schurawitzki H, *et al.* "Interstitial lung disease in progressive systemic sclerosis: high-resolution CT versus radiography". *Radiology* 176.3 (1990): 755-759.
36. Taormina VJ, *et al.* "Progressive systemic sclerosis subgroups: variable pulmonary features". *American Journal of Roentgenology* 137.2 (1981): 277-285.
37. Remy-Jardin M, *et al.* "Pulmonary involvement in progressive systemic sclerosis: sequential evaluation with CT, pulmonary function tests, and bronchoalveolar lavage". *Radiology* 188.2 (1993): 499-506.
38. Arroliga AC, *et al.* "Pulmonary manifestations of scleroderma". *Journal of Thoracic Imaging* 7.2 (1992): 30-45.
39. Seely JM, *et al.* "Systemic sclerosis: using high-resolution CT to detect lung disease in children". *American Journal of Roentgenology* 170.3 (1998): 691-697.
40. Wechsler RJ, *et al.* "The relationship of thoracic lymphadenopathy to pulmonary interstitial disease in diffuse and limited systemic sclerosis: CT findings". *American Journal of Roentgenology* 167.1 (1996): 101-104.
41. Griffin MT, *et al.* "Diffuse alveolar haemorrhage associated with progressive systemic sclerosis". *Thorax* 45.11 (1990): 903-904.
42. Rockall AG, *et al.* "Imaging of the pulmonary manifestations of systemic disease". *Postgraduate Medical Journal* 77.912 (2001): 621-638.
43. Trisolini R, *et al.* "Diffuse lung disease in neurofibromatosis". *Lung* 190.2 (2012): 249-250.
44. Zamora AC, *et al.* "Neurofibromatosis-associated lung disease: a case series and literature review". *European Respiratory Journal* 29.1 (2007): 210-214.
45. Hewitt MG, *et al.* "The relative frequencies of causes of widespread ground-glass opacity: a retrospective cohort". *European Journal of Radiology* 83.10 (2014): 1970-1976.
46. Franquet T, *et al.* "Human metapneumovirus infection in hematopoietic stem cell transplant recipients: high-resolution computed tomography findings". *Journal of Computer Assisted Tomography* 29.2 (2005): 223-227.
47. Voloudaki AE, *et al.* "Q fever pneumonia: CT findings". *Radiology* 215.3 (2000): 880-883.
48. Traill ZC, *et al.* "Pseudomonas aeruginosa bronchopulmonary infection in patients with advanced human immunodeficiency virus disease". *British Journal of Radiology* 69.828 (1996): 1099-1103.
49. Osler William. "Principles and Practice of Medicine, 4th Edition". New York: D. Appleton and Company (1901): 108.
50. Robbins Stanley, *et al.* "Robbins and Cotran pathologic basis of disease". St. Louis, Mo: Elsevier Saunders (2005): 749.

51. Wagner AL, et al. "Radiologic manifestations of round pneumonia in adults". *American Journal of Roentgenology* 170.3 (1998): 723-726.
52. Stern EJ and White CS. "Chest radiology companion". Lippincott Williams and Wilkins (1999).
53. Kim YW and Donnelly LF. "Round pneumonia: imaging findings in a large series of children". *Pediatric Radiology* 37.12 (2007): 1235-1240.
54. Burrill J, et al. "Tuberculosis: a radiologic review". *Radiographics* 27.5 (2007): 1255-1273.
55. Harisinghani MG, et al. "Tuberculosis from head to toe". *Radiographics* 20.2 (2000): 449-470.
56. McShane PJ and Glassroth J. "Pulmonary Disease Due to Nontuberculous Mycobacteria: Current State and New Insights". *Chest* 148.6 (2015): 1517-1527.
57. Henkle E and Winthrop KL. "Nontuberculous mycobacteria infections in immunosuppressed hosts". *Clinics in Chest Medicine* 36.1 (2015): 91-99.
58. Ronald P Bologna, et al. "Dermatology: 2-Volume Set". St. Louis: Mosby (2007).
59. Ryan KJ and Ray CG. "Sherris Medical Microbiology (4th Edition)". McGraw Hill (2004): 674-676.
60. Aliouat-Denis CM, et al. "Pneumocystis species, co-evolution and pathogenic power". *Infection, Genetics and Evolution* 8.5 (2008): 708-726.
61. Kanne JP, et al. "Pneumocystis jiroveci pneumonia: high-resolution CT findings in patients with and without HIV infection". *American Journal of Roentgenology* 198.6 (2012): W555-W561.
62. Medrano FJ, et al. "Pneumocystis jirovecii in general population". *Emerging Infectious Diseases* 11.2 (2005): 245-250.
63. Stern A, et al. "Prophylaxis for Pneumocystis pneumonia (PCP) in non-HIV immunocompromised patients". *Cochrane Database of Systematic Reviews* 10 (2014): CD005590.
64. Ryan KJ and Ray CG. "Sherris Medical Microbiology (4th edition)". McGraw Hill (2004).
65. Postgrad J. "Nitrogen Fixation (3rd edition)". Cambridge University Press (1998).
66. Riggs PJ, et al. "Enhanced maize productivity by inoculation with diazotrophic bacteria". *Australian Journal of Plant Physiology* 29.8 (2001): 829-836.
67. Podschun R and Ullmann U. "Klebsiella spp. as Nosocomial Pathogens: Epidemiology, Taxonomy, Typing Methods, and Pathogenicity Factors". *Clinical Microbiology Reviews* 1.41 (1998): 589-603.
68. Cunha BA, et al. "Legionnaires' disease". *Lancet* 387.10016 (2016): 376-385.
69. "Legionella (Legionnaires' Disease and Pontiac Fever) About the Disease". CDC (2016).
70. "Legionella (Legionnaires' disease and Pontiac Fever) Signs and Symptoms". CDC (2016).
71. "Legionella (Legionnaires' disease and Pontiac Fever) Causes and Transmission". CDC (2016).
72. "Legionella (Legionnaires' Disease and Pontiac Fever) People at Risk". CDC (2016).

73. "Legionella (Legionnaires 'disease and Pontiac Fever) Diagnostic Testing". CDC (2015).
74. "Legionella (Legionnaires 'disease and Pontiac Fever) Treatment and Complications". CDC (2016).
75. "Legionella (Legionnaires' Disease and Pontiac Fever)". CDC (2016).
76. Sawicki GS, *et al.* "Necrotising pneumonia is an increasingly detected complication of pneumonia in children". *European Respiratory Journal* 31.6 (2008): 1285-1291.
77. Hodina M, *et al.* "Imaging of cavitory necrosis in complicated childhood pneumonia". *European Radiology* 12.2 (2002): 391-396.
78. Pande A, *et al.* "The incidence of necrotizing changes in adults with pneumococcal pneumonia". *Clinical Infectious Diseases* 54.1 (2012): 10-16.
79. Gadkowski LB and Stout JE. "Cavitory pulmonary disease". *Clinical Microbiology Reviews* 21.2 (2008): 305-333.
80. Hansell DM, *et al.* "Fleischner Society: glossary of terms for thoracic imaging". *Radiology* 246.3 (2008): 697-722.
81. Fox DL and Müller NL. "Pulmonary cryptococcosis in immunocompetent patients: CT findings in 12 patients". *American Journal of Roentgenology* 85.3 (2005): 622-626.
82. Al-Ghanem Sara, *et al.* "Bronchiolitis obliterans organizing pneumonia: Pathogenesis, clinical features, imaging and therapy review". *Annals of Thoracic Medicine* 3.2 (2008): 67-75.
83. Bouchardy LM, *et al.* "CT findings in bronchiolitis obliterans organizing pneumonia (BOOP) with radiographic, clinical, and histologic correlation". *Journal of Computer Assisted Tomography* 17.3 (1993): 352-357.
84. Epler GR, *et al.* "Bronchiolitis obliterans organizing pneumonia". *New England Journal of Medicine* 312.3 (1985): 152-158.
85. Izumi T, *et al.* "Bronchiolitis obliterans organizing pneumonia. Clinical features and differential diagnosis". *Chest* 102.3 (1992): 715-719.
86. Katzenstein AL and Myers JL. "Nonspecific interstitial pneumonia and the other idiopathic interstitial pneumonias: classification and diagnostic criteria". *American Journal of Surgical Pathology* 24.1 (2000): 1-3.
87. Mayberry JP, *et al.* "Thoracic manifestations of systemic autoimmune diseases: radiographic and high-resolution CT findings". *Radiographics* 20.6 (2000): 1623-1635.
88. Muller NL and Coiby TV. "Idiopathic interstitial pneumonias: high-resolution CT and histologic findings". *Radiographics* 17.4 (1997): 1016-1022.
89. Nagai S, *et al.* "Classification and recent advances in idiopathic interstitial pneumonia". *Current Opinion in Pulmonary Medicine* 4.5 (1998): 256-260.
90. Stover DE, *et al.* "A newly recognized syndrome--radiation-related bronchiolitis obliterans and organizing pneumonia. A case report and literature review". *Respiration* 68.5 (2001): 540-544.
91. Kaestel M, *et al.* "Pulmonary aspergilloma - clinical findings and surgical treatment". *Thoracic and Cardiovascular Surgery* 47.5 (1999): 340-345.
92. Regnard JF, *et al.* "Aspergilloma: a series of 89 surgical cases". *Annals of Thoracic Surgery* 69.3 (2000): 898-903.

93. Rumbak M., *et al.* "Topical treatment of life threatening haemoptysis from aspergillomas". *Thorax* 51.3 (1996): 253-255.
94. Chatzimichalis A., *et al.* "Bronchopulmonary aspergilloma: a reappraisal". *Annals of Thoracic Surgery* 65.4 (1998): 927-929.
95. van der Maarek-Wierink CD., *et al.* "Risk factors for aspiration pneumonia in frail older people: a systematic literature review". *Journal of American Medical Directors Association* 12.5 (2011): 344-354.
96. Taylor GW., *et al.* "Impact of Oral Diseases on Systemic Health in the Elderly: Diabetes Mellitus and Aspiration Pneumonia". *Journal of Public Health Dentistry* 60.4 (2000): 313-320.
97. Mukhopadhyay S and Katzenstein AL. "Pulmonary disease due to aspiration of food and other particulate matter: a clinicopathologic study of 59 cases diagnosed on biopsy or resection specimens". *American Journal of Surgical Pathology* 31.5 (2007): 752-759.
98. Visscher MB. "The genesis of pulmonary edema". *Circulation Research* 2.4 (1954): 291-293.
99. Ali Nawaz Khan., *et al.* "Reading chest radiographs in the critically ill (Part II): Radiography of lung pathologies common in the ICU patient". *Annals of Thoracic Medicine* 4.3 (2009): 149-157.
100. Shah PL., *et al.* "Pulmonary alveolar proteinosis: clinical aspects and current concepts on pathogenesis". *Thorax* 55.1 (2000): 67-77.
101. Webb WR and Higgins CB. "Consolidation and atelectasis". In *Thoracic Imaging: Pulmonary and Cardiovascular Radiology*. Lippincott Williams & Wilkins, Chapter 2 (2004).
102. Swensen SJ., *et al.* "High-resolution CT of the lungs: findings in various pulmonary diseases". *American Journal of Roentgenology* 158.5 (1992): 971-979.
103. Gluecker T., *et al.* "Clinical and radiologic features of pulmonary edema". *Radiographics* 19.6 (1999): 1507-1531.
104. Attias D., *et al.* "Prevalence, characteristics, and outcomes of patients presenting with cardiogenic unilateral pulmonary edema". *Circulation* 122.11 (2010): 1109-1115.
105. Myrianthefs P., *et al.* "Rare roentgenologic manifestations of pulmonary edema". *Current Opinion in Critical Care* 17.5 (2011): 449-453.
106. Miyatake K., *et al.* "Localisation and direction of mitral regurgitant flow in mitral orifice studied with combined use of ultrasonic pulsed Doppler technique and two dimensional echocardiography". *British Heart Journal* 48.5 (1982): 449-458.
107. Roach James M and Schoene Robert B. "High-Altitude Pulmonary Edema". In Pandolf, Kent B. Burr, Robert E. *Medical Aspects of Harsh Environments (PDF)* 2. Washington, DC: Borden Institute. (2002): 789-814.
108. Khan SU., *et al.* "Acute pulmonary edema after lung transplantation: the pulmonary reimplantation response". *Chest* 116.1 (1999): 187-194.
109. Marom EM., *et al.* "Reperfusion edema after lung transplantation: effect of daclizumab". *Radiology* 221.2 (2001): 508-514.
110. Ablett MJ., *et al.* "The correlation of the radiologic extent of lung transplantation edema with pulmonary oxygenation". *American Journal of Roentgenology* 171.3 (1998): 587-589.
111. Ng YL., *et al.* "Imaging of lung transplantation: review". *American Journal of Roentgenology* 192.3 (2009): S1- S19.
112. Rumbak MJ. "The etiology of pulmonary edema in fresh water near-drowning". *American Journal of Emergency Medicine* 14.2 (1996): 176-179.

113. Cohen DS., *et al.* "Pulmonary edema associated with salt water near-drowning: new insights". *American Review of Respiratory Disease* 146.3 (1992): 794-796.
114. Fanelli Vito and Ranieri V Marco. "Mechanisms and clinical consequences of acute lung injury". *Annals of the American Thoracic Society* 12.1 (2015): S3-S8.
115. Rubenfeld Gordon D., *et al.* "Incidence and Outcomes of Acute Lung Injury". *New England Journal of Medicine* 353.16 (2005): 1685-1693.
116. Bernard G., *et al.* "The American-European Consensus Conference on ARDS. Definitions, mechanisms, relevant outcomes, and clinical trial coordination". *American Journal of Respiratory and Critical Care Medicine* 149 (1994): 818-824.
117. Bain GA and Flower CD. "Pulmonary eosinophilia". *European Journal of Radiology* 23.1 (1996): 3-8.
118. Rossi SE., *et al.* "Pulmonary drug toxicity: radiologic and pathologic manifestations". *Radiographics* 20.5 (2000): 1245-1259.
119. Arakawa H., *et al.* "Nonspecific interstitial pneumonia associated with polymyositis and dermatomyositis: serial high-resolution CT findings and functional correlation". *Chest* 123.4 (2003): 1096-1103.
120. Kim TS., *et al.* "Nonspecific interstitial pneumonia with fibrosis: high-resolution CT and pathologic findings". *American Journal of Roentgenology* 171.6 (1998): 1645-1650.
121. Elliot TL., *et al.* "High-resolution computed tomography features of nonspecific interstitial pneumonia and usual interstitial pneumonia". *Journal of Computer Assisted Tomography* 29.3 (2005): 339-345.
122. Hartman TE., *et al.* "Nonspecific interstitial pneumonia: variable appearance at high-resolution chest CT". *Radiology* 217.3 (2000): 701-705.
123. Miller BH and Putman CE. "The chest radiograph and sarcoidosis. Reevaluation of the chest radiograph in assessing activity of sarcoidosis: a preliminary communication". *Sarcoidosis* 2.2 (1985): 85-90.
124. Criado E., *et al.* "Pulmonary Sarcoidosis: Typical and Atypical Manifestations at High-Resolution CT with Pathologic Correlation". *RadioGraphics* 30.6 (2010): 1567-1586.
125. A Khan., *et al.* "Thoracic Sarcoidosis Imaging". Medscape (2013).
126. Miller BH., *et al.* "Thoracic sarcoidosis: radiologic-pathologic correlation". *Radiographics* 15.2 (1995): 421-437.
127. Godwin JD., *et al.* "Pulmonary alveolar proteinosis: CT findings". *Radiology* 169.3 (1988): 609-613.
128. Holbert JM., *et al.* "CT features of pulmonary alveolar proteinosis". *American Journal of Roentgenology* 176.5 (2001): 1287-1294.
129. Johkoh T., *et al.* "Crazy-paving appearance at thin-section CT: spectrum of disease and pathologic findings". *Radiology* 211.1 (1999): 155-160.
130. Kariman K., *et al.* "Pulmonary alveolar proteinosis: prospective clinical experience in 23 patients for 15 years". *Lung* 162.4 (1984): 223-231.
131. Lee KN., *et al.* "Pulmonary alveolar proteinosis: high-resolution CT, chest radiographic, and functional correlations". *Chest* 111.4 (1997): 989-995.

132. Murch CR and Carr DH. "Computed tomography appearances of pulmonary alveolar proteinosis". *Clinical Radiology* 40.3 (1989): 240-243.
133. Parker LA and Novotny DB. "Recurrent alveolar proteinosis following double lung transplantation". *Chest* 111.5 (1997): 1457-1458.
134. Schumacher RE., et al. "Pulmonary alveolar proteinosis in a newborn". *Pediatric Pulmonology* 7.3 (1989): 178-182.
135. Wang BM., et al. "Diagnosing pulmonary alveolar proteinosis. A review and an update". *Chest* 111.2 (1997): 460-466.
136. Qin L., et al. "Non-Hodgkin's lymphoma with diffuse ground-glass opacity on chest CT: a report of 6 cases". *Zhonghua Yi Xue Za Zhi* 90.46 (2010): 3283-3286.
137. Tokuyasu H., et al. "Non-Hodgkin's lymphoma accompanied by pulmonary involvement with diffuse ground-glass opacity on chest CT: a report of 2 cases". *Internal Medicine* 48.2 (2009): 105-109.
138. M Yc., et al. "Computed tomography features of pulmonary non-Hodgkin's lymphoma and special emphasis on Richter's syndrome". *Journal of Clinical Oncology* 26.15 (2008): 19526.
139. Arana S., et al. "Choriocarcinoma syndrome in a 24-year-old male". *JRSM Open* 3.6 (2012): 44.
140. Chen X., et al. "Testicular choriocarcinoma metastatic to skin and multiple organs. Two case reports and review of literature". *Journal of Cutaneous Pathology* 37.4 (2010): 486-490.
141. Moon JH., et al. "Cytomegalovirus pneumonia: high-resolution CT findings in ten non-AIDS immunocompromised patients". *Korean Journal of Radiology* 1.2 (2002): 73-78.
142. Aafedt BC., et al. "Cytomegalovirus pneumonia: computed tomography findings". *Canadian Association of Radiologists Journal* 41.5 (1990): 276-280.
143. Horger MS., et al. "Cytomegalovirus pneumonia after stem cell transplantation: correlation of CT findings with clinical outcome in 30 patients". *American Journal of Roentgenology* 187.6 (2006): W636-W643.
144. McGuinness G., et al. "Cytomegalovirus pneumonitis: spectrum of parenchymal CT findings with pathologic correlation in 21 AIDS patients". *Radiology* 192.2 (1994): 451-459.
145. Franquet T., et al. "Thin-section CT findings in 32 immunocompromised patients with cytomegalovirus pneumonia who do not have AIDS". *American Journal of Roentgenology* 181.4 (2003): 1059-1063.
146. Kang EY., et al. "Cytomegalovirus pneumonia in transplant patients: CT findings". *Journal of Computer Assisted Tomography* 20.2 (1996): 295-299.
147. Gasparetto EL., et al. "Cytomegalovirus pneumonia after bone marrow transplantation: high resolution CT findings". *British Journal of Radiology* 77.921 (2004): 724-727.
148. Vogel MN., et al. "Differences and similarities of cytomegalovirus and pneumocystis pneumonia in HIV-negative immunocompromised patients thin section CT morphology in the early phase of the disease". *British Journal of Radiology* 80.955 (2007): 516-523.
149. RAL Bisset., et al. "Differential Diagnosis in Abdominal Ultrasound". Elsevier (2012): 470.
150. Mylona Mylonakis E., et al. "Pulmonary aspergillosis and invasive disease in AIDS: review of 342 cases". *Chest* 114.1 (1998): 251-262.

151. McGuinness G. "Changing trends in the pulmonary manifestations of AIDS". *Radiologic Clinics of North America* 35.5 (1997): 1029-1082.
152. Gruden JF, et al "High-resolution CT in the evaluation of clinically suspected *Pneumocystis carinii* pneumonia in AIDS patients with normal, equivocal, or nonspecific radiographic findings". *American Journal of Roentgenology* 169.4 (1997): 967-975.
153. Wolff SD, et al. "Thoracic Kaposi sarcoma in AIDS: CT findings". *Journal of Computer Assisted Tomography* 17.1 (1993): 60-62.
154. Gupta N., et al. "Diffuse Cystic Lung Disease. Part I". *American Journal of Respiratory and Critical Care Medicine* 191.12 (2015): 1354-1366.
155. Walsh SL, et al. "Interstitial lung disease related to smoking: imaging considerations". *Current Opinion in Pulmonary Medicine* 21.4 (2015): 407-416.
156. Margaritopoulos GA, et al. "Smoking and interstitial lung diseases". *European Respiratory Review* 24.137 (2015): 428-435.
157. Margaritopoulos GA, et al. "Smoking-related idiopathic interstitial pneumonia: A review". *Respirology* 21.1 (2016): 57-64.
158. Fraire AE. "Hypersensitivity pneumonitis: a commentary". *Archives of Pathology and Laboratory Medicine* 132.2 (2008): 192-194.
159. Madison JM. "Hypersensitivity pneumonitis: clinical perspectives". *Archives of Pathology and Laboratory Medicine* 132.2 (2008): 195-198.
160. Babu KS and Marshall BG. "Drug-induced airway diseases". *Clinics in Chest Medicine* 25.1 (2004): 113-122.
161. Camus P, et al. "Drug-induced and iatrogenic infiltrative lung disease". *Clinics in Chest Medicine* 25.3 (2004): 479-519.
162. Camus PH, et al. "Drug-induced infiltrative lung disease". *European Respiratory Journal. Supplement* 32 (2001): 93s-100s.
163. Erasmus JJ, et al. "Drug-induced lung injury". *Seminars in Roentgenology* 37.1 (2002): 72-81.
164. Fraser RS, et al. "Drugs". In: Fraser RS, Mueller NL, Colman N, Pare PD, eds. *Diagnosis of Diseases of the Chest*. 4th edition. Philadelphia, PA: WB Saunders (1999): 2537-2583.
165. Huggins JT and Sahn SA. "Drug-induced pleural disease". *Clinics in Chest Medicine* 25.1 (2004): 141-153.
166. Limper AH and Rosenow EC. "Drug-induced interstitial lung disease". *Current Opinion in Pulmonary Medicine* 2.5 (1996): 396-404.
167. Lock BJ, et al. "Infiltrative lung disease due to noncytotoxic agents". *Clinics in Chest Medicine* 25.1 (2004): 47-52.
168. Morelock SY and Sahn SA. "Drugs and the pleura". *Chest* 116.1 (1999): 212-221.
169. Ozkan M, et al. "Drug-induced lung disease". *Cleveland Clinic Journal of Medicine* 68.9 (2001): 782-795.
170. Sylvester KP, et al. "Computed tomography and pulmonary function abnormalities in sickle cell disease". *European Respiratory Journal* 28.4 (2006): 832-838.
171. Lee JW, et al. "Cryptogenic organizing pneumonia: serial high-resolution CT findings in 22 patients". *American Journal of Roentgenology* 195.4 (2010): 916-922.
172. Lee HY, et al. "High-resolution CT findings in fibrotic idiopathic interstitial pneumonias with little honeycombing: serial changes and prognostic implications". *American Journal of Roentgenology* 199.5 (2012): 982-989.

173. Rao PN, *et al.* "Monitoring of acute lung rejection and infection by bronchoalveolar lavage and plasma levels of hyaluronic acid in clinical lung transplantation". *Journal of Heart and Lung Transplantation* 13.6 (1995): 958-962.
174. Martinu T, *et al.* "Acute rejection and humoral sensitization in lung transplant recipients". *Proceedings of the American Thoracic Society* 6.1 (2009): 54-65.
175. Mangi AA, *et al.* "Predictors of acute rejection after lung transplantation". *Annals of Thoracic Surgery* 91.6 (2011): 1754-1762.
176. Gotway MB, *et al.* "Acute rejection following lung transplantation: limitations in accuracy of thin-section CT for diagnosis". *Radiology* 221.1 (2001): 207-212.
177. Garg K, *et al.* "Lung transplantation: indications, donor and recipient selection, and imaging of complications". *Radiographics* 16.2 (1996): 355-367.
178. Loubeyre P, *et al.* "High-resolution computed tomographic findings associated with histologically diagnosed acute lung rejection in heart-lung transplant recipients". *Chest* 107.1 (1995): 132-138.
179. Arakawa H and Webb WR. "Air trapping on expiratory high-resolution CT scans in the absence of inspiratory scan abnormalities: correlation with pulmonary function tests and differential diagnosis". *American Journal of Roentgenology* 170.5 (1998): 1349-1353.
180. Aronson S, *et al.* "The value of routine admission chest radiographs in adult asthmatics". *Annals of Emergency Medicine* 18.11 (1989): 1206-1208.
181. "BMJ: Editorial: chest radiographs in asthma". *British Medical Journal* 4.5937 (1974): 123-124.
182. Carr DH, *et al.* "Peripheral airways obstruction on high-resolution computed tomography in chronic severe asthma". *Respiratory Medicine* 92.3 (1998): 448-453.
183. Dalton AM. "A review of radiological abnormalities in 135 patients presenting with acute asthma". *Archives of Emergency Medicine* 8.1 (1991): 36-40.
184. Gershel JC, *et al.* "The usefulness of chest radiographs in first asthma attacks". *New England Journal of Medicine* 309.6 (1983): 336-339.
185. Roback MG and Dreitlein DA. "Chest radiograph in the evaluation of first time wheezing episodes: review of current clinical practice and efficacy". *Pediatric Emergency Care* 14.3 (1998): 181-184.
186. Snider GL, *et al.* "The definition of emphysema. Report of the National Heart, Lung and Blood Institute, Division of Lung Diseases Workshop". *American Review of Respiratory Disease* 132.1 (1985): 182-185.
187. Gurney JW. "Pathophysiology of obstructive airways disease". *Radiologic Clinics of North America* 36.1 (1998): 15-27.
188. Coxson H, *et al.* "A Quantification of the Lung Surface Area In Emphysema Using Computed Tomography". *American Journal of Respiratory and Critical Care Medicine* 159.3 (1999): 355-361.
189. Klein JS, *et al.* "High-resolution CT diagnosis of emphysema in symptomatic patients with normal chest radiographs and isolated low diffusing capacity". *Radiology* 182.3 (1992): 817-821.
190. Foster WL, *et al.* "Centrilobular emphysema: CT pathologic correlation". *Radiology* 159.1 (1986): 27-32.

191. Kinsella M., *et al.* "Quantitation of emphysema by computed tomography using a "density mask" program and correlation with pulmonary function tests". *Chest* 97.2 (1990): 315-321.
192. Coxson HO., *et al.* "Measurement of lung expansion with computed tomography and comparison with quantitative histology". *Journal of Applied Physiology* 79.5 (1995): 1525-1530.
193. Knudson RJ., *et al.* "Expiratory computed tomography for assessment of suspected pulmonary emphysema". *Chest* 99.6 (2003): 1357-1366.
194. Hayhurst MD., *et al.* "Diagnosis of pulmonary emphysema by computerized tomography". *Lancet* 2.8398 (1984): 320-322.
195. Blechschmidt RA., *et al.* "Automated CT image evaluation of the lung: a morphology-based concept". *IEEE Transactions on Medical Imaging* 20.5 (2001): 434-442.
196. Falaschi F., *et al.* "Quantification of pulmonary emphysema with computerized tomography. Comparison with various methods". *La Radiologia Medica* 90.1-2 (1995): 16-23.
197. Hruban RH., *et al.* "High resolution computed tomography of inflation fixed lungs: pathologic-radiologic correlation of centrilobular emphysema". *American Review of Respiratory Disease* 136.4 (1987): 935-940.
198. Muller NL., *et al.* "Density mask: an objective method to quantitate emphysema using computed tomography". *Chest* 94.4 (1988): 782-787.
199. Gould GA., *et al.* "CT measurements of lung density in life can quantitate distal airspace enlargement: an essential defining feature of human emphysema". *American Review of Respiratory Disease* 137.2 (1988): 380-392.
200. Gevenois PA., *et al.* "Comparison of computed density and macroscopic morphometry in pulmonary emphysema". *American Journal of Respiratory and Critical Care Medicine* 152 (1995): 653-665.
201. Gevenois PA., *et al.* "Comparison of computed density and microscopic morphometry in pulmonary emphysema". *American Journal of Respiratory and Critical Care Medicine* 154.1 (1996): 187-192.
202. Bankier AA., *et al.* "CT of pulmonary emphysema: subjective assessment and objective quantification by densitometry and macroscopic morphometry". *Radiology* 211.3 (1999): 851-858.
203. Stern EJ and Frank MS. "CT of the lung in patients with pulmonary emphysema: diagnosis, quantification, and correlation with pathologic and physiologic findings". *American Journal of Roentgenology* 162.4 (1994): 791-798.
204. Sanders C., *et al.* "Detection of emphysema with computed tomography: correlation with pulmonary function tests and chest radiography". *Investigative Radiology* 23.4 (1988): 262-266.
205. Newell JD., *et al.* "Report of a workshop: quantitative computed tomography scanning in longitudinal studies of emphysema". *European Respiratory Journal* 23.5 (2004): 769-775.
206. Park KJ., *et al.* "Quantitation of emphysema with three-dimensional CT densitometry: comparison with two-dimensional analysis, visual emphysema scores, and pulmonary function test results". *Radiology* 211.2 (1999): 541-547.
207. Madani A., *et al.* "Pulmonary emphysema: objective quantification at multi-detector row CT--comparison with macroscopic and microscopic morphometry". *Radiology* 238.3 (2006): 1036-1043.

208. Gierada DS, *et al.* "Repeatability of quantitative CT indexes of emphysema in patients evaluated for lung volume reduction surgery". *Radiology* 220.2 (2001): 448-454.
209. Kauczor HU and Heussel CP. "Assessment of lung volumes using helical CT at inspiration e expiration: comparison with pulmonary function tests". *American Journal of Roentgenology* 171 (1998): 1091-1095.
210. Mergo PJ, *et al.* "Three dimensional volumetric assessment of abnormally low attenuation of the lung from routine helical CT: Inspiratory and expiratory quantification". *American Journal of Roentgenology* 170.5 (1998): 1355-1360.
211. Hoffman EA and McLennan G. "Assessment of the Pulmonary Structure-Function Relationship and Clinical Outcomes Measures: Quantitative Volumetric CT of the Lung". *Academic Radiology* 4.11 (1997): 758-776.
212. Arakawa A, *et al.* "Assessment of lung volumes in pulmonary emphysema using multidetector helical CT: comparison with pulmonary function tests". *Computerized Medical Imaging and Graphics* 25.5 (2001): 399-404.
213. Kollef M." Critical care parameters e formulas". In: Ewald GA, McKenzie CR. Manual of medical therapeutics. Little Brown e Company 1 (1995): 577.
214. Becker MD, *et al.* "Lung volumes before and after lung volume reduction surgery: quantitative CT analysis". *American Journal of Respiratory and Critical Care Medicine* 157 (1998): 1593-1599.
215. Boedeker KL, *et al.* "Emphysema: Effect of Reconstruction Algorithm on CT Imaging Measures". *Radiology* 232.1 (2004): 295-301.
216. Stern EL, *et al.* "Dynamic quantitative computed tomography: a predictor of pulmonary function in obstructive lung disease". *Investigative Radiology* 29.5 (1994): 564-569.
217. Rienmuller R, *et al.* "Standardized quantitative high resolution CT in lung diseases". *Journal of Computer Assisted Tomography* 15.5 (1991): 742-749.
218. Kalender WA, *et al.* "Measurement of pulmonary parenchymal attenuation: use of spirometric gating with quantitative CT". *Radiology* 175.1 (1990): 265-268.
219. Kemerink GJ, *et al.* "Scanner conformity in CT densitometry of the lungs". *Radiology* 197.3 (1995): 749-752.
220. Lamers RJ, *et al.* "Chronic obstructive pulmonary disease: evaluation with spirometrically controlled CT lung densitometry". *Radiology* 193.1 (1994): 109-113.
221. Cederlund K, *et al.* "Visual classification of emphysema heterogeneity compared with objective measurements: HRCT vs spiral CT in candidates for lung volume reduction surgery". *European Radiology* 12.5 (2002): 1045-1051.
222. Madani A, *et al.* "Quantitative computed tomography assessment of lung structure and function in pulmonary emphysema". *European Respiratory Journal* 18.4 (2001): 720-730.
223. Goldman HI and Beck lake MR. "Respiratory function tests: normal values at median altitudes and the prediction of normal results". *American Review of Tuberculosis* 79.4 (1959): 457-467.
224. Vikgren J, *et al.* "Detection of mild emphysema by computed tomography density measurements". *Acta Radiologica* 46.3 (2005): 237-245.

Volume 5 Issue 2 October 2017

©All rights reserved by Ali Nawaz Khan, *et al.*